Chapter 4

Test beam performance of the TileCal prototypes

The Tile Calorimeter test beam program started in 1993 with a standalone setup. The reduced hadron calorimeter prototype consisted of an azimuthal stack of five modules. Each module covering $2\pi/64$ in azimuth and 1 m length along the z direction.

The five prototypes were exposed to high-energy pion, electron and muon beams at the CERN SPS. The energy resolution for pions was studied in the energy range from 20 to 300 GeV and for incident angles from $\theta = 0^o$ to 45^o. Uniformity was studied with pions of 40 and 80 GeV at $\theta = 10^o$. The calorimeter response to muons was investigated using 225 GeV muons at various incident angles.

The results from this test beam data can be summarized as follows:

• The hadronic energy resolution was compatible with the design goal of $\frac{\sigma}{E} = \frac{50\%}{\sqrt{E}} \oplus 3\%$.

• Linearity between 20 and 300 GeV of the order of a few percent can be achieved with the Tile Calorimeter alone.

• The e/π ratio for the Tile Calorimeter prototype was found to be between 1.1 and 1.2, a relatively small deviation from the ideal compensation.

Recent test beam results related to the hadron response for prototypes and modules zero of the barrel and extended barrel are presented in this Chapter. The energy resolution, linearity and e/π ratio are also given. Up to date, we can categorize the test beam setups as follows:

• 1997 test beam with two Extended Barrel Modules 0.

- 1998 test beam with a full scale barrel sector (Module 0).

Early measurements were performed in the H8 beam line at the SPS at CERN. The beam lines were instrumented in a standard fashion with one threshold Cherenkov counter used for π/e separation for $E \leq 20$ GeV, a pair of delay-line wire chambers for both x and y coordinates, and a set of scintillators to define the trigger beam. The scintillators could define a beam spot of around 2-3 cm, while the chambers allowed the reconstruction of the impact point on the calorimeter face to better than ± 1 mm. Data were taken with muons, pions and electrons between 10 and 400 GeV.

For the needs of the Tile Calorimeter a full simulation package based on the GEANT program [1] has been developed, which describes in full detail the detector prototypes that have been used for the test beam runs. A comparison between the test beam data of the Tile Calorimeter prototype modules and the GCALOR [2] package in the framework of the GEANT program has been done for the 1998 test beam.

This program of test beam data taking has been carried out demonstrating the good performance of the calorimeter, which fulfils the requirements for the ATLAS hadronic barrel calorimetry.

4.1 The 1997 test beam

The extended barrel modules of Tilecal are smaller than the barrel ones, with a front face area of 259×22 cm^2. The sizes of the barrel and extended barrel tiles are the same, but a different fiber configuration allows a different radial segmentation to adapt the modules to the higher η values where they will be located.

Two extended barrel modules 0 were built for the test, one in Barcelona (BCN), Spain, and the other at Argonne (ANL), USA. The cell structure of the modules is shown in figure 4.1, where two different routing of the fibers have been used, resulting in different fibre lengths in the modules. We used two different routing because the USA group insisted to make a different one, where the routing has a more clean path. The fibres used to equip the modules were the Kuraray multi-clad Y11(200)MS, dopped with 600 ppm of UV Absorber. Both modules were equipped with white fibre profiles. The modules have 3 segments in depth, corresponding to 1.37, 2.48 and 3.14 interaction lengths at $\eta = 0$. A semi-projective cell geometry is defined as it will be in ATLAS.

The modules were tested at CERN in October 1997 together with the five 1 meter old modules. In order to improve the transverse leakage for both, the two extended barrel modules were sandwiched between the 1 m prototype modules, as it is shown in figure 4.2. The ANL module was located on the top of the BCN module. The readout of the

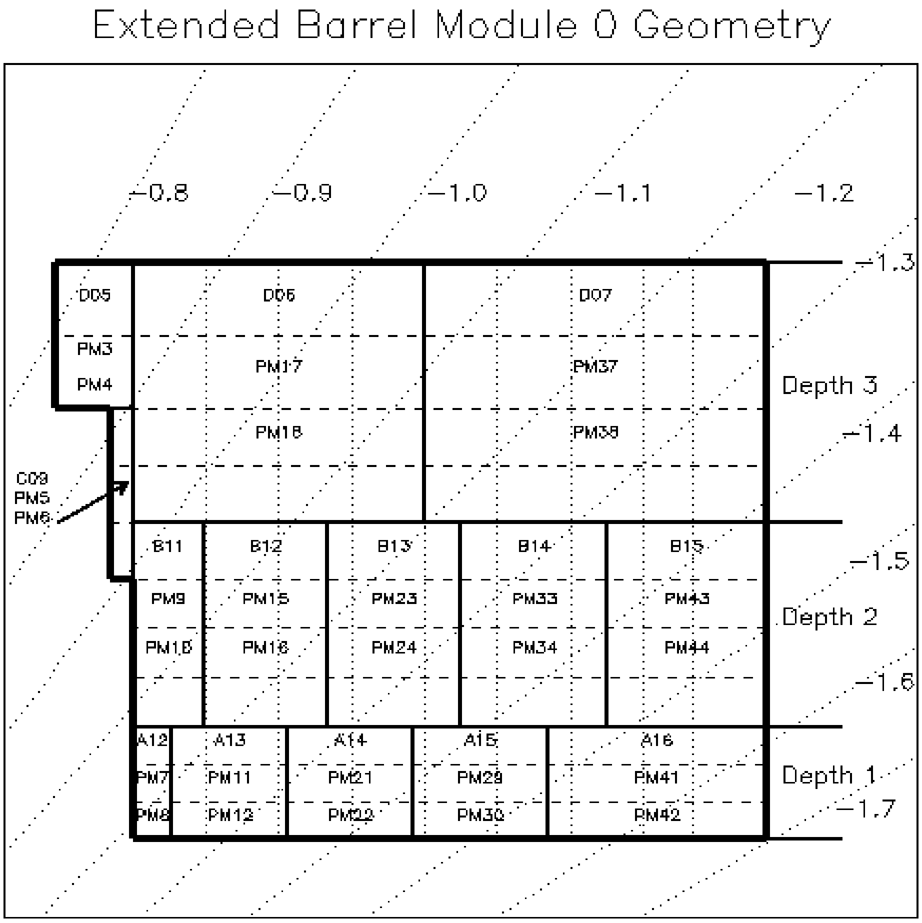

Figure 4.1: Configuration of the Extended Barrel Module 0 built in Barcelona.

ANL module used the Fermi system (1 ADC) [3], while part of the Barcelona module was equipped with a bi-gain 12 bit ADC readout. The photomultipliers (PMT's) were the Hamamatsu 8-stage R5900.

The calorimeter modules were installed on a table that moves horizontally and perpendiculary to the beam line (z direction). They can also be rotated around its vertical axis, allowing to change the θ angle, accesing the towers of different η values. The table can also be rotated around a horizontal axis, allowing to scan in the azimuthal incidence angle (ϕ).

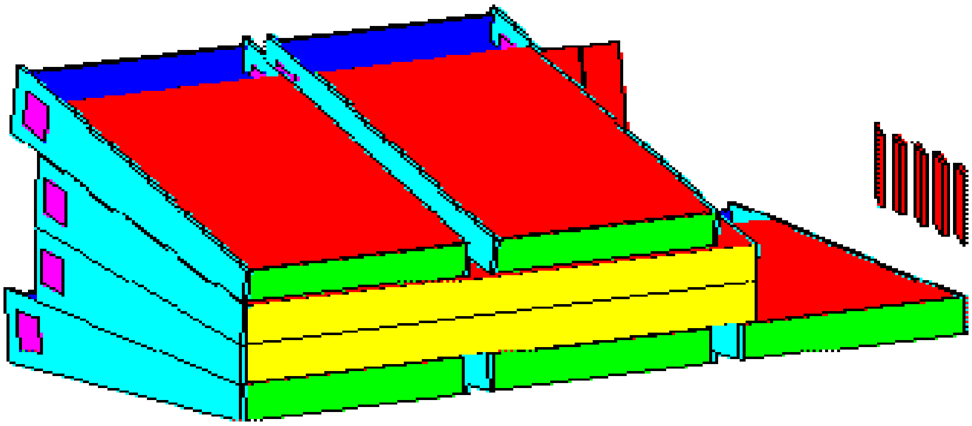

Figure 4.2: Extended barrel modules 0 in the test beam.

Test beam energies (20, 40, 50, 80, 100, 180, 300 and 400 GeV) along different values of η, from $\eta = -0.8$ up to $\eta = -1.4$ have been used in this analysis. On average, about ten thousand events are available for each energy. Cuts were applied on the beam chambers data to eliminate the beam halo and events with simultaneous particles in the scintillator chambers; finally 60% of the events were removed including pedestal events supression. The cut on the beam chamber coordinates remove around 10-20% of the sample data, whilst the scintillator chambers remove 15%. All the applied cuts have been taken from reference [4]. The cuts were applied with the agreement of the colaboration members.

Figures 4.3 and 4.4 show examples of the applied cuts effects.

This test beam experience has revealed the cross-talk effect. The high trasparency

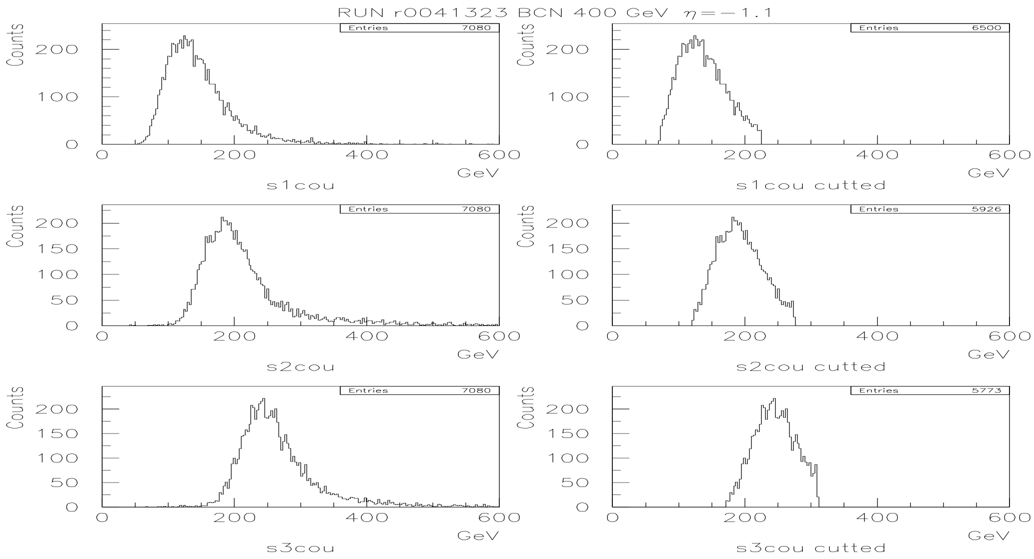

Figure 4.3: *Effects of the cuts in the scintillator chambers.*

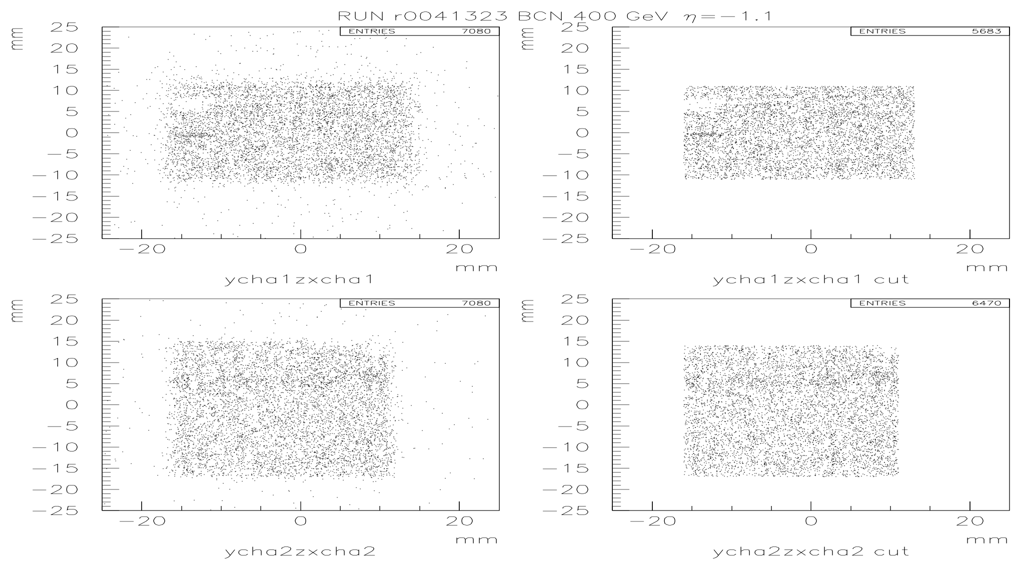

Figure 4.4: *Effects of the cuts in the beam chambers.*

of the plastic profiles used to group the fibres and stick them in the proper grooves, induced that the light produced in a given calorimeter cell from the third or second depth was transported by the same group of fibres to the first or second depth.

Let be E_i, $i = 1, 2, 3$, the energy measured in the i depth and ϵ_i the true energy deposited in the i depth. Because of the cross-talk between the depth 1 and the depths 2 and 3, and of the cross-talk between the depth 2 and 3, we can write:

$$E_1 = \epsilon_1 + x_{21}\epsilon_2 + x_{31}\epsilon_3 \tag{4.1}$$

$$E_2 = \epsilon_2 + x_{32}\epsilon_3$$

$$E_3 = \epsilon_3$$

where x_{ij} is the fraction of the energy measured in the j-th depth, due to a particle passing through the i-th depth.

In terms of measured energy:

$$\epsilon_1 = E_1 - x_{21}(E_2 - x_{32}E_3) - x_{31}E_3 \tag{4.2}$$

$$\epsilon_2 = E_2 - x_{32}E_3$$

$$\epsilon_3 = E_3$$

The total energy E_{total} can be written as:

$$E_{tot} = \epsilon_1 + \epsilon_2 + \epsilon_3 = E_1 + (1 - x_{21})E_2 + (1 - x_{31} - x_{32} + x_{21}x_{32})E_3 \tag{4.3}$$

the values of x_{ij} are between 0.2/0.3 as calculated from the muon and electron data, and the Cs calibration analysis [5]. We can then write:

$$E_{tot} = E_1 + \alpha E_2 + \beta E_3 \tag{4.4}$$

where the α and β coefficients are:

$$\alpha \cong 0.75, \quad \beta \cong 0.6 \tag{4.5}$$

4.2 Analysis of the 1997 pion data for the Extended Barrel Modules 0

The different energy values of the pion data taken with the setup described in the last section were reconstructed with two algorithms which are explained in detail in reference [6]. In this Section, we will briefly describe the two algorithms and will present a new method to reconstruct the pion energy; we will compare our strategy and results with previous approaches.

Before going into the energy reconstruction of the pion data, we will briefly discuss a crucial phenomenon for the understanding of the different techniques that will be explained. This concept is the so-called *non-compensation* (see chapter 3) in hadron calorimetry and is the main physical motivation for the algorithms applied in the reconstruction of the extended barrels and barrel pion data.

A high energy hadron which enters a calorimeter interacts inelastically with the nuclei of the calorimeter and develops a shower of particles that can be grouped as follows:

• High-energy secondaries, such as π^+, π^-, $\pi^0 \to \gamma\gamma$, p, n,... Note that the hadronically produced π^0's will immediately decay into $\gamma\gamma$ and develop an electromagnetic shower.

• Low-energy fragments emitted from the excited target nucleus, such as photons with energy in the range $\sim$ 1 - 10 MeV, neutrons and protons (*boil off* particles) with energy between $\sim$ 1 and 10 MeV. The binding energy to boil off these nucleons is *robbed* from the energy of the cascade and in most cases will not contribute to a measurable (*visible*) energy.

The picture of the hadronic cascade suggests to qualitatively distinguish between an electromagnetic component (mostly due to the π^0 production) and a purely hadronic component, which will invert a considerable fraction ($\sim$ 15-20% at 10 GeV incident energy) of its energy to overcome the binding energy of nucleons.

In order to study the performance of the calorimeters (see Section 3.4), it is very useful to compare the visible energy released by electrons with the signal released by pions of equal incident energy; this ratio is usually named e/π in calorimetry and allows us to introduce the concept of non-compensation: $e/\pi \neq 1$.

In most sampling calorimeters $e/\pi > 1$; this is mostly caused by the energy loss to overcome the binding energy of the excited nucleus in the hadronic shower development; the low-energy products produced in the boiling-off of nucleus will in general be registered very differently at the read-out level compared with the energetic cascade component.

Nevertheless, it is possible to achieve compensation. Two different strategies have been adopted, which may result in $e/\pi \cong 1$:

• designing an intrisically compensated calorimeter (U, Pb, etc.).

• achieving compensation in off-line analysis using different weights for the electromagnetic and hadronic components of the shower.

The previous approaches applied to the extended barrel data and our new approach use just the latter method in trying to achieve compensation. We will further see the characteristics of the different techniques and the results obtained in resolution and linearity.

In the next section we study in three steps the evolution of the linearity and resolution parameters in the data reconstruction, from raw data to H1 weighting method going through the benchmark method. The e/h ratio is determined from these data using the response obtained for electrons and pions.

4.2.1 Raw data

The first step in the linearity and resolution study was the direct analysis of the raw data. The three components of the total raw energy are the energy detected in the BCN, ANL and in the five 1 m modules. The energy in BCN and ANL modules has been corrected for the cross-talk problem [4], and the conversion factors from pC to GeV were calculated to be 1.26 GeV/pC for extended barrels (this electromagnetic scale is determined using electron data) and 0.1613 GeV/pC for old modules (it was determined several times in the past using electron runs of the test beam prototype modules). So finally:

$$E_{Raw} = E^{corr}_{ANL} + E^{corr}_{BCN} + E_{old} \tag{4.6}$$

According to this expresion we present the results of the mean reconstructed energy (μ), σ and resolution (σ/μ) in table 4.1. Also the plots of linearity, defined as E/E_{beam} and energy resolution can be seen in figures 4.5 and 4.6.

The linearity presents the typical shape of a non-compensated calorimeter, the slope is due to the increase of the electromagnetic component in the shower produced by a pion. The *rms* is around 4.3% for both modules and both values of η, which is one of the characteristics to improve.

Table 4.1: *Nominal energy, mean reconstructed energy, σ and resolution at various beam energies at two different η for BCN and ANL modules obtained from raw data.*

BCN	η=-1.1		
Beam Energy (GeV)	μ (GeV)	σ (GeV)	σ/μ(%)
20	16.55±0.04	2.03±0.03	12.2±0.2
40	34.17±0.10	3.30±0.08	9.6±0.2
50	42.25±0.10	3.37±0.09	7.97±0.21
80	69.01±0.11	5.32±0.09	7.71±0.13
100	86.24±0.12	5.94±0.10	6.89±0.12
180	160.6±0.3	9.16±0.23	5.71±0.14
300	275.5±0.3	16.8±0.3	6.09±0.10
400	373.8±0.4	23.5±0.4	6.28±0.11
ANL	η=-1.1		
Beam Energy (GeV)	μ (GeV)	σ (GeV)	σ/μ(%)
20	15.80±0.04	2.06±0.03	13.0±0.2
40	33.19±0.09	3.17±0.08	9.56±0.23
50	42.09±0.11	3.61±0.09	8.57±0.21
80	68.22±0.11	5.18±0.10	7.59±0.14
100	85.47±0.12	6.1±0.1	7.09±0.12
180	158.7±0.2	9.9±0.2	6.25±0.11
300	268.4±0.3	15.4±0.3	5.74±0.10
400	364.7±0.4	22.2±0.4	6.07±0.11
BCN	η=-1.2		
Beam Energy (GeV)	μ (GeV)	σ (GeV)	σ/μ(%)
20	16.11±0.05	2.23±0.02	13.9±0.2
40	33.72±0.08	3.30±0.08	9.8±0.2
50	44.74±0.13	4.09±0.08	9.15±0.21
80	72.20±0.13	5.90±0.09	8.17±0.15
100	90.98±0.15	6.98±0.11	7.67±0.12
180	168.5±0.3	11.7±0.2	6.94±0.11
300	282.3±0.4	19.6±0.3	6.95±0.10
400	380.0±0.5	24.9±0.3	6.55±0.10
ANL	η=-1.2		
Beam Energy (GeV)	μ (GeV)	σ (GeV)	σ/μ(%)
20	16.58±0.04	1.98±0.02	11.9±0.2
40	34.00±0.09	3.29±0.08	9.7±0.2
50	42.4±0.1	3.33±0.08	7.9±0.2
80	69.2±0.1	4.75±0.08	6.87±0.15
100	86.3±0.1	5.38±0.10	6.24±0.11
180	160.6±0.2	8.7±0.2	5.44±0.11
300	276.5±0.3	15.3±0.3	5.54±0.10
400	373.8±0.4	23.5±0.4	6.28±0.10

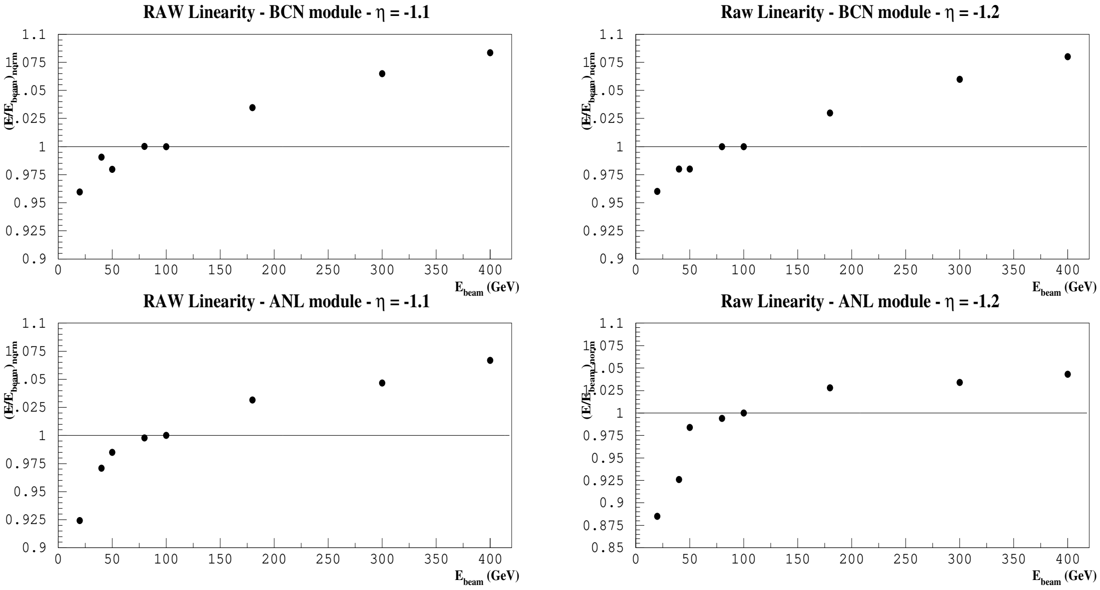

Figure 4.5: *Lineatiry of raw data. Left: for η=-1.1 BCN (top) and ANL (bottom) modules. Right: for η=-1.2 BCN and ANL respectivily.*

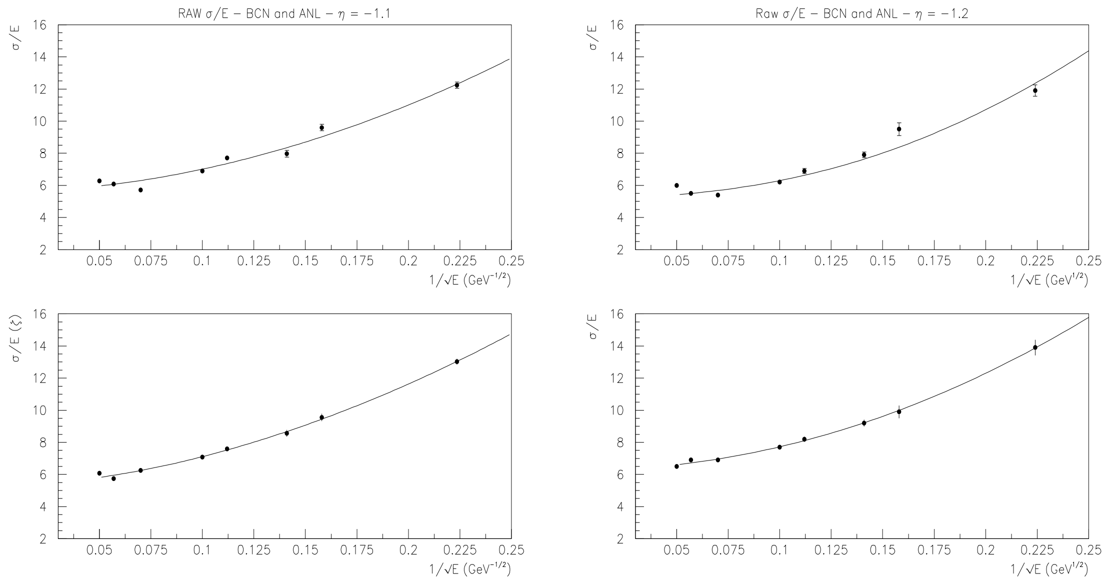

Figure 4.6: *Energy resolution of raw data. Left: for η=-1.1 BCN (top) and ANL (bottom) modules. Right: for η=-1.2 BCN and ANL respectively.*

A fit of the data is performed in the way:

$$\frac{\sigma}{E} = \frac{\mathbf{a}\%}{\sqrt{E}} \oplus \mathbf{b}\% \oplus \frac{\mathbf{c}}{E} \tag{4.7}$$

where **a** represents the statistical fluctuations in the shower development, **b** is the constant term dominant at high energies and **c** is the noise term. E is given in GeV and the $\oplus$ symbol indicates sum in quadrature.

The fit results for BCN and ANL modules at η = -1.1 and -1.2 are presented in the table 4.2.

Table 4.2: *Statistical (a), constant (b), and noise (c) terms at two different η for the BCN and ANL modules obtained from raw data.*

η	BCN			ANL		
	a (%)	b (%)	c	a (%)	b (%)	c
-1.1	40.88	5.61	1.26	45.01	5.35	1.27
-1.2	31.10	5.17	1.74	43.30	6.24	1.56

The **c** parameter in the expresison 4.7 takes into account the different noise contributions in the detector. It can be measured independently of the resolution studies and has been estimated from noise *rms* which mean value is around 0.06 GeV (figure 4.12) [8].

If we fit this expresison with the three parameters free, then the **c** parameter can take no representative values, it is due to the characteristics of the experimental data. These values affect directly to the **a** values as it can be seen in figure 4.7, impeding to compare the **a** parameters obtained from different methods.

In figure 4.7 is shown the strong relation between the two parameters **a** and **c** when we do the fit of the typical resolution expression.

In this analysis all the resolution fits have been done fixing $\mathbf{c}$ = 0.06 GeV (according to the mean in figure 4.12) and fitting with **a** and **b** free in order to obtain less aleatory results in the **a** value and to compare with other fits. In figure 4.7 it can be seen that at $\mathbf{c}$ = 0.06 GeV the **a** value reach a *plateau*.

The figure 4.8 shows the same data but fitted with this new consideration.

The results taking into account this idea are presented in the table 4.3. About the resolution, we can conclude that in general the requirement is reached. Moreover it can be seen that BCN module has better resolution than ANL.

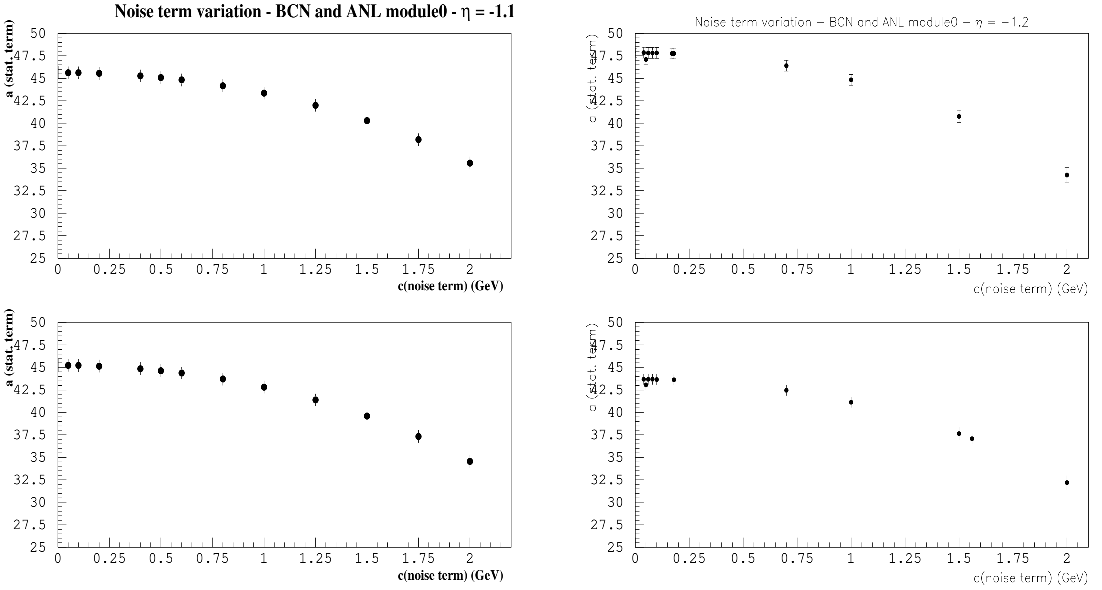

Figure 4.7: *Variation of parameter* **a** *as a function of* **c**.

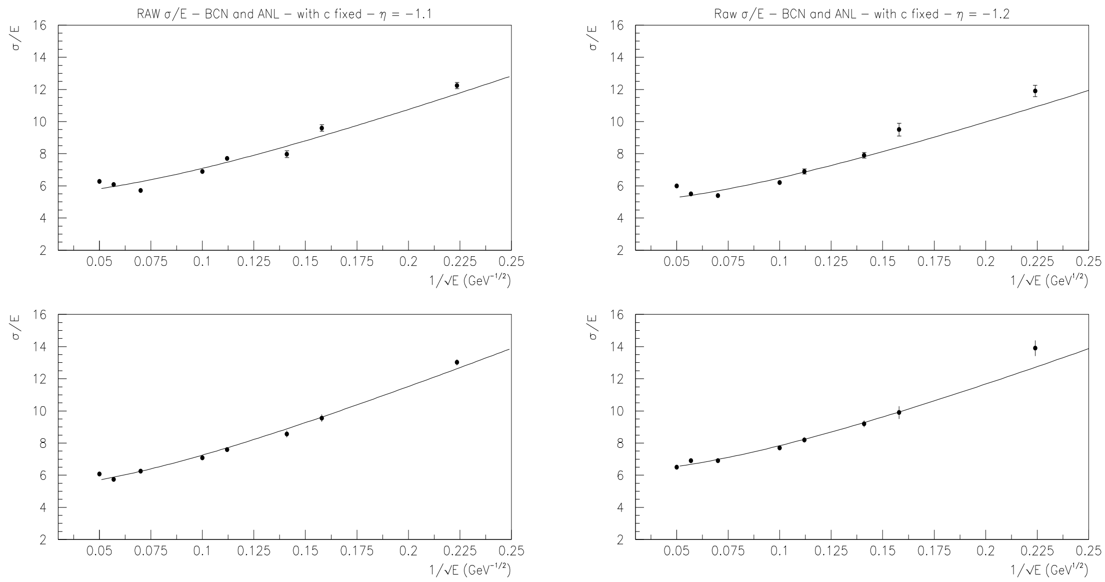

Figure 4.8: *Energy resolution of raw data with parameter* **c** *fixed at 0.06 GeV. Left: for η=-1.1 BCN (top) and ANL (botton) modules. Right: for η=-1.2 BCN and ANL respectively.*

Table 4.3: *Statistical (a), constant (b), and noise (c) terms at two different η for the BCN and ANL modules obtained from raw data fixing the* **c** *parameter.*

η	BCN			ANL		
	a (%)	b (%)	c	a (%)	b (%)	c
-1.1	46.70	5.34	0.06	51.71	5.09	0.06
-1.2	43.71	4.80	0.06	49.90	6.04	0.06

4.2.2 A Benchmark approach

In the *benchmark* algorithm, a one step procedure is adopted to reconstruct the nominal beam energy: the energy of the particle is obtained as the sum of several terms, and the involved parameters are optimized by minimizing the fractional energy resolution σ/E.

This method tries to correct the effect of the lateral and longitudinal leakage in the prototype [4].

The used algorithm is:

$$E_{TOT} = X[E_{tot}^{ANL} + E_{tot}^{BCN} + (A-1)(E_{S3}^{ANL} + E_{S3}^{BCN})] + BE_{old} \tag{4.8}$$

where E_{tot}^{ANL}, E_{tot}^{BCN} are the energy values corrected by cross-talk (in pC) detected in the ANL and BCN modules, and E_{S3}^{ANL}, E_{S3}^{BCN} are the energies detected in sample three of ANL and BCN modules. Finally E_{old} is the energy detected in the five 1 meter modules.

X =1.26 GeV/pC is the conversion factor from pC to GeV for the extended barrel.

(*A-1*) is the parameter that corrects the energy losses due to the longitudinal leakage of the shower. It is calculated looking at the dependence of the total energy with the energy deposited in sample three. It is logic to assume that the longitudinal leakage is proportional to the energy deposited in the last sample.

Finally, B takes into account the transversal leakage of the shower. The transversal losses are proportional to the energy deposited in the old modules due to the set up of the experiment. To obtain this parameter, the total energy is plotted as a function of the energy in the old modules. Moreover in this factor we included the conversion factor 0.1613 GeV/pC for the 1 meter modules. An example of this representation is shown in figure 4.9.

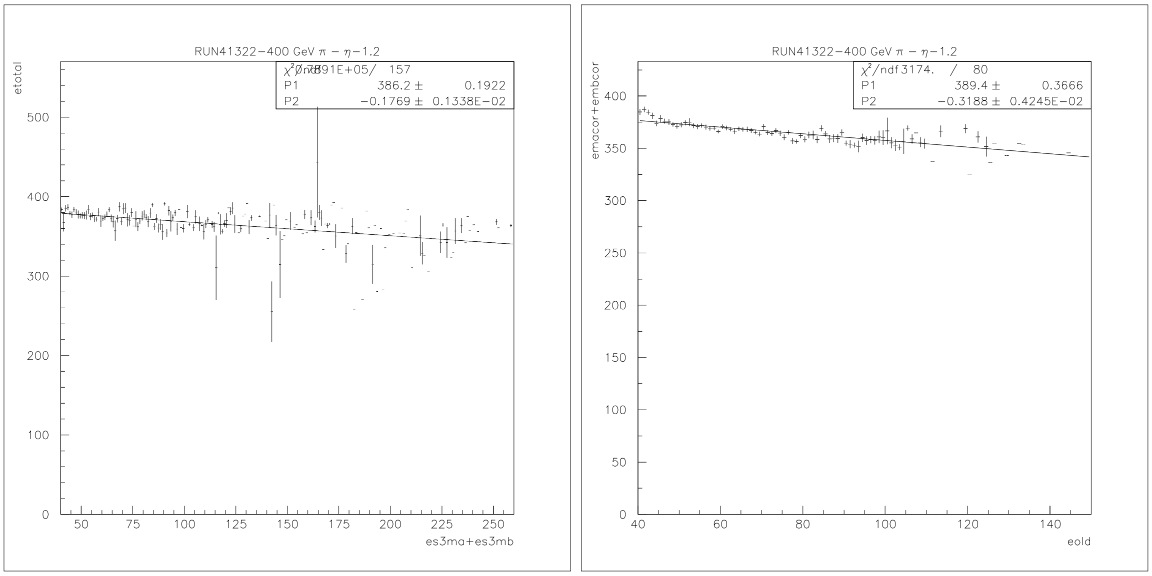

Figure 4.9: *Left: Total energy as a function of the deposited energy in the last samples. Right: Total energy as a function of the energy deposited in the old modules.*

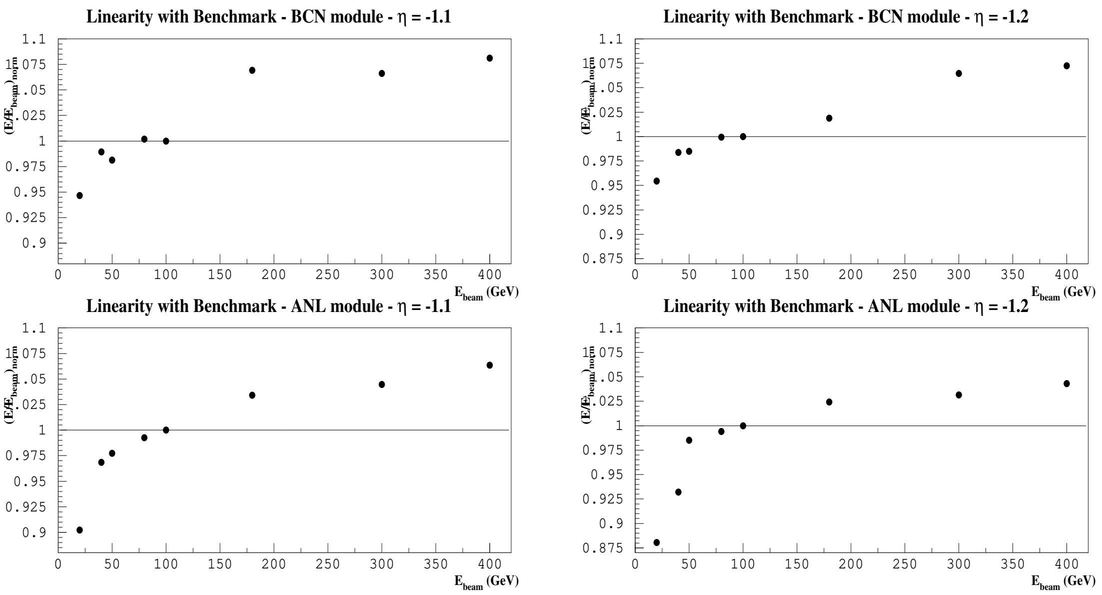

Figure 4.10: *Linearity plots obtained with the benchmark method. Left: for η=-1.1 BCN (top) and ANL (bottom) modules. Right: for η=-1.2, BCN and ANL modules, respectively.*

Table 4.4: *Nominal energy, mean reconstructed energy, σ and resolution at various beam energies and two different η for BCN and ANL modules obtained from benchmark method.*

BCN	η=-1.1		
Beam Energy (GeV)	μ (GeV)	σ (GeV)	σ/μ(%)
20	17.69±0.05	2.40±0.05	13.6±0.3
40	36.97±0.08	3.54±0.06	9.58±0.22
50	45.84±0.10	3.70±0.09	8.07±0.21
80	74.88±0.12	5.52±0.09	7.37±0.15
100	93.42±0.11	6.22±0.11	6.66±0.14
180	179.80±0.16	10.3±0.2	5.74±0.11
300	298.8±0.2	15.5±0.3	5.18±0.10
400	404.0±0.2	19.8±0.4	4.9±0.1
ANL	η=-1.1		
Beam Energy (GeV)	μ (GeV)	σ (GeV)	σ/μ(%)
20	16.73±0.05	2.5±0.03	15.0±0.3
40	35.92±0.04	3.5±0.07	10.0±0.3
50	45.31±0.12	3.9±0.09	8.7±0.3
80	73.62±0.12	5.7±0.10	7.7±0.2
100	92.72±0.13	6.3±0.11	6.79±0.15
180	172.6±0.3	10.3±0.2	5.99±0.15
300	290.6±0.3	17.6±0.3	6.07±0.11
400	394.4±0.4	18.1±0.4	4.60±0.15
BCN	η=-1.2		
Beam Energy (GeV)	μ (GeV)	σ (GeV)	σ/μ(%)
20	17.26±0.05	2.37±0.05	13.8±0.3
40	35.57±0.09	3.46±0.11	9.7±0.3
50	44.52±0.11	3.47±0.10	7.8±0.2
80	72.27±0.09	4.71±0.07	6.52±0.10
100	90.40±0.11	5.21±0.09	5.76±0.10
180	167.4±0.2	7.65±0.17	4.57±0.10
300	288.7±0.2	12.44±0.17	4.31±0.06
400	387.8±0.2	15.90±0.23	4.10±0.06
ANL	η=-1.2		
Energy	μ (GeV)	σ (GeV)	σ/μ(%)
20	16.68±0.05	2.53±0.05	15.2±0.3
40	35.32±0.05	3.52±0.07	9.96±0.19
50	46.65±0.12	4.05±0.10	8.7±0.2
80	75.34±0.12	5.63±0.09	7.48±0.12
100	94.72±0.13	6.60±0.10	6.97±0.12
180	174.6±0.3	9.6±0.3	5.48±0.16
300	293.1±0.3	16.7±0.3	5.7±0.1
400	345.2±0.4	19.3±0.3	5.6±0.1

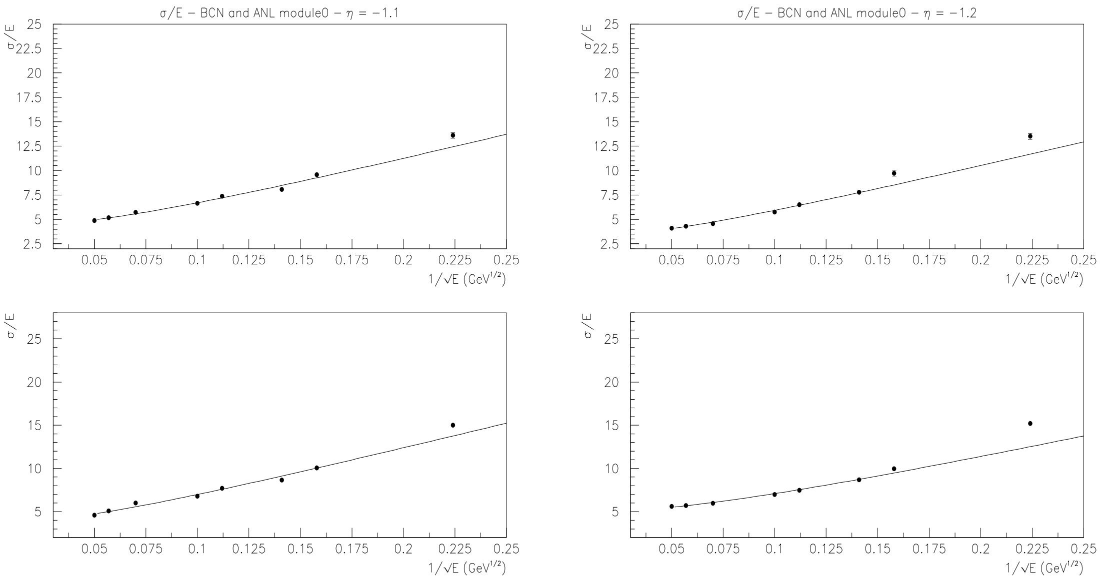

Figure 4.11: *Energy resolution plots obtained with the benchmark method. Left: for η = -1.1 BCN (top) and ANL (bottom) modules. Right: for η=-1.2, BCN and ANL modules, respectively. The* **c** *parameter has been fixed.*

In table 4.4 are shown the results obtained with the present method.

A similar behaviour as for direct raw data is obtained for linearity (figure 4.10). The *rms* changes from 4.3% to 4.5% in this analysis. This is logic if we consider that the benchmarck method does not correct the non-compensation of the detector. A short improvement can be seen in the linearity of points at high energies.

The fit results (figure 4.11) for BCN and ANL modules at η = -1.1 and -1.2 are presented in the table 4.5. There is a clear improvement in **b**, the dominant parameter at high energies, where the Benchmark method corrects the leakage.

Table 4.5: *Statistical (a), constant (b), and noise (c) terms at two different η for the BCN and ANL modules obtained from the Bechmark method.*

η	BCN			ANL		
	a (%)	b (%)	c	a (%)	b (%)	c
-1.1	50.10	3.10	0.06	51.50	4.87	0.06
-1.2	52.21	4.21	0.06	59.10	3.71	0.06

Applying the cell-by-cell cross-talk correction and the benchmark techniques to correct for the longitudinal and lateral behaviour of the hadronic shower, we have obtained an improvement in σ/E. The next step is the application of a weighting technique that could improve the poor linearity results obtained so far.

4.2.3 A new energy reconstruction of the pion energy (H1 method)

As it has been pointed out, the previous results were not quite satisfactory: after applying a benchmark technique an improvement in the **b** parameter of the resolution was obtained but the linearity is still quite poor.

We then decided to try an independent approach inspired in the H1 collaboration [9]. The correction strategy chosen in previous calorimeter studies [7] was to adjust *downwards* the response of read-out cells with a large signal to compensate for the response to large EM energy clusters, typically due to π^0 production. This method is based in correcting *upwards* the energy of the cells instead of *downwards* as the weighting techniqued applied to TILECAL standalone [10].

As a preliminary step, the signal in every calorimeter cell (ANL, BCN and five 1 meter modules) is expressed in GeV, using the signal-to-energy conversion constant obtained from electron runs [4].

The energy in each cell, E_{cell}, is corrected multiplying its value by a parameter a_i [9] which depends on the energy of the cell:

$$E_{Cell}^{Cor} = a_i \times E_{Cell} \tag{4.9}$$

As a first step, a simple minimization technique [11] is used to obtain a set of n correction parameters a_i (i = 1.,,,.n) for each beam energy. As second step the a_i are expressed as a function of the cell and beam energies.

In this analysis a noise cut has been applied to the energy of the cells; this helps in parametrizing the a_i because of their unstable behaviour in the noise region. The cut applied is the following:

$$|E_{cells}| > 0.056\ GeV/Cell \tag{4.10}$$

The reason for making a symmetric cut is that the electronic noise with its "zero suppression" appears as symmetric around zero. This sign-symmetric noise cut [12] has the advantage of statistically cancelling the noise signals beyond the cut; the bias introduced on the signal, inevitable with any cut, will in general be smaller than with an asymmetric cut.

The cut value was chosen from the plot shown in figure 4.12; the criteria are the *RMS* of the pedestal noise in the two modules.

4.2.3.1 Obtaining sets of a_i at each energy

For each beam energy the cell energy spectrum is divided into n intervals and a correction paramater a_i is calculated for each interval.

To obtain stable results it is useful to have about the same number of entries per interval. Also, in view of the subsequent a_i parametrization it is useful to develop a simple interval definition algorithm that can be applied at all beam energies.

The algorithm is based on selecting equal area intervals on an exponential cell energy distribution, as schematically is shown in figure 4.13, for the 20 GeV data.

The limits of the intervals are defined from the 20 GeV data and are unchanged at all other beam energies; hence the number of intervals is invariant, but the mean value of the cell energy in each interval changes somewhat with the energy.

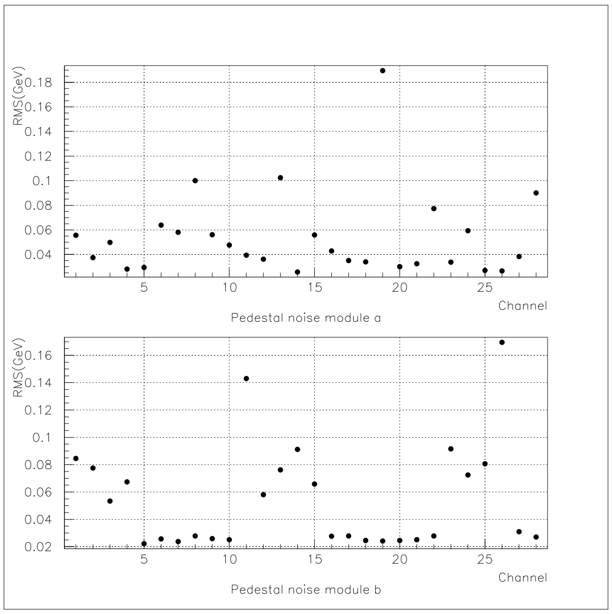

Figure 4.12: *RMS study of the pedestal noise for the ANL module (top) using only compressors and for the BCN module using compressors and bigain (bottom) [8].*

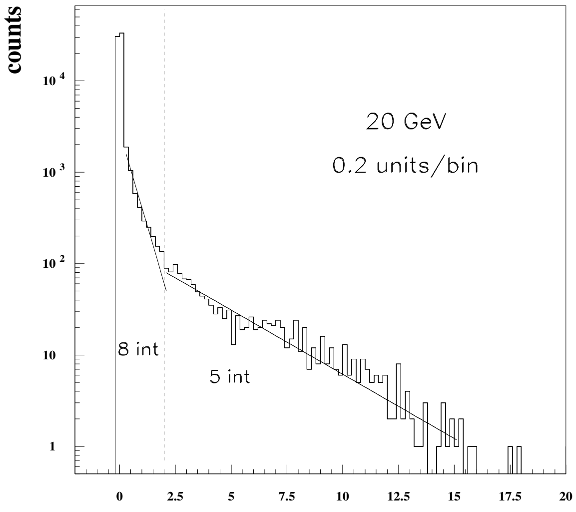

Figure 4.13: *Cell energy spectrum of the Tile calorimeter for 20 GeV pions. Two region are shown with the corresponding number of chosen intervals in each zone.*

A total of 13 intervals were defined at first. Two sets of parameters are calculated for the ANL and BCN module, respectively.

The a_i are obtained from de data at each energy, writing the corrected energy of the k event as

$$E_{cor}^K = a_1 \; E_1^K + ... + a_n \; E_n^K + B \; E_{old} \tag{4.11}$$

In this expression:

- E_i^K is the energy sum of all the cells within i interval, i.e.

$$E_i^K = \sum_{cells \in i} E_{Cell} \tag{4.12}$$

- E_{old} is the energy released in the old modules.

The set of correction parameters a_i is determined from the data by minimizing the expression

$$N \; \sigma^2 = \sum_{K=1,N} (E_{cor}^K - E_{Beam})^2 + \lambda \sum_{K=1,N} (E_{cor}^K - E_{Beam}) \tag{4.13}$$

in which the constraint that the mean reconstructed energy has to reproduce the nominal beam energy is introduced by means of a Lagrange multiplier.

The corrected total energy spectra were fitted with Gaussian distributions over a $\pm 2\sigma$ range. From the mean values of the fits we obtain plots of the deviation from a linear response. Such *linearity plots*, are shown in figure 4.14, left η=-1.1 and right -1.2, respectively. The improvement when including the *energy conservation* constraint is very clear; with this constraint, the *rms* deviation from linearity is 0.34% and 0.12% for ANL module at η=-1.1 and -1.2, respectively. For BCN module the *rms* is 0.4% for both η values.

The energy resolution (σ/E *vs.* the beam energy) is given in figure 4.15. The resolution obtained here can be parametrized for the BCN and ANL modules as shows the table 4.6.

The results of the fits to the reconstructed pion energies are given in table 4.7.

Before moving we can remark some observations:

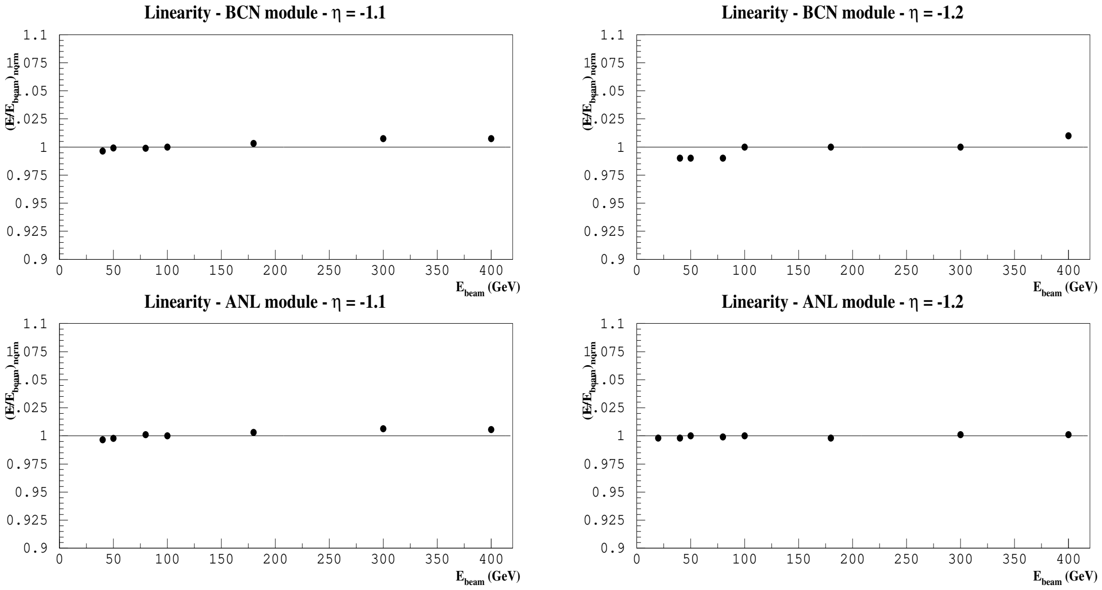

Figure 4.14: *Linearity plot minimizing the functional with the Lagrange multiplier. Left: η=-1.1, (top) BCN module and (bottom) ANL module. Right: η=-1.2, (top) BCN module and (bottom) ANL module. The points are obtained normalizing the mean reconstructed energy values from the Gaussian fits to the value of 100 GeV.*

Table 4.6: *Statistical (a), constant (b), and noise (c) terms at two different η for the BCN and ANL modules obtained with the constraint to the beam energy.*

η	BCN			ANL		
	a (%)	b (%)	c	a (%)	b (%)	c
-1.1	36.90	3.90	0.06	40.50	3.90	0.06
-1.2	40.51	3.21	0.06	36.30	4.91	0.06

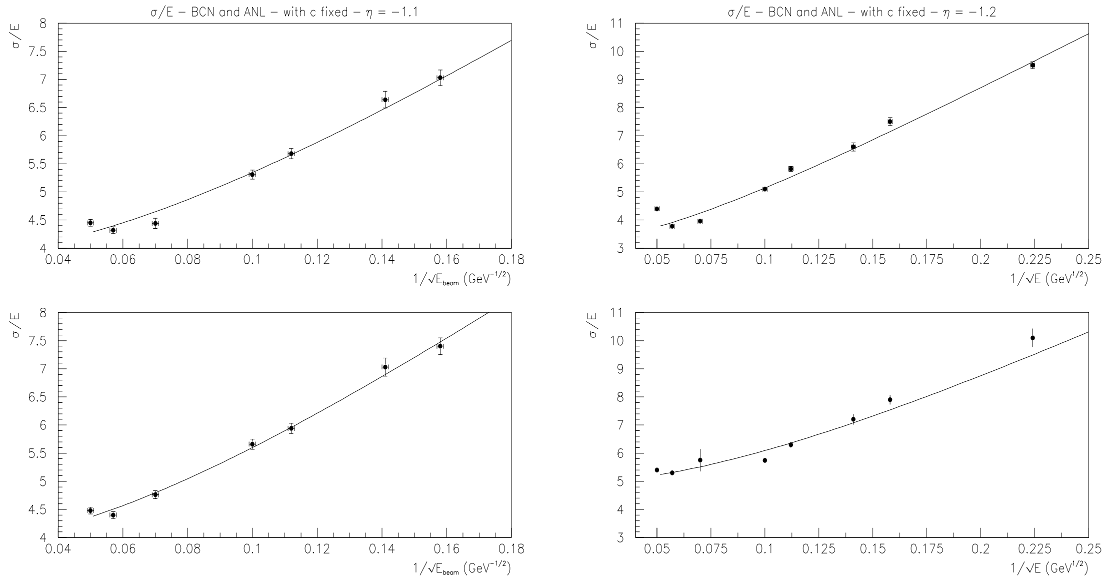

Figure 4.15: *Resolution plot minimizing the functional with the Lagrange multiplier. Left: η =-1.1, (top) BCN module and (bottom) ANL module. Right: η =-1.2, (top) BCN module and (bottom) ANL module.*

Table 4.7: *Nominal energy, mean reconstructed energy, σ and resolution at various beam energies at two different η for BCN and ANL modules obtained with the constraint to the beam energy.*

BCN	η=-1.1		
Beam energy (GeV)	μ (GeV)	σ (GeV)	σ/μ(%)
40	39.98 $\pm$ 0.07	2.81 $\pm$ 0.06	7.03 $\pm$ 0.14
50	50.11 $\pm$ 0.10	3.33 $\pm$ 0.07	6.64 $\pm$ 0.15
80	80.14 $\pm$ 0.09	4.55 $\pm$ 0.07	5.68 $\pm$ 0.09
100	100.3 $\pm$ 0.11	5.32 $\pm$ 0.08	5.31 $\pm$ 0.08
180	179.6 $\pm$ 0.64	7.13 $\pm$ 0.72	4.44 $\pm$ 0.09
300	303.2 $\pm$ 0.22	13.09 $\pm$ 0.20	4.32 $\pm$ 0.06
400	404.2 $\pm$ 0.23	15.00$\pm$ 0.25	4.45 $\pm$ 0.06
ANL	η=-1.1		
Beam energy (GeV)	μ (GeV)	σ (GeV)	σ/μ(%)
40	39.98 $\pm$ 0.07	2.96 $\pm$ 0.06	7.40 $\pm$ 0.15
50	50.04 $\pm$ 0.11	3.52 $\pm$ 0.08	7.03 $\pm$ 0.16
80	80.34 $\pm$ 0.10	4.77 $\pm$ 0.07	5.94 $\pm$ 0.09
100	100.30 $\pm$0.11	5.68 $\pm$ 0.09	5.66 $\pm$ 0.09
180	182.1 $\pm$ 0.10	10.21 $\pm$ 0.09	4.76 $\pm$ 0.07
300	302.8 $\pm$ 0.22	13.31 $\pm$ 0.20	4.40 $\pm$ 0.06
400	403.5 $\pm$ 0.23	15.05 $\pm$ 0.25	4.48 $\pm$ 0.06
BCN	η=-1.2		
Beam energy (GeV)	μ (GeV)	σ (GeV)	σ/μ(%)
20	19.95 $\pm$ 0.06	2.01 $\pm$ 0.06	9.5 $\pm$ 0.1
40	39.95 $\pm$ 0.07	3.01 $\pm$ 0.06	7.5 $\pm$ 0.1
50	49.93 $\pm$ 0.09	3.29 $\pm$ 0.08	6.6 $\pm$ 0.2
80	79.99 $\pm$ 0.09	4.65 $\pm$ 0.08	5.82 $\pm$ 0.09
100	100.1 $\pm$ 0.09	5.11 $\pm$ 0.08	5.1 $\pm$ 0.1
180	180.3 $\pm$ 0.15	7.15 $\pm$ 0.12	3.96 $\pm$ 0.06
300	300.5 $\pm$ 0.13	11.36 $\pm$ 0.10	3.78 $\pm$ 0.04
400	404.2 $\pm$ 0.23	18.01 $\pm$ 0.21	4.4 $\pm$ 0.06
ANL	η=-1.2		
Beam energy (GeV)	μ (GeV)	σ (GeV)	σ/μ(%)
20	19.97 $\pm$ 0.06	2.02 $\pm$ 0.05	10.1 $\pm$ 0.3
40	39.92 $\pm$ 0.08	3.15 $\pm$ 0.07	7.9 $\pm$ 0.2
50	50.01 $\pm$ 0.11	5.04 $\pm$ 0.09	7.2 $\pm$ 0.2
80	79.98 $\pm$ 0.10	5.74 $\pm$ 0.09	6.3 $\pm$ 0.1
100	100.00 $\pm$ 0.11	10.33$\pm$ 0.09	5.74 $\pm$ 0.09
180	179.70 $\pm$ 0.87	3.59 $\pm$ 0.38	5.75 $\pm$ 0.11
300	300.50 $\pm$ 0.26	15.90 $\pm$ 0.24	5.30 $\pm$ 0.06
400	400.30 $\pm$ 0.34	21.65 $\pm$ 0.32	5.40 $\pm$ 0.07

• The improvement in resolution and linearity with respect to other weighting techniques is not surprising. The two terms of eq. 4.13 and the large number of parameters practically guarantee this result.

However, the good news is that the a_i vary smoothly with cell energy, and do not vary too much with E_{beam}. This simplifies the parametrizations which are described further in this work.

• The individual cell energies can be corrected using this method with a variety of similar algorithms: for instance, the a_i parameters can be defined by a distribution of volume energy density E_{cell}/V_{cell}. This latter approach was found to give significantly worse resolutions. Other approaches (such as normalizing the cell energies to the total energy) were tried; the choice of correcting the cell energies as a function only of the cell energy gives the best results and was chosen for this analysis.

4.2.3.2 Parametrizing the a_i

A total of 112 parameters are used to reconstruct the pion energy in the Tile Calorimenter: (13 + 1) at each of the 8 beam energies. To reduce the number of parameters we proceed as follows:

• The a_i are parametrized as a function of the cell energy in the way: $y = p_1 + p_2/E_{cell}$ (with different values p_1, p_2 for the BCN and ANL modules). The results are shown in figures 4.16, 4.17, 4.18 and 4.19 for various beam energies at η=-1.1 and -1.2, respectively.

The errors on the a_i shown in the figures are the *rms* values of ten independent sets of a_i obtained by classifing the data in 10 independent subsamples at each energy and solving the minimization equations for each set.

The corrected energy of the K event is expressed as:

$$E^K_{cor} = \sum_{cells}(p_1 + \frac{p_2}{E_{cell}})E^K_{cell} + BE_{old} \tag{4.14}$$

• Next, the parameters p_1, p_2 and B (the old modules parameter) are expressed as a function of the beam energy using two parameter dependence for p_1 and B (i.e., $p'_1 + p'_2 \times E_{beam}$) and three parameter for p_2 (i.e., $p'_1 + p'_2 \times E_{beam} + p'_3 \times E^2_{beam}$). This is shown in figures 4.20, 4.21 and 4.22; for ANL and BCN modules at η=-1.1 and -1.2.

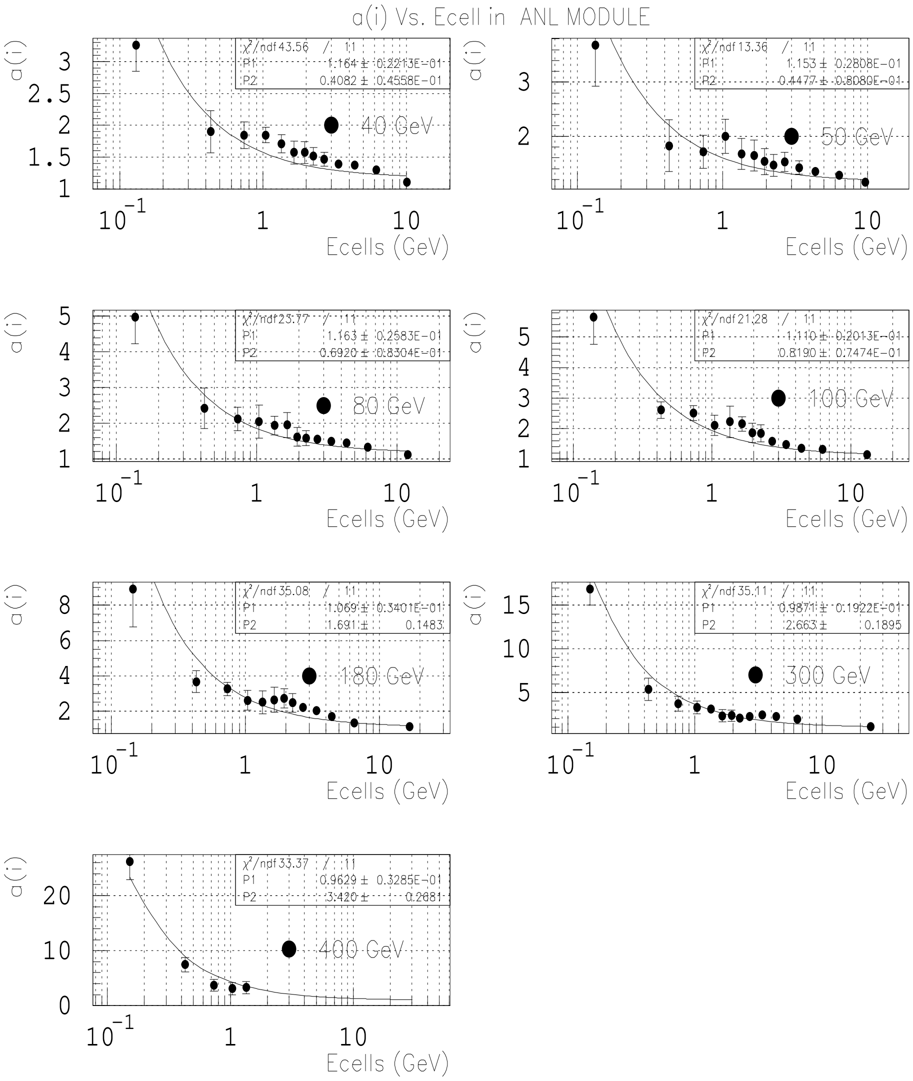

Figure 4.16: *Fits for the a_i parameters (ANL module) at various beam energies and η=-1.1. The parameters p_1 and p_2 obtained for ANL are also shown on the plots.*

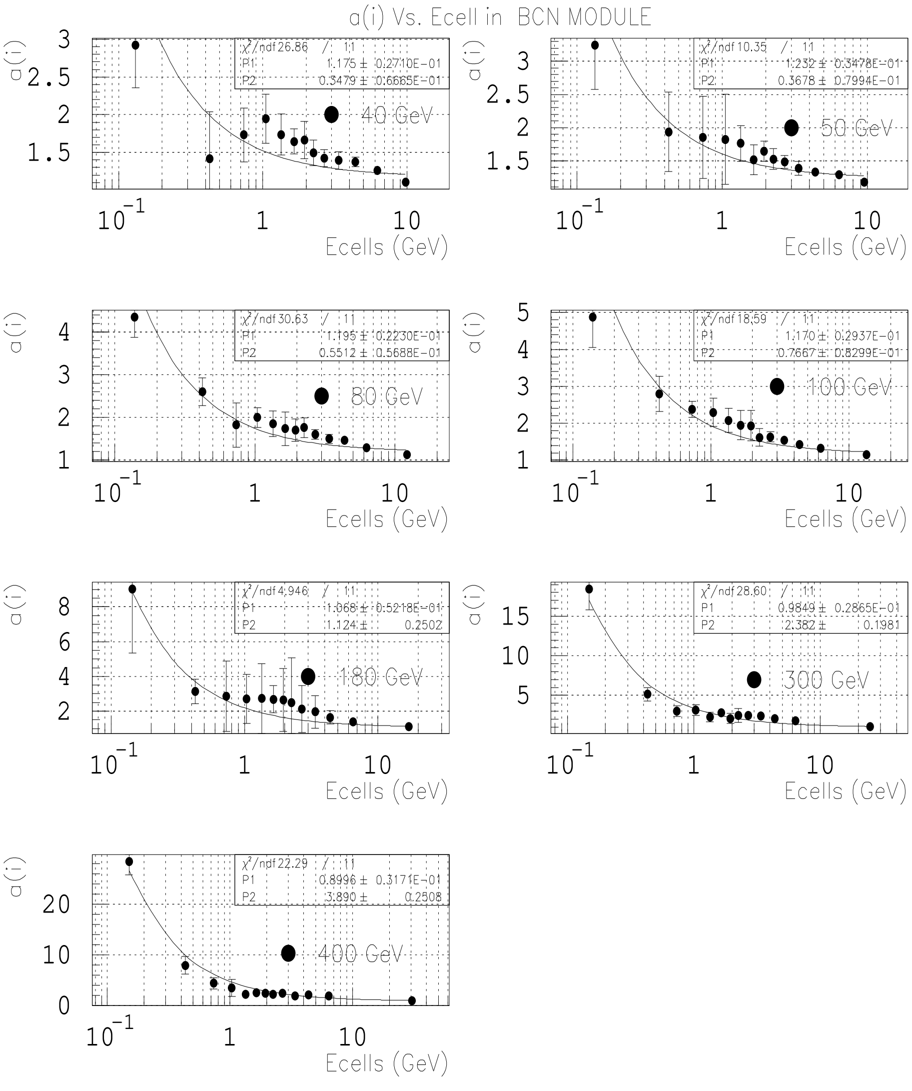

Figure 4.17: *Fits for the a_i parameters (BCN module) at various beam energies and η=-1.1. The parameters p_1 and p_2 obtained for BCN are also shown on the plots.*

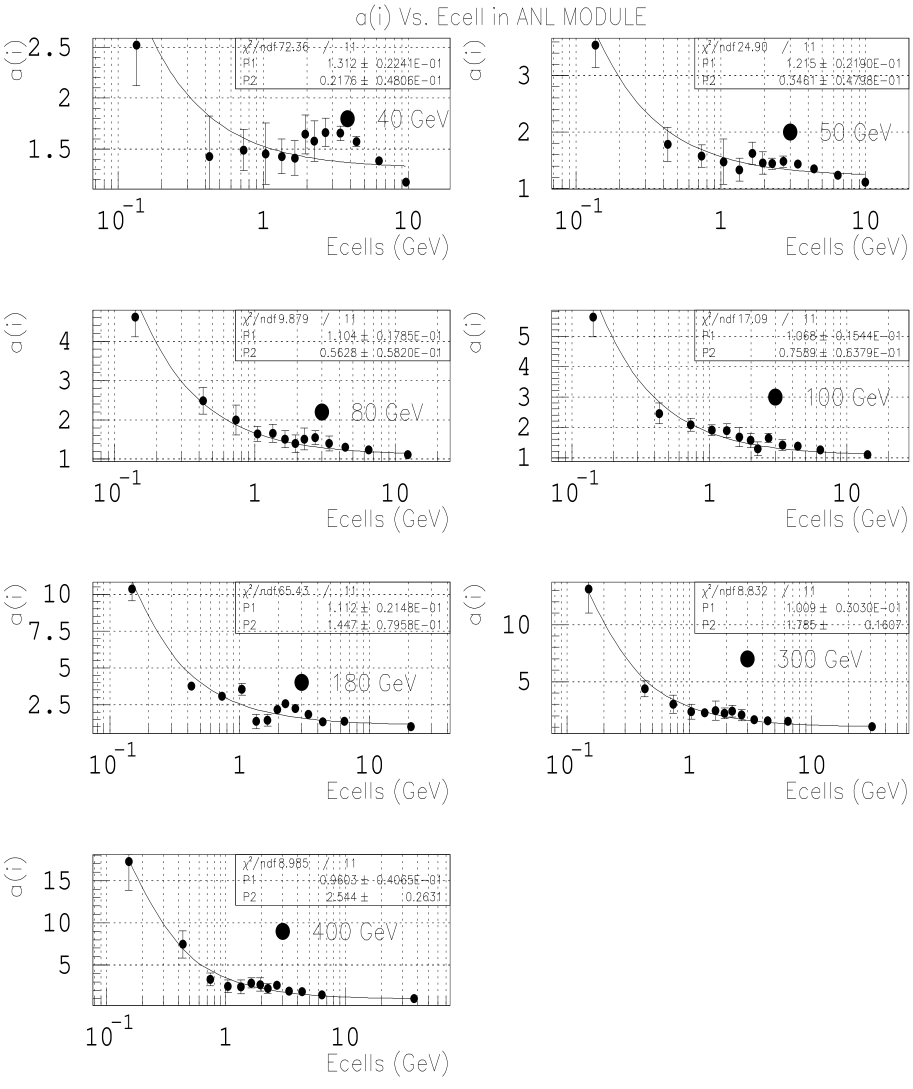

Figure 4.18: *Fits for the a_i parameters (ANL module) at various beam energies and η=-1.2. The parameters p_1 and p_2 obtained for ANL are also shown on the plots.*

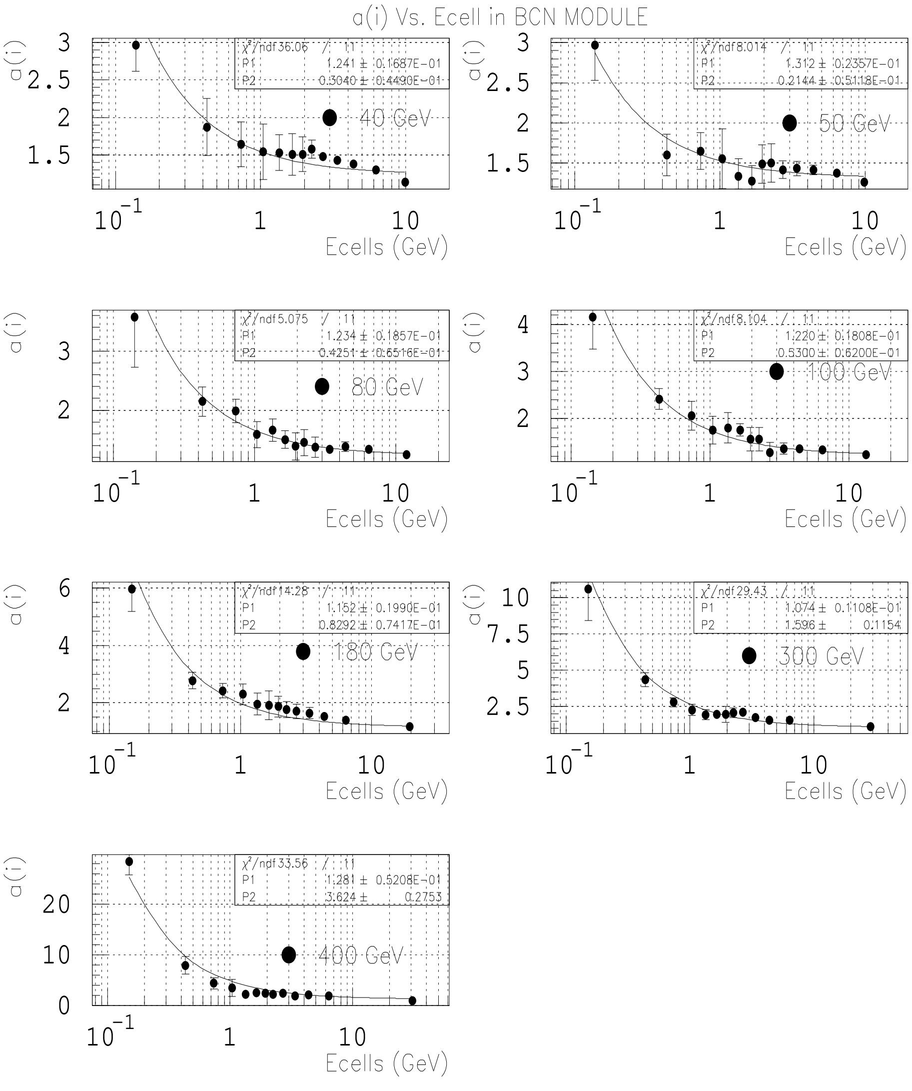

Figure 4.19: *Fits for the a_i parameters (BCN module) at various beam energies and η=-1.2. The parameters p_1 and p_2 obtained for BCN are also shown on the plots.*

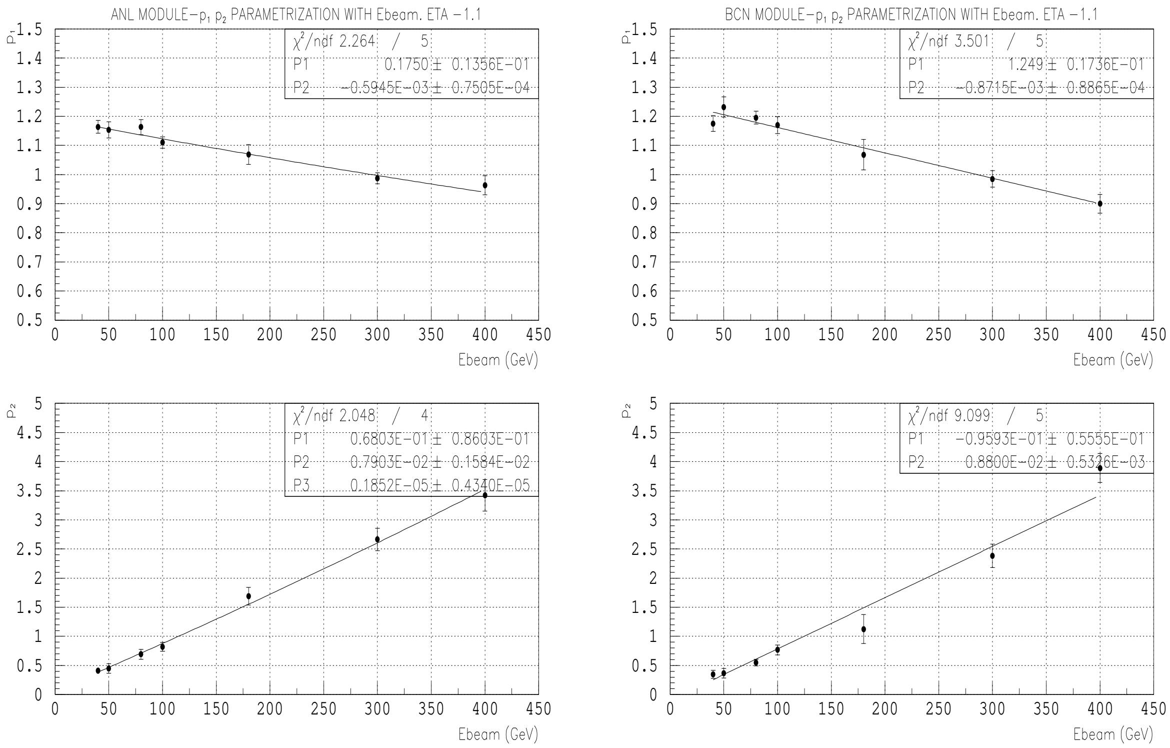

Figure 4.20: *For η=-1.1, the top plots show the parametrization with the beam energy of p_1 for the ANL (left) and BCN (right) modules; the bottom plots shown the same for the p_2. The values of the parameters p_1', p_2' and p_3' from the fits are also presented on the plots.*

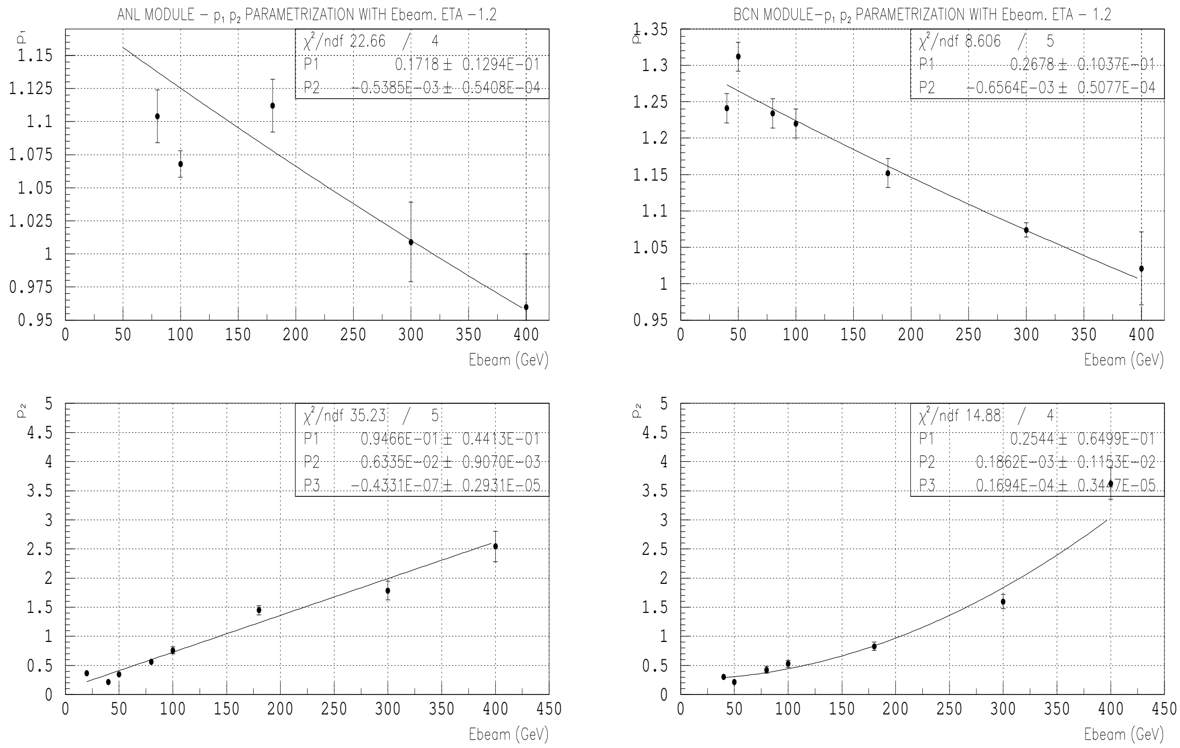

Figure 4.21: *For η=-1.2, the top plots show the parametrization with the beam energy of p_1 for the ANL (left) and BCN (right) modules; the bottom plots show the same for p_2. The values of the parameters p'_1, p'_2 and p'_3 from the fits are also presented on the plots.*

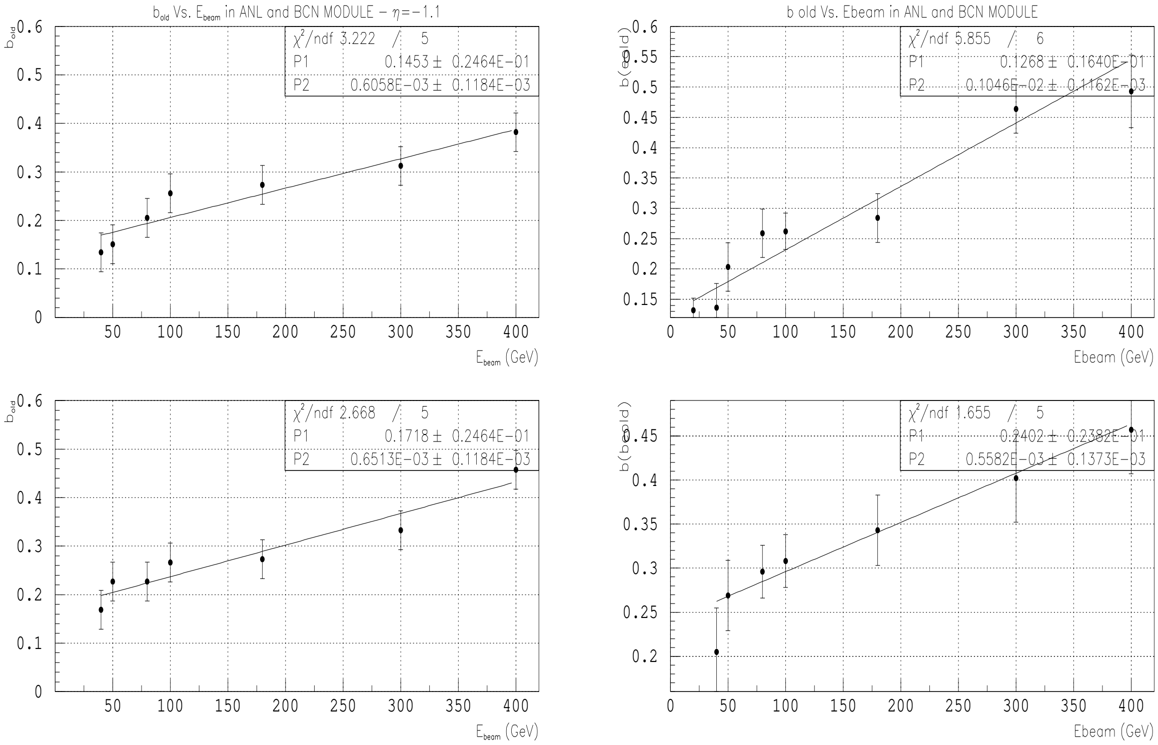

Figure 4.22: *The top plot show the parametrization with the beam energy of B for the ANL module; the bottom plots show the same for the BCN module. On the left η=-1.1 and on the right η=-1.2. The values of the parameters p_1' and p_2' from the fits are also presented on the plots.*

Following theses parametrizations, we have expressed the entire set of corrections by two sets of simple functions, containing only a total of seven parameters. The aim now is to check whether the reconstructed energies with 7 rather than 112 parameters are less precise. The mean, σ and resolution values obtained from this a_i parametrization are given in the table 4.8; the linearity and resolution plots are in figures 4.23 and 4.24. Comparing to the results previously obtained with 112 parameters (see table 4.6) it is seen that despite the dramatic reduction of correction parameters the resolution is negligibly worse and the linearity has degraded because the energy reconstruction is not good enough at low energies (discussed in subsection 4.2.3.4). Quantitatively, the *rms* deviation from linearity is now σ = 2.9% and 3.0% for ANL and BCN modules, respectively, at η=-1.2 instead of 0.12% and 0.4%. For η=-1.1 we get σ = 2.1% and 2.8% instead of 0.34% and 0.4%.

The resolution is now parametrized for the BCN and ANL modules as shows the table 4.9. Comparing with the results previously obtained in table 4.6 the statistical term has worsed but is less than 50% and the constant term has improved, being around 3%.

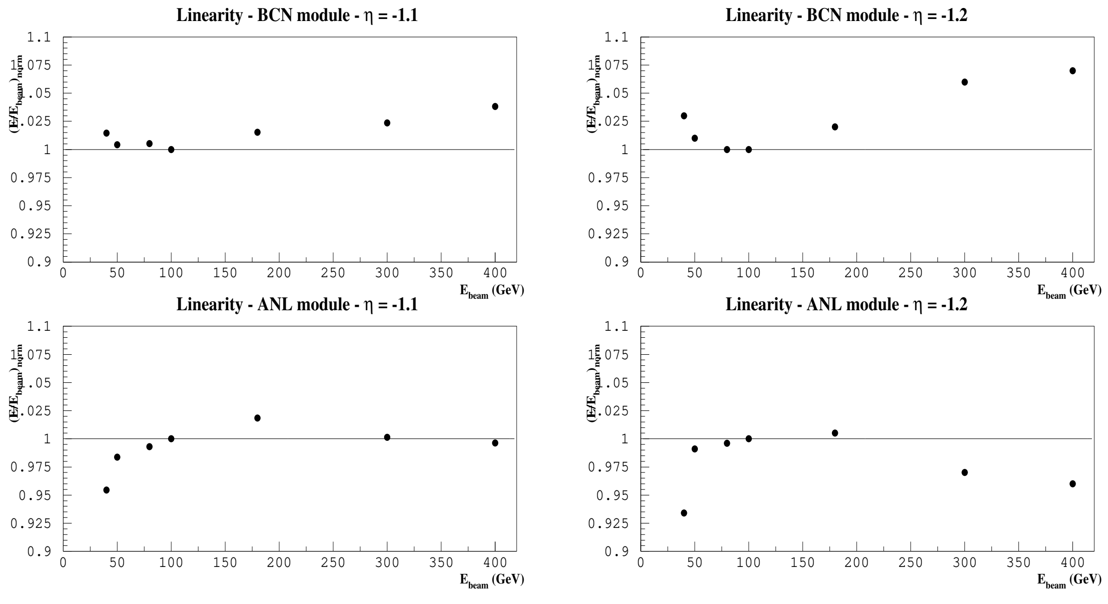

Figure 4.23: *Linearity with the beam energy after the parametrization. Left: For η= -1.1, BCN (Top) and ANL (Bottom) modules. Right: For η= -1.2, BCN (Top) and ANL (Bottom) modules.*

Table 4.8: *Nominal energy, mean reconstructed energy, σ and resolution at various beam energies at two different η for BCN and ANL modules obtained after the parametrization.*

BCN	η=-1.1		
Beam energy (GeV)	μ (GeV)	σ (GeV)	σ/μ(%)
40	40.30 $\pm$ 0.07	3.11 $\pm$ 0.06	7.61 $\pm$ 0.17
50	49.88 $\pm$ 0.11	3.44$\pm$ 0.08	6.73$\pm$ 0.16
80	79.93 $\pm$ 0.09	4.73$\pm$ 0.07	5.83 $\pm$ 0.09
100	99.23$\pm$ 0.11	5.24$\pm$ 0.08	5.26$\pm$ 0.09
180	181.90 $\pm$ 0.22	7.47$\pm$ 0.17	4.13 $\pm$ 0.10
300	306.40 $\pm$ 0.14	11.10 $\pm$ 0.15	3.54 $\pm$ 0.05
400	417.7 $\pm$ 0.19	15.59 $\pm$ 0.21	3.63$\pm$ 0.05
ANL	η=-1.1		
Beam energy (GeV)	μ (GeV)	σ (GeV)	σ/μ(%)
40	40.30$\pm$0.08	3.11$\pm$ 0.06	7.66$\pm$ 0.15
50	49.88$\pm$0.11	3.45$\pm$ 0.08	6.89$\pm$ 0.16
80	79.93 $\pm$0.09	4.73 $\pm$ 0.07	6.05$\pm$ 0.11
100	99.23$\pm$ 0.11	5.24 $\pm$ 0.08	5.43$\pm$ 0.08
180	181.9$\pm$ 0.22	7.47$\pm$ 0.17	4.52$\pm$ 0.07
300	306.4 $\pm$ 0.14	11.10$\pm$ 0.15	3.92$\pm$ 0.05
400	415.5 $\pm$ 0.19	15.69 $\pm$0.22	3.72$\pm$ 0.05
BCN	η=-1.2		
Beam energy (GeV)	μ (GeV)	σ (GeV)	σ/μ(%)
20	20.47 $\pm$ 0.06	2.05 $\pm$ 0.05	10.0 $\pm$ 0.3
40	38.60 $\pm$ 0.08	3.25 $\pm$ 0.06	8.4 $\pm$ 0.2
50	48.58 $\pm$ 0.09	3.29 $\pm$ 0.08	6.9 $\pm$ 0.2
80	76.62 $\pm$ 0.09	4.39 $\pm$ 0.08	5.81 $\pm$ 0.09
100	95.62 $\pm$ 0.09	4.80 $\pm$ 0.08	5.13 $\pm$ 0.07
180	175.6 $\pm$ 0.13	6.76 $\pm$ 0.12	3.92 $\pm$ 0.06
300	298.9 $\pm$ 0.17	10.70 $\pm$ 0.15	3.58 $\pm$ 0.04
400	402.3 $\pm$ 0.26	14.28 $\pm$ 0.25	3.55 $\pm$ 0.05
ANL	η=-1.2		
Beam energy (GeV)	μ (GeV)	σ (GeV)	σ/μ(%)
20	19.46 $\pm$ 0.07	2.34 $\pm$ 0.05	12.1 $\pm$ 0.5
40	39.50 $\pm$ 0.08	3.37 $\pm$ 0.07	8.6 $\pm$ 0.4
50	52.01 $\pm$ 0.12	3.78 $\pm$ 0.10	7.5 $\pm$ 0.2
80	79.40 $\pm$ 0.11	5.30 $\pm$ 0.09	6.4 $\pm$ 0.1
100	100.60 $\pm$ 0.12	5.89 $\pm$ 0.10	5.57 $\pm$ 0.09
180	186.90 $\pm$ 0.21	8.34 $\pm$ 0.19	5.10 $\pm$ 0.11
300	302.37 $\pm$ 0.23	14.50 $\pm$ 0.21	4.65 $\pm$ 0.06
400	403.50 $\pm$ 0.33	18.74 $\pm$ 0.31	4.60 $\pm$ 0.07

Table 4.9: *Statistical (a), constant (b), and noise (c) terms at two different η for the BCN and ANL modules obtained after the parametrization.*

η	BCN			ANL		
	a (%)	b (%)	c	a (%)	b (%)	c
-1.1	45.10	2.70	0.06	45.41	3.00	0.06
-1.2	45.20	2.60	0.06	47.50	3.70	0.06

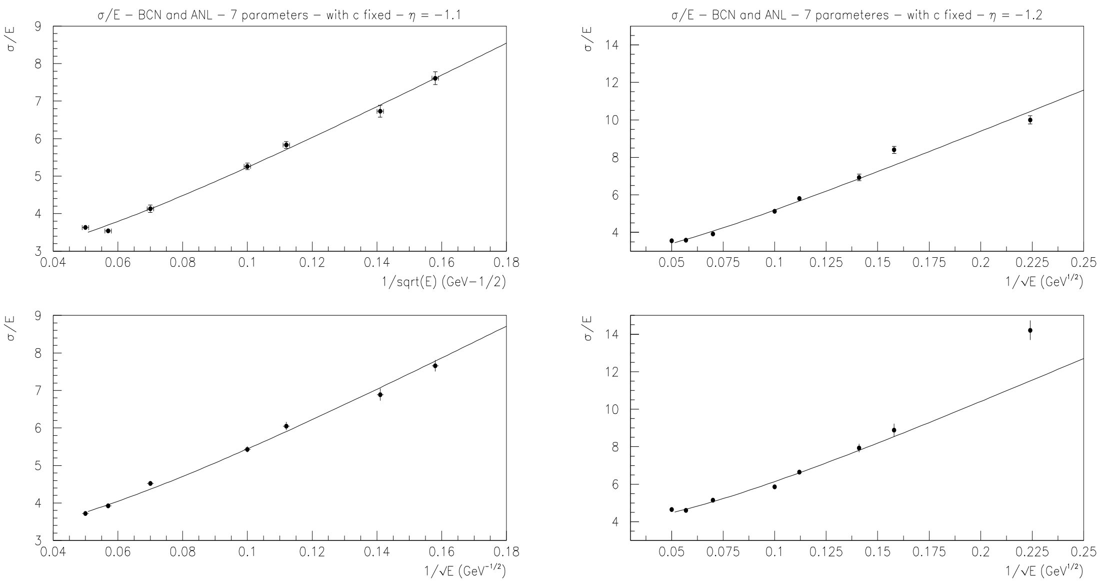

Figure 4.24: *Resolution as a function of the beam energy after the parametrization. Left: For η= -1.1, BCN (Top) and ANL (Bottom) modules. Right: For η= -1.2, BCN (Top) and ANL (Bottom) modules.*

4.2.3.3 Realistic energy reconstruction assuming no knowledge of the beam energy

The method described above cannot be used just *as it is* because the particle energy (needed to calculate the correction parameters) is unknown in a real life experiment. The aim of this section is to reconstruct the pion energy assuming no knowledge of the beam energy.

A more realistic energy reconstruction can be done by obtaining an initial estimate of the particle energy from the raw data and using this estimate as a first approximation of the true energy; the procedure may be iterated until it converges.

Two different algorithms have been considered to obtain the initial estimate of the particle energy:

The first one assumes that the sum of the cell energies (plus the old modules correction) follows a linear behaviour [13]:

$$E_{initial} = \frac{E^{ANL} + E^{BCN} + \alpha}{\beta} + \gamma\ E_{old} \tag{4.15}$$

where α, β and γ are 2.45, 0.88 and 0.31. The two first factors represent the electromagnetic scale determined using the 100 GeV electrons data at 90°, while the last has been determined several times in the past using electron runs of the protype modules test beams

The second uses the raw signal value as the initial estimated particle energy.

Both algorithms converge practically to the same total energy value after 3 or 4 iterations. The first was used for η=-1.2 and the second for η=-1.1.

The mean, σ and resolution of the reconstructed energies are presented in table 4.10. In figure 4.25 the linearity obtained by the *realistic* method is shown; the linearity remains as good as before. For ANL module the non-linearity ranges from 1.8% to 2.2% for η=-1.1 and from 2.9% to 3.4% for η = -1.2. For BCN module it goes from 1.2% to 2% and 3.0% to 3.5% for η=-1.1 and -1.2 respectively.

The resolutions obtained with the realistic algorithm, as we see in figure 4.26 present a slight degradation with respect to the values given in the preceding parametrization that uses the nominal beam energy. This result is unavoidable due to event-to-event fluctuations of hadronic showers. The figure shows that the degradation of the resolution is more pronounced at low energy, as expected from the energy dependence of σ/E.

Table 4.10: *Nominal energy, mean reconstructed energy, σ and resolution at various beam energies at two different η for BCN and ANL modules obtained assuming no knowledge of the beam energy.*

BCN	η=-1.1		
Beam energy (GeV)	μ (GeV)	σ (GeV)	σ/μ(%)
40	40.32±0.08	3.07 ±0.06	7.71 ± 0.15
50	49.89±0.11	3.56 ±0.07	6.93± 0.16
80	79.91±0.09	4.66± 0.07	5.92± 0.09
100	99.36±0.11	5.23± 0.08	5.27± 0.08
180	181.60±0.21	7.50± 0.18	4.11± 0.09
300	305.10±0.14	10.80± 0.15	3.62± 0.05
400	412.60±0.27	14.98± 0.23	3.76± 0.06
ANL	η=-1.1		
Beam energy (GeV)	μ (GeV)	σ (GeV)	σ/μ(%)
40	38.71± 0.07	2.99± 0.06	7.49±0.15
50	49.87± 0.11	3.45± 0.07	7.14± 0.11
80	80.56± 0.10	4.86± 0.08	6.07± 0.10
100	101.4 ± 0.10	5.47± 0.08	5.50± 0.09
180	185.9± 0.17	8.27± 0.13	4.57± 0.07
300	304.6± 0.15	11.93± 0.16	4.00± 0.06
400	404.1± 0.16	14.95± 0.22	3.78± 0.06
BCN	η=-1.2		
Beam energy (GeV)	μ (GeV)	σ (GeV)	σ/μ(%)
20	19.34 ± 0.06	2.08 ± 0.05	10.8 ± 0.3
40	37.97 ± 0.09	3.37 ± 0.06	8.9 ± 0.2
50	47.11 ± 0.10	3.27 ± 0.08	6.96 ± 0.21
80	75.79 ± 0.09	4.47 ± 0.08	5.91 ± 0.09
100	94.44 ± 0.09	4.95 ± 0.08	5.24 ± 0.07
180	175.3 ± 0.14	6.94 ± 0.12	3.96 ± 0.06
300	306.6 ± 0.13	10.70 ± 0.11	3.49 ± 0.04
400	410.6 ± 0.27	14.13 ± 0.25	3.40 ± 0.05
ANL	η=-1.2		
Beam energy (GeV)	μ (GeV)	σ (GeV)	σ/μ(%)
20	19.41 ± 0.07	2.31 ± 0.05	11.9 ± 0.5
40	39.40 ± 0.08	3.31 ± 0.07	8.4 ± 0.4
50	52.85 ± 0.12	3.89 ± 0.10	7.4 ± 0.2
80	85.16 ± 0.12	5.40 ± 0.09	6.34 ± 0.11
100	105.60 ± 0.12	6.02 ± 0.10	5.63 ± 0.09
180	193.20 ± 0.20	9.70 ± 0.18	4.98 ± 0.11
300	309.86 ± 0.23	14.19 ± 0.21	4.58 ± 0.06
400	404.73 ± 0.33	18.69 ± 0.30	4.62 ± 0.07

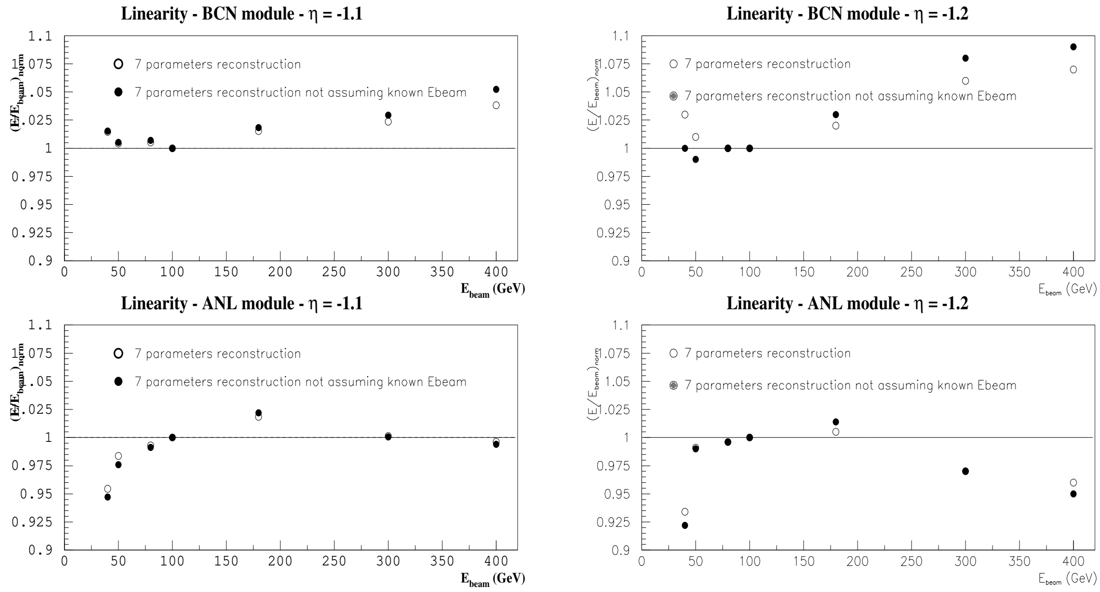

Figure 4.25: *Linearity plot comparing the method which does not use the beam energy with the one which does. Left: For η=-1.1 BCN, (Top) and ANL (Bottom) modules. Right: For η=-1.2, BCN (Top) and ANL (Bottom) modules.*

Table 4.11: *Statistical (a), constant (b), and noise (c) terms at two different η for the BCN and ANL modules obtained assuming no knowledge of the beam energy.*

η	BCN			ANL		
	a (%)	b (%)	c	a (%)	b (%)	c
-1.1	45.60	2.70	0.06	45.20	3.10	0.06
-1.2	47.80	2.60	0.06	44.50	3.90	0.06

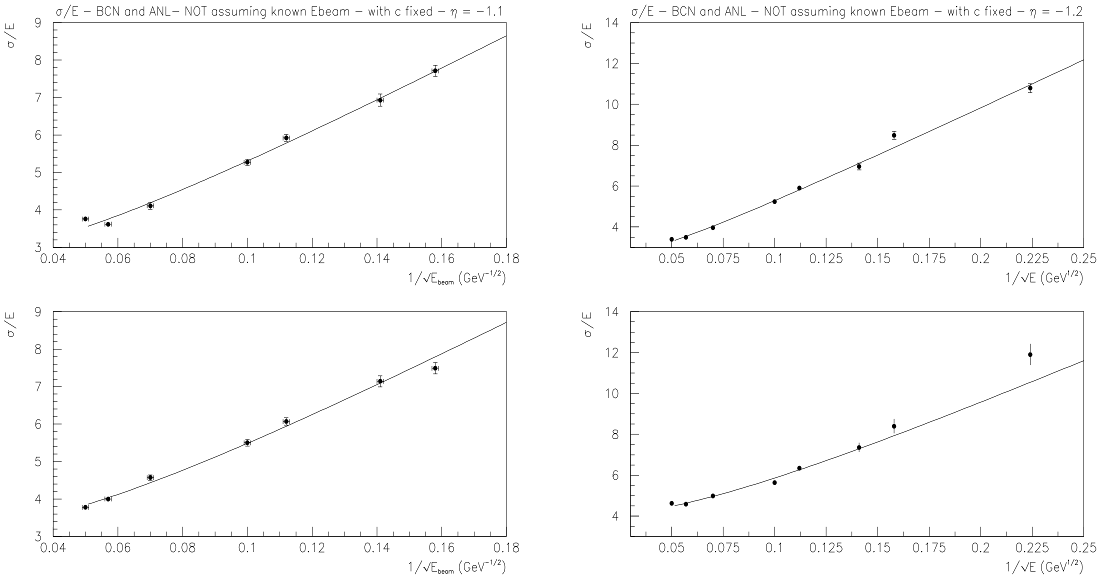

Figure 4.26: *Resolution plots without using the beam energy. Left: For η=-1.1, BCN (Top) and ANL (Bottom) modules. Right: For η=-1.2, BCN (Top) and ANL (Bottom) modules.*

The final results for the BCN and ANL modules are shown in the table 4.11

In this study we have proved that the linearity and resolution of the Tile Calorimeter prototypes improve using the H1 method. Also these results are compatible for the two modules used in the 1997 test beam and at two different values of η.

Respect to the linearity, the benchmark approach gives aproximately the same *rms* than the raw data, improving a little at high energies due to the leakage corrections. Using Lagrange multipliers we found a very linear response over the range of energies studied, because 112 weights have been used for each module. With the parametrization of these weights using a total of 7 constants and assuming no knowledge of the particle energy the linearity is degraded appreciably. This degradation is not seen in the 1994 [17] combined test analysis and it is caused by the difficulty in the parametrization, due to the bad quality of data; however it is still better than with the benchmark method.

For the resolution, figure 4.27 shows that the use of all those weights improves significantly the resolution respect to the raw data algorithm. As expected, the resolution degrades somewhat when no knowledge of the particle energy is assumed, been better than the obtained with the other methods.

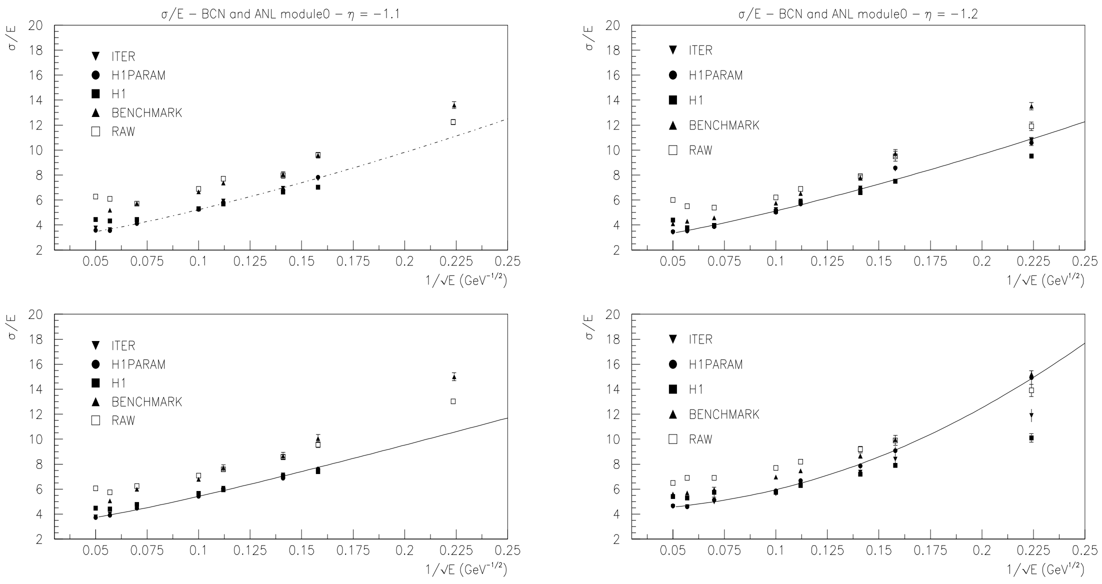

Figure 4.27: *Resolution plots applying all the described methods. Left: For η=-1.1, BCN (Top) and ANL (Bottom) modules. Right: For η=-1.2, BCN (Top) and ANL (Bottom) modules.*

4.2.3.4 Treatment of the low beam energy region

At low beam energies (below 50 GeV) the resolution deteriorates appreciably, as observed with all the reconstruction methods. This confirms that the problem is intrinsic to the data set. We describe here the results obtained for the linearity and resolution if we only consider energies greater than 40 GeV and the energy is reconstructed as in point 4.2.3.2.

The resolution is now parametrized as shows the table 4.12.

Table 4.12: *Statistical (a), constant (b), and noise (c) terms at two different η for the BCN and ANL modules obtained using beam energies greater than 40 GeV.*

η	BCN			ANL		
	a (%)	b (%)	c	a (%)	b (%)	c
-1.1	45.70	2.70	0.06	47.20	3.00	0.06
-1.2	44.30	2.50	0.06	41.10	4.10	0.06

The mean, σ and resolution values obtained are given in the table 4.13; the linearity and resolution plots are in figure 4.28 and 4.29. Comparing to the results previously obtained with beam energies below 50 GeV it is seen that the resolution is practically the same and the linearity has improved. Quantitatively, the *rms* deviation from linearity is now 2.0% and 0.6% instead of 2.12% and 2.8% for η=-1.1 and ANL and BCN modules respectively. For η=-1.2 the *rms* is now 2.0% and 1.5% instead of 2.9% and 3% for ANL and BCN modules.

4.2.4 e/π response

The Tile Calorimeter has not been designed to have a good electron performance, since it will have in front of it an electromagnetic compartment. However, it is important to understand the electron response, namely to study the e/π ratio. When studying the Tile Calorimeter response to electrons, the hadronic calorimeter can be considered as a set of different calorimeters, with variable absorber and scintillator thicknesses: from $t_{Fe} = 81$ to 28 mm, and from $t_{Scin} = 17$ to 6 mm for a θ angle between 10 and 30 degree, where t_{Fe} and t_{Scin} are the effective thicknesses of the absorber and the scintillator plates respectively [14]. Therefore, the electron response is a rather complicated function of E_{beam} and η.

Table 4.13: *Nominal energy, mean reconstructed energy, σ and resolution at various beam energies at two different η for BCN and ANL modules obtained with beam energies greater than 40 GeV.*

BCN	η=-1.1		
Beam energy (GeV)	μ (GeV)	σ (GeV)	σ/μ(%)
50	50.63±0.11	3.47±0.07	6.86±0.16
80	80.90 ± 0.09	4.74±0.07	5.86± 0.09
100	100.50 ± 0.11	5.33 ± 0.08	5.31 ± 0.08
180	182.60 ± 0.21	7.48± 0.16	4.09± 0.09
300	304.60 ± 0.19	11.02± 0.16	3.62± 0.05
400	409.70 ± 0.19	15.00± 0.20	3.66± 0.06
ANL	η=-1.1		
Beam energy (GeV)	μ (GeV)	σ (GeV)	σ/μ(%)
50	48.67 ±0.11	3.52 ± 0.07	7.22 ±0.15
80	80.17 ± 0.10	4.87± 0.08	6.07± 0.10
100	101.50 ± 0.11	5.62± 0.08	5.53± 0.09
180	187.40± 0.17	8.57± 0.14	4.57± 0.07
300	305.50 ± 0.32	12.11± 0.19	3.96 ±0.06
400	402.20 ± 0.20	15.11± 0.22	3.76± 0.06
BCN	η=-1.2		
Beam energy (GeV)	μ (GeV)	σ (GeV)	σ/μ(%)
50	49.81 ± 0.10	3.41 ± 0.08	6.85 ± 0.18
80	80.85 ± 0.09	4.57 ± 0.08	5.66 ± 0.09
100	100.9 ± 0.09	5.07 ± 0.08	5.03 ± 0.07
180	182.8 ± 0.14	6.94 ± 0.12	3.91 ± 0.06
300	299.6 ± 0.11	10.43 ± 0.09	3.48 ± 0.04
400	385.6 ± 0.17	13.31 ± 0.15	3.47 ± 0.05
ANL	η=-1.2		
Beam energy (GeV)	μ (GeV)	σ (GeV)	σ/μ(%)
50	49.76 ± 0.11	3.68 ± 0.09	7.4 ± 0.2
80	82.29 ± 0.11	5.16 ± 0.09	6.27 ± 0.14
100	104.3 ± 0.12	5.70 ± 0.10	5.47 ± 0.09
180	193.1 ± 0.21	9.56 ± 0.18	4.95 ± 0.07
300	309.0 ± 0.23	14.12 ± 0.21	4.57 ± 0.06
400	401.1 ± 0.26	18.77 ± 0.23	4.68 ± 0.07

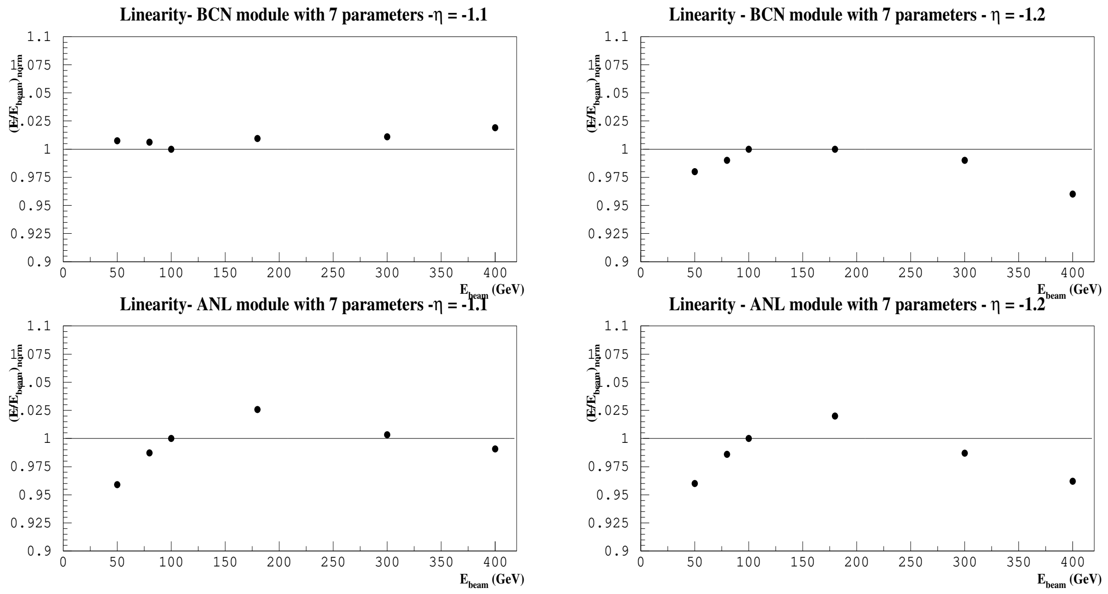

Figure 4.28: *Linearity plot minimising the functional with the Lagrange multiplier and beam energies greater than 40 GeV. Left: For η=-1.1, BCN (Top) and ANL (Bottom) modules. Right: For η=-1.2, BCN (Top) and ANL (Bottom) modules.*

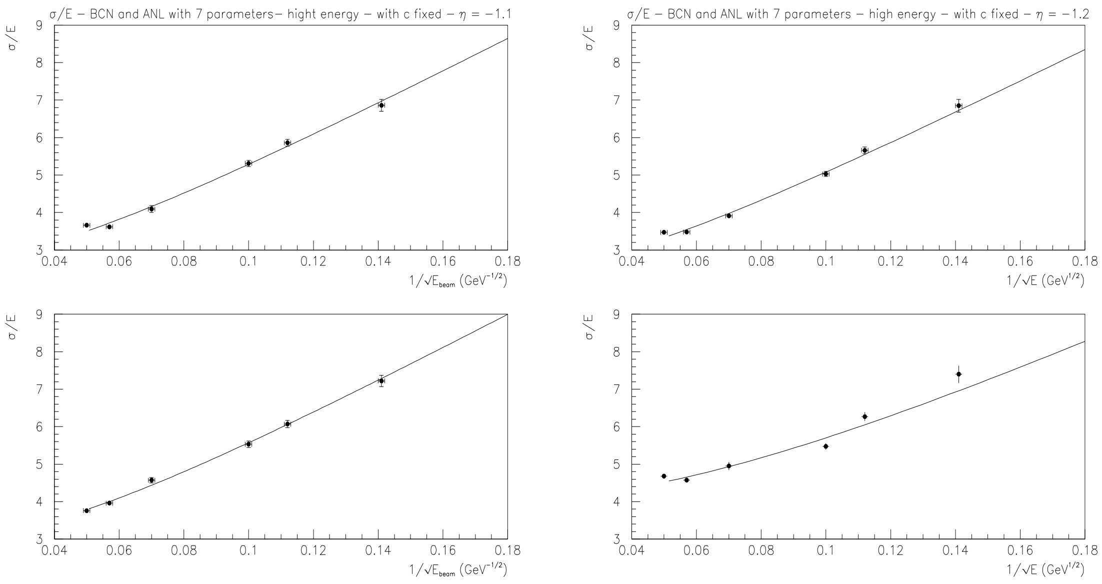

Figure 4.29: *Resolution plots minimizing the functional with the Lagrange multiplier and beam energies greater than 40 GeV. Left: For η=-1.1, BCN (Top) and ANL (Bottom) modules. Right: For η=-1.2, BCN (Top) and ANL (Bottom) modules.*

The response obtained for electrons and pions gives the possibility to extract the e/h value, that is the ratio of the calorimeter responses to the electromagnetic and non-electromagnetic (purely hadronic) components of hadron showers. An e/h value different from 1 causes deviation from linearity in the hadronic response versus energy, besides broadening the energy resolution and introducing tails in the energy distribution [15]. The value of the e/h ratio depends on a number of factors such as the thickness of the passive and active layers, and the sampling fraction. The e/h ratio of a sampling calorimeter with an iron-scintillator ratio less than 20 (in the case of the Tile Calorimeter this ratio is 4.7) is expected to be > 1 for the conventional orientation of tiles perpendicular to incident hadrons [16]. The Tile Calorimeter structure does not favour a simple relation, but rather a function such as $e/\pi = f(E, \eta)$.

The present study corresponds to the data taken in 1997 for the Extended Barrel Module 0 built in Barcelona (BCN), Spain.

The e/h ratio was extracted from the data by fitting the expression:

$$e/\pi = \frac{e/h}{1 + (e/h - 1) \times 0.11 \times ln(E)} \tag{4.16}$$

where $0.11 \times ln(E)$ is the average fraction of the incident hadron energy into π^0 production [15].

Figure 4.30 shows the e/π ratio as a function of the beam energy for BCN Extended Barrel module at four different η values. The response to pions relative to electrons is seen to increase with energy as expected, because the fraction of electromagnetic energy in a pion shower increases logarithmically with energy.

From the data we got four values for the e/h ratio; the results are presented in table 4.14. The table shows the results (e/h) as a function of η. The e/h value increases as the η increases, this is because the shower is better contained for $\eta = -1.1$ than for $\eta = -1.4$. Deviations from $e/h = 1$ contribute to the constant term in the energy resolution (see equation 4.7). This constant term is about 3% for the BCN Extended Barrel module.

The value $e/h = 1.38$ corresponding to η = -1.1 is in good agreement with the 1.36 obtained from previous precise studies and reported in the TDR [17].

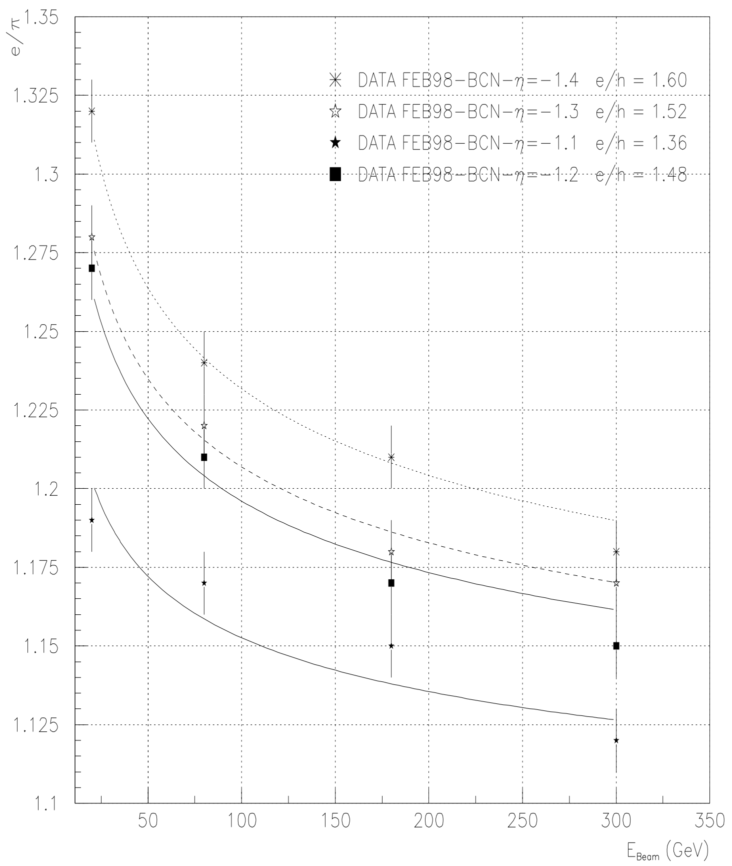

Figure 4.30: *The e/π ratio as a function of the beam energy for the BCN Extended Barrel module tested in the 1997 test beam at four differents η's. The lines are the fits of the equation (4.16).*

Table 4.14: *The values of the e/h ratio for the BCN Extended Barrel module at four differents η's using the equation (4.16).*

Module	η	e/h
BCN	-1.1	1.38 $\pm$0.013
BCN	-1.2	1.48 $\pm$0.014
BCN	-1.3	1.52 $\pm$0.015
BCN	-1.4	1.60 $\pm$0.016

4.3 The 1998 test beam

The Barrel Module 0 was tested in the beam area in 1998 using the same scanning table as for the test beam in 1997. In order to improve the transverse leakage for the Barrel Module 0, the five original one meter prototype modules (Old modules) were placed on either sides (in ϕ) of Module 0, three on one side and two on the other as shown in figure 4.31. Unlike the 1 m prototype modules, which had non-projective tower read-out, Module 0 had fibre routing in such a way that the scintillating tiles were grouped in a projective way with towers forming a minimun of granularity 0.1 in η. This is shown in figure 4.32. This projective tower structure defined by the fibre routing in Module 0 will most likely be the projective geometry used in ATLAS. For the test beam run, only half of the module was equipped with read-out electronics (η = 0 on the figure was actually the physical center of the structure).

The Tilecal modules have three segmentations in depth and the showers are sampled with 11 tiles varying their size in depth from 97 to 187 mm. The iron structure of the barrel Module 0 consists of 305 repeated periods sandwiched between two iron end plates of 20 mm thickness. Each period consists of four layers. The first and third layers are formed by 5 mm thick trapezoidal steel plates, spanning the full radial dimension of the module (master plates, 152 cm long). In the second and fourth layer, smaller trapezoidal steel plates and scintillator tiles alternate along the radial dimension. The front face area of the barrel modules is 560 $\times$ 22 cm^2. The granularity in $\Delta\eta \times \Delta\phi$ is 0.1 $\times$ 0.1 for the first two samplings and 0.2 $\times$ 0.1 for the last sampling. The thickness of the module at $\eta = 0$ is 1.5 λ in the first sampling which groups the 3 smallest tiles, 4.2 λ in the second which groups 6 tiles, and 1.9 λ in the third which is composed by the 2 largest tiles.

The negative η side of the module was equipped with Bicron multi-clad fibres. The cells of the sampling A (inner sampling) were equipped with fibers BCF99-28 dopped with 60 ppm of UV Absorber, and the other cells with fibres BCF91A without UV Absorber. The positive η side of the module was equipped with Pol.Hi.Tech multi-clad

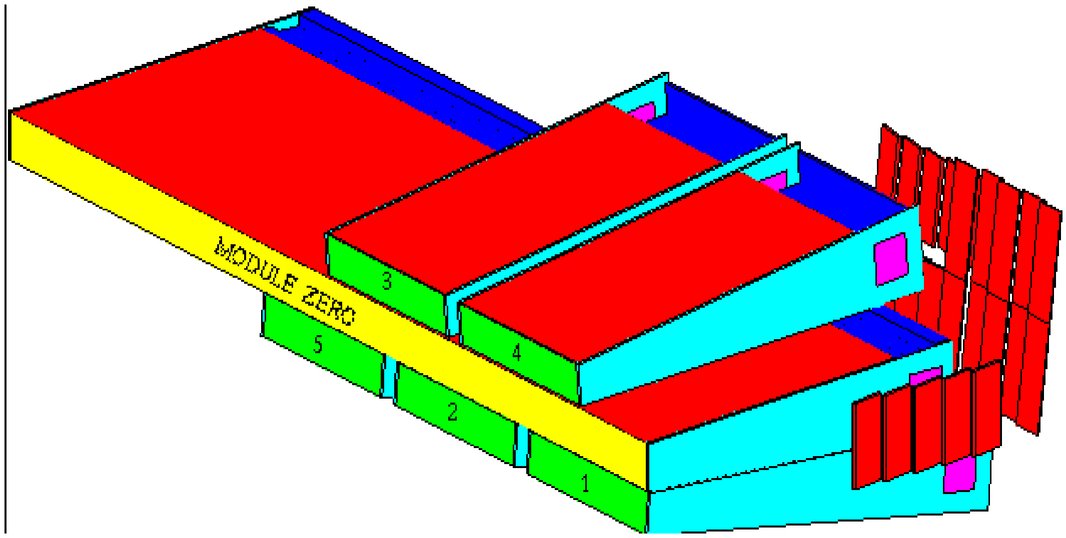

Figure 4.31: Barrel module 0 in the 1998 test beam.

S250-100 fibres dopped with UV Absorber. The full module was equipped with black fibre profiles (and a few gray near the ends) which were painted white in the face that ensures the tile-fibre optical coupling. The reason to use white painting is because a large fraction of the light is going to the fiber profiles and if they are white the light gets reflected back inside the fibers.

The PMT's used are the Hamamatsu 8-stage R5900. In the 1998 test an improved version of these PMT's was used in the positive η side of the module.

The phototube signals were sampled at 40 MHz with the FERMI system and the drawers were equipped with bi-gain 3-in-1 readout cards into FERMI ADC modules. Each drawer is equipped with 45 PMTs.

Pion calibration beams of different energies (20, 50, 80, 100, 150, 180, 300 and 400 GeV) at η = -0.25, -0.35, -0.45 and -0.55 have been analysed from the test beam data. On average, about ten thousand events are available for each energy. Cuts were applied in the beam chambers to eliminate the beam halo and events with simultaneous particle in the scintillator chambers (the same idea that in 1997 test beam); finally 60% of the events were removed including pedestal events supression.

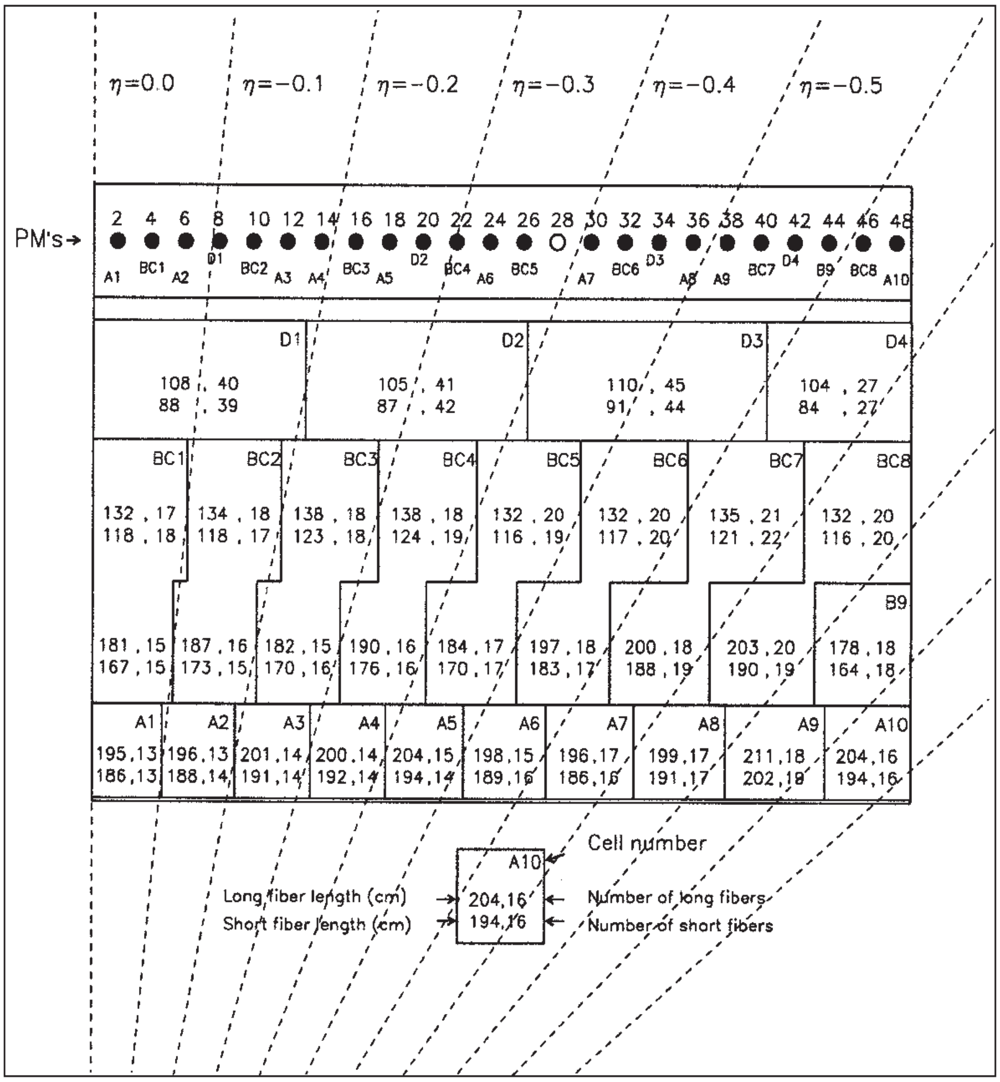

Figure 4.32: Cell geometry of the barrel module 0 tested in 1998.

4.4 Monte Carlo simulation

The data obtained in the test beam has been compared with Monte Carlo simulation. The test beam setup was simulated in the framework of GEANT3.21 [1] using DICE [18], [19] to simulate the geometry. The GCALOR [2] package was used to simulate the hadronic interactions.

The GEANT package has been used to simulate in detail the detector characteristics and performance. Version 3.21 is the best one suited for describing some of the very complex aspects of the detector geometry, while still providing a reasonable performance in terms of accuracy of the simulation and of CPU time needed to track particles through the complete detector. In addition to describing the detector geometry and tracking particles through it, the GEANT framework is used to describe the materials constituting the detector, to visualise the detector components, and to simulate and record the response of the sensitive elements of the various systems.

The DICE package contains general-purpose routines, which control the simulation flow, together with detector geometry modules, digitisation routines, and dedicated routines.

The final choice for the hadronic model was to use the GEANT interface to the CALOR package (GCALOR) because, although still far from an optimal fit to the data, it reproduces better than other procedures (FLUKA and GEISHA packages [20]) the experimental results. A cut set at 1 MeV for most of the hadronic processes has been used for event production, again as trade-off for performance.

The description of the Module 0 geometry in GEANT is probably the most critical issue for the detector-simulation program, since it must represent the right compromise between accuracy and performance. To simplify this procedure, a FORTRAN-based macro-language [21] has been used to set up detector-description banks, to implement the detector geometry, and to define HITS and DIGI structures associated with it. The advantage of this approach for the user is the possibility of having a generic interface to ZEBRA [22], while still maintaining a high level of flexibility.

The event-generation phase is normally run separately in order to have a consistent input stream which can be used many times. Event generation facilities are implemented within SLUG by using GENZ package, which provides a common interface between the most widely used event generators (PYTHIA [23], HERWIG [24], ISAJET [25]) and GEANT via the standard HEPEVT common block and ZEBRA banks.

We have simulated samples of two thousand pion events for different energy values in the range from 20 to 400 GeV and at different η values.

The simulation program is not complete and many features of the module 0 are not yet implemented in the simulation source code, namely:

- The fluctuations on the response of the fibres and tiles, including tile-to-tile and fibre-to-fibre fluctuations;

- The electronic of the read-out system, including the photostatistic effect and the electronic noise effect in the response of the module 0 to the particle beams.

4.5 Analysis of the 1998 pion data for the Barrel Module 0

When a particle develops a shower in a block of matter such a sampling calorimeter, some fraction of its energy is transformed into a measurable signal, usually a pulse of electrical charge. This pulse is the result of all the charged particles generated in the shower development which traverse and ionise the active layers of the detector. The energy resolution for detecting the original particle is determined by the fluctuations occuring in this process. This has consequences for calorimetric hadron detection (see chapter 3). Firstly, the signal distribution for hadrons of energy E will be broader than for electromagnetic showers at the same energy. Secondly, the average response (signal per unit of energy) will have a different value for electromagnetic and hadronic showers $e/h > 1$.

For hadrons the resolution and linearity of a non-compensated calorimeter ($e/h \neq 1$) are degraded by the different response to the electromagnetic and hadronic components of the hadronic shower [26]. The dependence of the e/h value with the energy affects the linearity, whereas the presence of the electromagnetic component in the shower generated by a hadron worses the resolution. All together, to these physical effects, which are limiting the intrinsic resolution of the detector, it has to be added the always experimental contributions, basically the losses due to leakage.

The purpose of weighting techniques is to compensate for this difference and to perform the energy reconstruction optimizing the linearity and resolution [30]. In the next subsections, the evolution of the linearity and resolution parameters with the data reconstruction is studied in two steps: from raw data to H1 weighting method. The benchmark approach is not used in this analysis, because the H1 method gives better results respect to the linearity and the resolution. The next point explains how to parametrize the leakage in order to improve the resolution. The e/h ratio is determined from the data taken in 1998 for Barrel Module 0. Finally, a comparison between Extended Barrel and Barrel Module 0 is presented.

4.5.1 Raw Data

The first step in the linearity and resolution study was the direct analysis of the test beam and Monte Carlo simulation raw data. The two components of the total raw energy are the energy detected in the barrel Module 0 and the energy measured in the five 1 m modules (old modules). The conversion factors from pC to GeV were calculated to be 1.26 and 36.1 for the barrel and 0.1613 and 29.2 for old modules, for the test beam data and Monte Carlo simulation respectively. So finally:

$$E_{Raw} = E_{M0}^{corr} + E_{old} \tag{4.17}$$

Using this formula we can reconstruct the beam energy as shown in Figure 4.33. The mean value is similar (for the test beam data is 65.7 GeV and for the Monte Carlo simulation 65.41 GeV) but the sigma parameter is bigger in the test beam data (6.3 GeV) than in the Monte Carlo simulation (5.2 GeV). This is because the simulation program does not have into account the fluctuations in the response of the fibres and tiles, and because of the limited knowledge of the hadronic showers development.

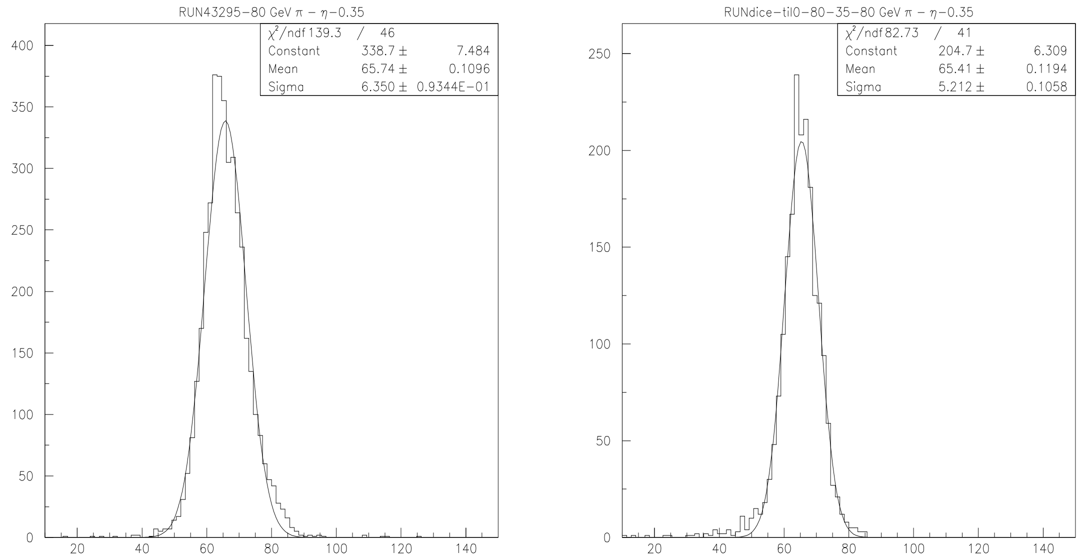

Figure 4.33: *Raw energy reconstruction for pions at 80 GeV and η=-0.35. Left: test beam data. Right: Monte Carlo simulation.*

According with the expresion (4.17) we present in table 4.15 the results of μ and σ for pion beams at η=-0.35 and in table 4.16 σ/μ for four different η values, obtained from the test beam data and from Monte Carlo simulation. Also the plots of linearity and energy resolution can be seen in figures 4.34 and 4.35, respectively.

Table 4.15: *Nominal energy, mean reconstructed energy and σ for pions at various beam energies at η=-0.35 for test beam data and Monte Carlo simulation obtained from raw data.*

η=-0.35	Test Beam data		MC simulation	
N. E. (GeV)	μ (GeV)	σ (GeV)	μ (GeV)	σ (GeV)
20	15.58±0.03	2.30±0.02	15.96±0.04	1.99±0.03
50	41.05±0.07	4.09±0.06	40.75±0.08	3.68±0.06
80	65.74±0.10	6.35±0.09	65.41±0.12	5.21±0.10
100	81.49±0.14	7.12±0.10	82.18±0.13	5.68±0.11
150	123.3±0.3	9.57±0.21	123.8±0.2	8.29±0.17
180	148.2±0.2	11.64±0.15	149.1±0.2	9.11±0.21
300	251.5±0.3	19.29±0.25	248.7±0.3	14.58±0.39
400	326.9±0.4	25.36±0.31	332.1±0.5	19.30±0.48

The linearity presents the typical shape of a non-compensated calorimeter, the slope is due to the increase of electromagnetic energy (π^0) with the incident pion energy in the shower. The big difference between the test beam data and the Monte Carlo simulation is found at high energies. The *rms* for the test beam data is greater (2% for all η's) than for the simulation (1.3%). This is mainly due to the data points at high energies, because the hadronic showers development knowledge is limited in the simulation program.

A fit of the data is performed using the expression (4.7). The study presented in the previous section 4.2.3 shows a strong correlation between parameters **a** and **c**, so that we have decided to fix the **c** value at 0.06 GeV in order to obtain less aleatory results in the **a** value and to compare with other fits.

The fit results for the test beam data and Monte Carlo simulation are presented in the table 4.17.

We obtain better resolution in the simulation than in the data. The figure 4.33 shows that in the Monte Carlo simulation the sigma parameter is lower than for the data, therefore as the mean value is similar for both, the resolution is better in the simulation.

Table 4.16: *Nominal energy and resolution for pions at various beam energies at four different η for test beam data and Monte Carlo simulation obtained from raw data.*

η=-0.25	Test Beam data	MC simulation
N. E. (GeV)	$\sigma/\mu(\%)$	$\sigma/\mu(\%)$
20	14.27±0.13	12.33±0.22
50	9.77±0.13	9.24±0.21
80	8.72±0.12	8.04±0.18
100	8.06±0.14	7.99±0.17
150	6.83±0.17	7.40±0.18
180	7.19±0.10	6.74±0.16
300	5.73±0.09	6.83±0.19
400	7.07±0.11	6.48±0.18
η=-0.35	Test Beam data	MC simulation
N. E. (GeV)	$\sigma/\mu(\%)$	$\sigma/\mu(\%)$
20	14.77±0.15	12.47±0.22
50	9.96±0.14	9.03±0.16
80	9.65±0.14	7.97±0.16
100	8.74±0.12	6.91±0.14
150	7.76±0.17	6.67±0.14
180	7.85±0.10	6.10±0.14
300	7.67±0.09	5.86±0.16
400	7.75±0.09	5.81±0.15
η=-0.45	Test Beam data	MC simulation
N. E. (GeV)	$\sigma/\mu(\%)$	$\sigma/\mu(\%)$
20	13.81±0.13	12.07±0.35
50	9.40±0.12	8.70±0.24
80	8.44±0.11	7.90±0.25
100	7.92±0.12	7.60±0.22
150	6.82±0.16	6.90±0.23
180	6.58±0.08	6.60±0.20
300	6.43±0.09	6.70±0.23
400	6.13±0.09	6.10±0.18
η=-0.55	Test Beam data	MC simulation
N. E. (GeV)	$\sigma/\mu(\%)$	$\sigma/\mu(\%)$
20	12.89±0.29	11.64±0.29
50	9.24±0.12	8.46±0.17
80	7.98±0.10	7.50±0.15
100	7.09±0.10	6.83±0.17
150	6.34±0.13	5.71±0.12
180	6.60±0.09	5.69±0.12
300	6.00±0.08	5.41±0.13
400	5.43±0.05	5.39±0.14

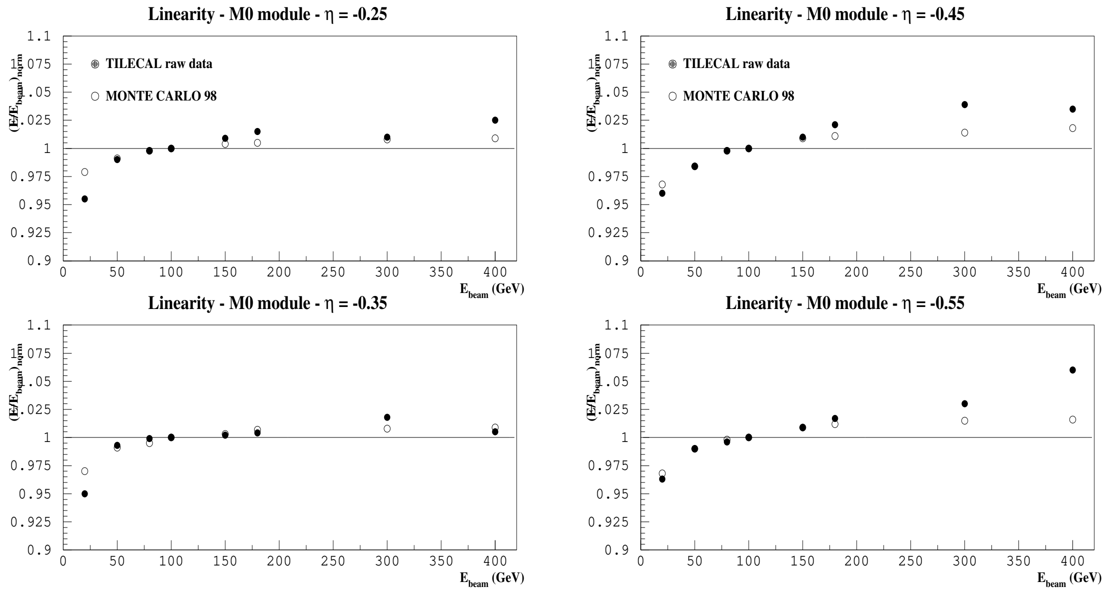

Figure 4.34: *Linearity of raw data for the test beam data and the Monte Carlo simulation. Left: for* η*=-0.25 (top) and* η*=-0.35 (bottom). Right: for* η*=-0.45 (top) and* η*=-0.55 (bottom).*

Table 4.17: *Statistical (a), constant (b), and noise (c) terms at four different* η *for test beam pion data and Monte Carlo simulation obtained from raw data.*

η	Test Beam data			MC simulation		
	a (%)	b (%)	c	a (%)	b (%)	c
-0.25	59.10	5.40	0.06	48.30	6.10	0.06
-0.35	56.30	6.88	0.06	56.30	6.88	0.06
-0.45	56.50	5.35	0.06	47.30	5.75	0.06
-0.55	55.20	5.10	0.06	48.80	5.20	0.06

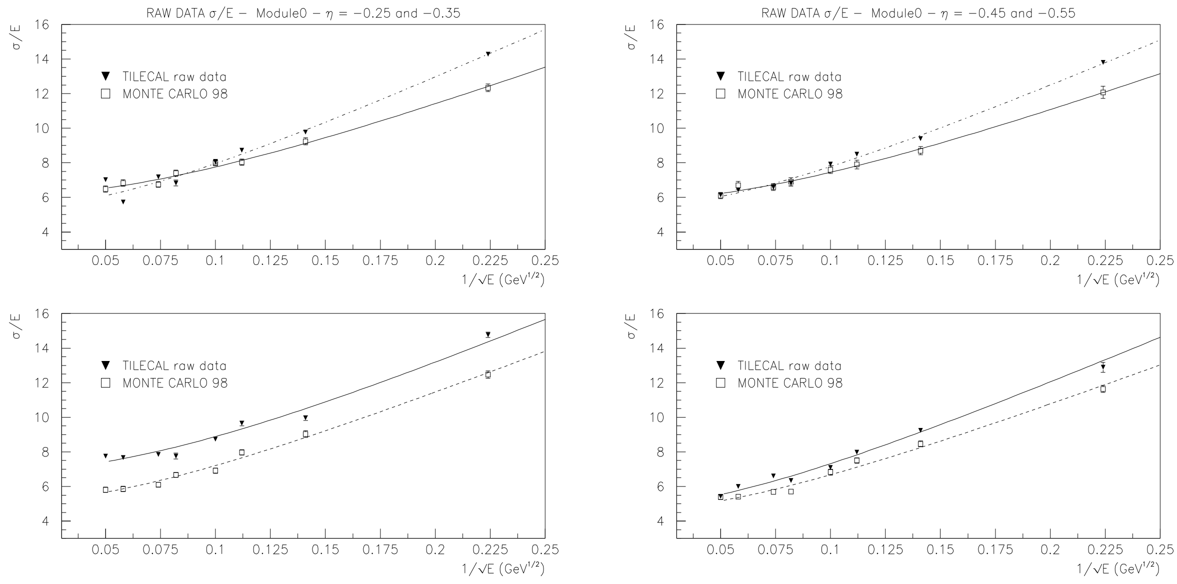

Figure 4.35: *Energy resolution of raw data for the test beam data and the Monte Carlo simulation. Left: for η=-0.25 (top) and η=-0.35 (bottom). Right: for η=-0.45 (top) and η=-0.55 (bottom).*

4.5.2 H1 Method

The linearity and the resolution are two characteristics which can be improved via software offline. Instead of correcting *upwards* the response of cells with relatively small signals, this method pretends to equalize their responses to the one of the cells with large (tipically electromagnetic) deposited energies (see section 4.2.3).

The energy in each cell, E_{cell}, is corrected multiplying its value by a parameter a_i [9] which depends on the energy of the cell (see formula 4.9).

The technical details of the method have been described in the section 4.2.3. As first step, for each beam energy, the cell energy spectrum is divided into n intervals [13] and a correction parameter a_i is calculated for each interval. Several sets of parameters are calculated for all the η values and for test beam data and Monte Carlo simulation.

The set of correction parameters a_i is determined from the data by minimizing the expression 4.13.

The corrected total energy spectra were fitted with Gaussian distributions over a $\pm 2\sigma$ range. From the mean values of the fits we obtain plots of the deviation from a linear response. Such linearity plots, are shown in figure 4.36, left η=-0.25 ,-0.35 and right η=-0.45, -0.55, respectively. The improvement when including the *energy conservation* constraint is very clear; with this constraint the *rms* deviation from linearity is 0.46% and 0.48% for the test beam data and Monte Carlo simulation, respectively. The two *rms* are very similar because we have reconstructed both energies minimizing the functional with the Lagrange multiplier.

The results of the fits to the reconstructed pion energies are given in table 4.18 and 4.19.

The energy resolution (σ/E *vs.* the beam energy) is given in figure 4.37. The resolution obtained here can be parametrized for the test beam data and Monte Carlo simulation as shows the table 4.20.

We obtain similar resolution in the simulation than in the real data because both functional have been minimized with the Lagrange multiplier.

4.5.2.1 Parametrizing the a_i

A total of 112 parameters are used to reconstruct the pion energy. To reduce the number of parameters we proceed as has been described in the section 4.2.3.2.

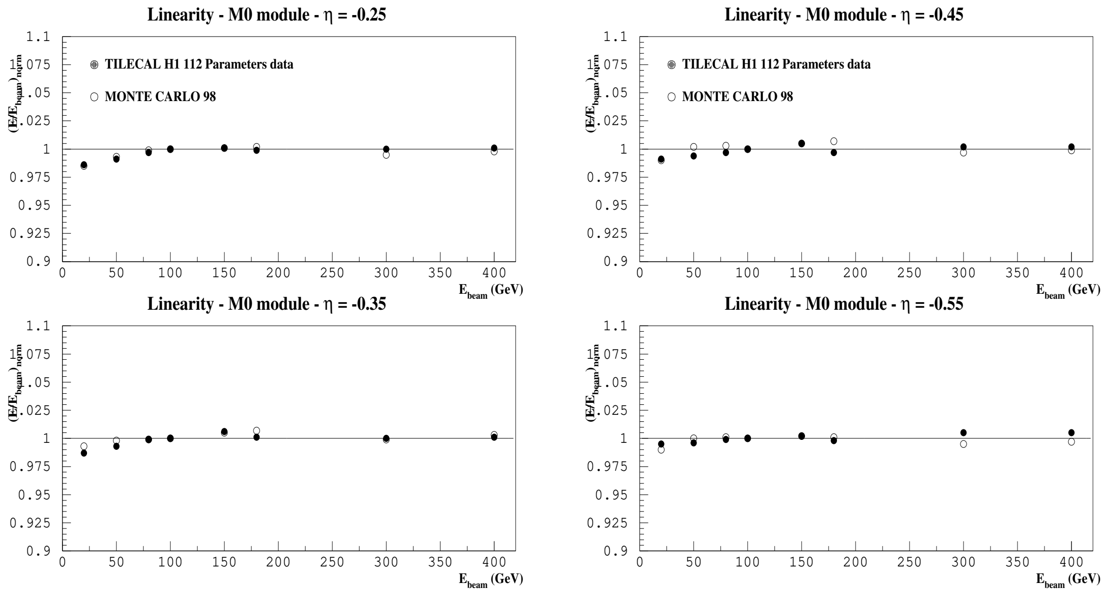

Figure 4.36: *Linearity plot minimizing the functional with the Lagrange multiplier for the test beam data and the Monte Carlo simulation. Left: for η=-0.25 (top) and η=-0.35 (bottom). Right: for η=-0.45 and η=-0.55. The points are obtained normalizing the mean reconstructed energy values from the Gaussian fits to the value of 100 GeV.*

Table 4.18: *Nominal energy, mean reconstructed energy and σ at various beam energies at η=-0.35 for test beam data and Monte Carlo simulation obtained with the constraint to the beam energy.*

η=-0.35	Test Beam data		MC simulation	
N. E. (GeV)	μ (GeV)	σ (GeV)	μ (GeV)	σ (GeV)
20	19.87±0.05	2.11±0.05	20.10±0.04	1.98±0.03
50	50.02±0.09	3.95±0.08	50.53 ±0.08	3.77±0.07
80	80.47±0.11	5.60±0.09	80.90±0.12	5.43±0.09
100	100.7±0.1	6.80±0.10	101.2±0.1	6.24±0.12
150	152.1±0.3	9.30±0.25	153.0±0.2	9.09±0.18
180	181.4±0.2	11.10±0.16	184.2±0.3	10.75±0.22
300	302.1±0.3	18.40±0.29	303.2±0.4	16.08±0.39
400	403.1±0.4	27.40±0.45	406.0±0.7	20.80±0.48

Table 4.19: *Nominal energy and resolution at various beam energies at four different η for test beam data and Monte Carlo simulation obtained with the constraint to the beam energy.*

η=-0.25	Test Beam data	MC simulation
N. E. (GeV)	$\sigma/\mu(\%)$	$\sigma/\mu(\%)$
20	10.63±0.27	10.10±0.29
50	7.95±0.17	7.76±0.17
80	7.39±0.13	7.51±0.16
100	6.99±0.13	7.35±0.16
150	6.98±0.18	7.09±0.15
180	6.92±0.11	6.78±0.16
300	5.93±0.11	5.98±0.15
400	7.40±0.11	5.59±0.15
η=-0.35	Test Beam data	MC simulation
N. E. (GeV)	$\sigma/\mu(\%)$	$\sigma/\mu(\%)$
20	10.62±0.25	9.85±0.27
50	7.90±0.17	7.46±0.15
80	6.95±0.12	6.71±0.12
100	6.75±0.11	6.17±0.13
150	6.11±0.17	5.94±0.13
180	6.12±0.10	5.83±0.13
300	6.09±0.09	5.30±0.13
400	6.69±0.12	5.12±0.12
η=-0.45	Test Beam data	MC simulation
N. E. (GeV)	$\sigma/\mu(\%)$	$\sigma/\mu(\%)$
20	10.41±0.28	10.40±0.27
50	7.52±0.15	7.85±0.28
80	7.00±0.11	7.31±0.29
100	6.56±0.09	6.81±0.27
150	5.85±0.17	6.70±0.24
180	5.86±0.09	6.50±0.19
300	5.36±0.07	5.92±0.25
400	5.75±0.10	5.16±0.14
η=-0.55	Test Beam data	MC simulation
N. E. (GeV)	$\sigma/\mu(\%)$	$\sigma/\mu(\%)$
20	8.85±0.49	9.70±0.15
50	7.55±0.15	7.70±0.17
80	6.81±0.11	7.06±0.19
100	6.14±0.09	6.81±0.18
150	6.08±0.19	6.78±0.19
180	6.03±0.09	6.63±0.18
300	5.58±0.09	5.42±0.16
400	5.40±0.07	5.25±0.17

Table 4.20: *Statistical (a), constant (b), and noise (c) terms at four different η for test beam data and Monte Carlo simulation obtained with the constraint to the beam energy.*

η	Test Beam data			MC simu lation		
	a (%)	b (%)	c	a (%)	b (%)	c
-0.25	35.10	6.30	0.06	39.30	5.10	0.06
-0.35	38.40	5.60	0.06	38.90	4.90	0.06
-0.45	41.30	5.00	0.06	41.70	5.30	0.06
-0.55	37.20	5.10	0.06	37.50	5.55	0.06

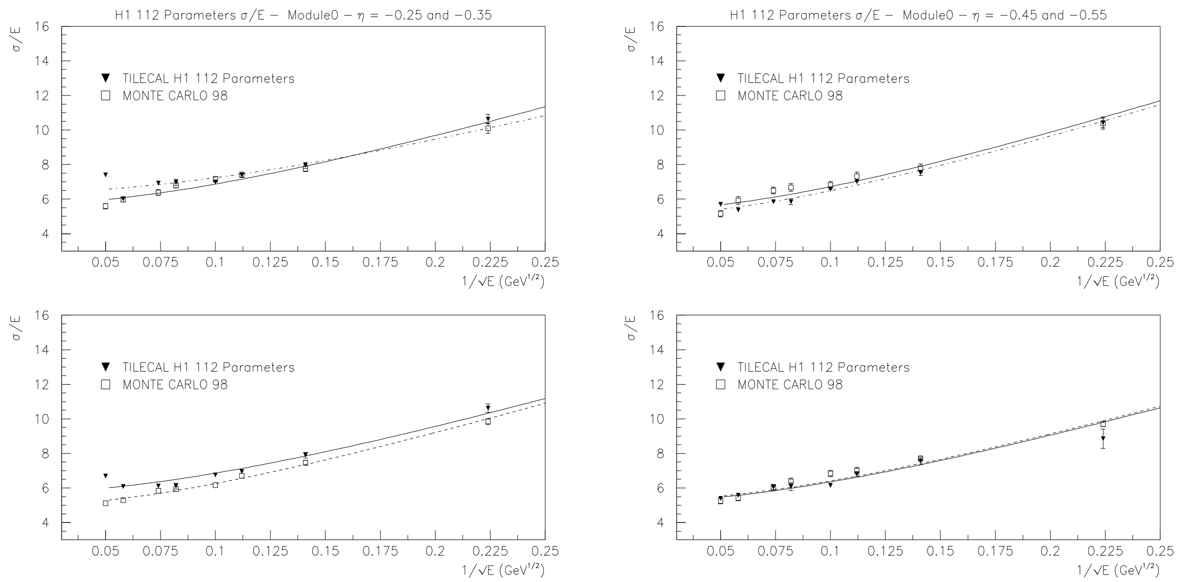

Figure 4.37: *Resolution plot minimizing the functional with the Lagrange multiplier for the test beam data and Monte Carlo simulation. Left: η =-0.25, (top) and η = -0.35 (bottom). Right: η =-0.45, (top) and η =-0.55(bottom) .*

The different values p_1, p_2 for the test beam data and Monte Carlo simulation are shown in figure 4.38 for test beam data and 4.39 for Monte Carlo simulation for various beam energies and η=-0.45. Applying the same parametrization similar results for the other η values have been obtained.

The parameters p_1, p_2 and B (the old modules parameter) are expressed as a function of the beam energy using two parameters dependence (i.e., $p_1' + p_2' \times E_{beam}$). This is shown in figures 4.40 and 4.41; for the test beam data and Monte Carlo simulation at η=-0.45. The same behaviour has been obtained for other η values.

Following theses parametrizations, we have expressed the entire set of corrections by two sets of simple functions, containing a total of only six parameters. The aim now is to check whether the energies reconstructed with 6 rather than 112 parameters are less precise. The mean, σ for η=-0.35 and resolution values for four η obtained from this a_i parametrization are given in the table 4.21 and 4.22; the linearity and resolution plots are given in figure 4.42 and 4.43. Comparing to the results previously obtained with 112 parameters one can see that despite the dramatic reduction of correction parameters the resolution is negligibly worse.

The linearity has degraded because the energy reconstruction is not good enough. This is due to the fact that the errors on the a_i, p_1, p_2 and B (the old modules parameter) are big, therefore the fit is worse than in 1997 test beam. Quantitatively, the *rms* deviation from linearity is now $\sigma = 1.19\%$ and 0.95% for the test beam data and Monte Carlo simulation, respectively, instead of 0.46% and 0.48%.

Table 4.21: *Nominal energy, mean reconstructed energy and σ at various beam energies at η=-0.35 for test beam data and Monte Carlo simulation obtained after the parametrization.*

η=-0.35	Test Beam data		MC simulation	
N. E. (GeV)	μ (GeV)	σ (GeV)	μ (GeV)	σ (GeV)
20	19.56±0.06	2.27±0.06	20.71±0.05	2.09±0.04
50	50.23±0.09	3.95±0.08	51.22 ±0.09	3.82±0.07
80	81.50±0.11	5.68±0.09	80.10±0.12	5.19±0.09
100	101.3±0.1	6.83±0.11	98.62±0.14	5.99±0.12
150	154.5±0.3	9.19±0.24	148.3±0.2	8.21±0.16
180	185.1±0.2	10.94±0.17	178.6±0.2	9.08±0.18
300	310.4±0.3	17.74±0.28	298.2±0.6	14.08±0.49
400	405.4±0.5	26.18±0.44	396.7±0.9	16.91±0.65

The resolution is now parametrized for the test beam data and Monte Carlo simulation as shows the table 4.23.

The *rms* obtained for the Monte Carlo simulation is less than for the test beam data.

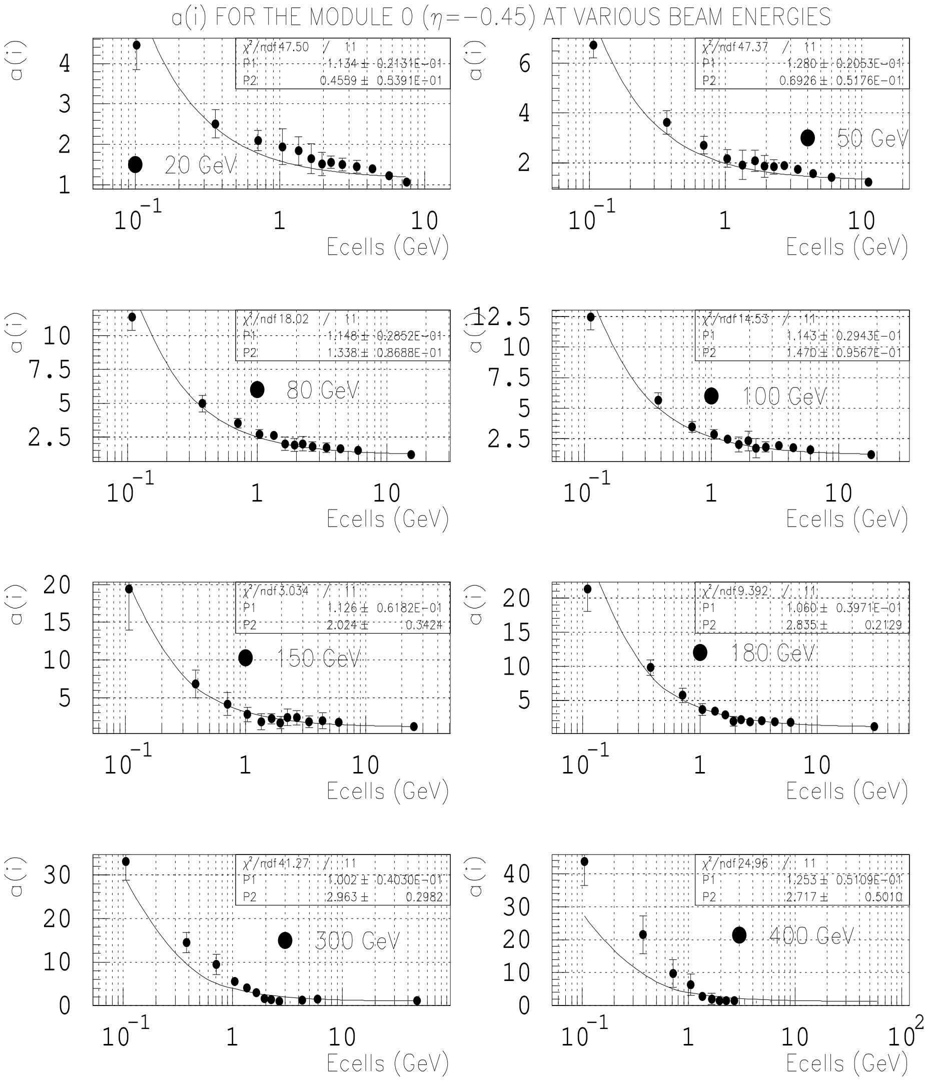

Figure 4.38: *Fits for the a_i parameters at various beam energies and η=-0.45 for the test beam data. The parameters p_1 and p_2 obtained are also shown on the plots.*

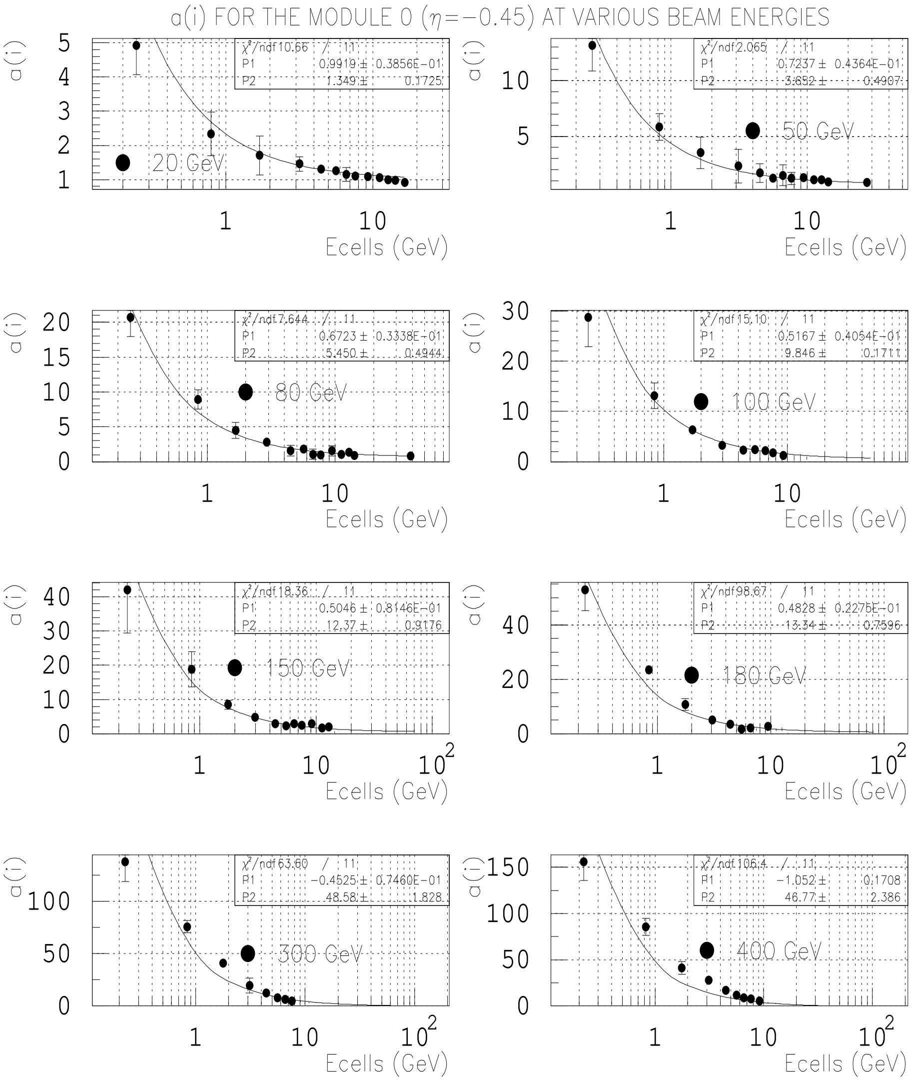

Figure 4.39: *Fits for the a_i parameters at various beam energies and η=-0.45 for the Monte Carlo simulation. The parameters p_1 and p_2 obtained are also shown on the plots.*

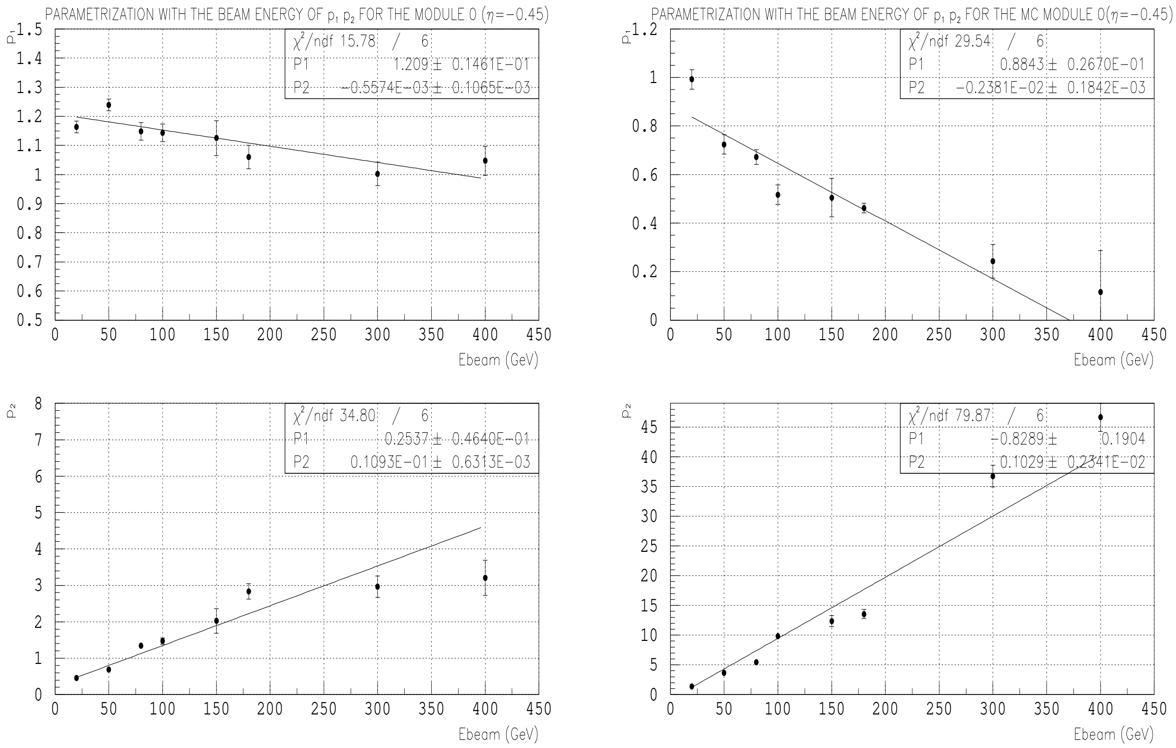

Figure 4.40: *For η=-0.45, the top plots show the parametrization with the beam energy of p_1 for the test beam data (left) and Monte Carlo simulation (right) modules; the bottom plots shown the same for p_2. The values of the parameters p_1' and p_2' from the fits are also presented on the plots.*

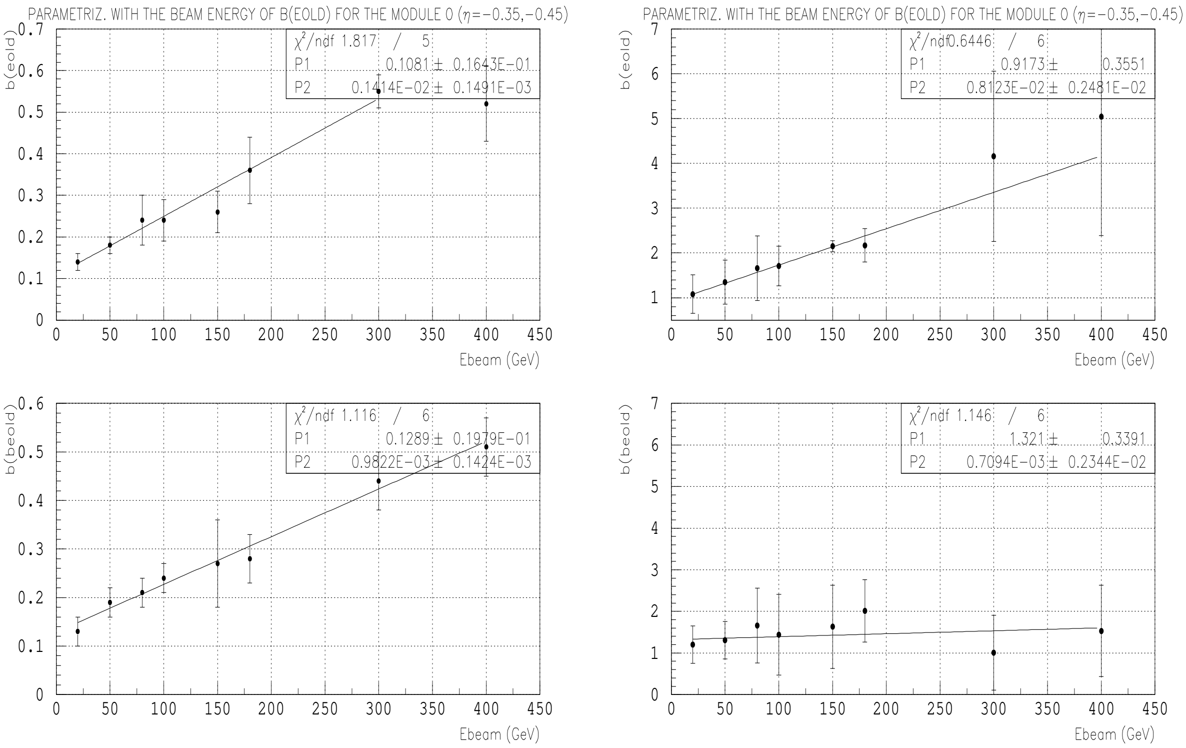

Figure 4.41: *The top plots show the parametrization with the beam energy of B for η=-0.35; the bottom plots show the same for η=-0.45. On the left test beam data and on the right Monte Carlo simulation. The values of the parameters p'_1 and p'_2 from the fits are also presented on the plots.*

Table 4.22: *Nominal energy and resolution at various beam energies at four different* η *for test beam data and Monte Carlo simulation obtained after the parametrization.*

η=-0.25	Test Beam data	MC simulation
N. E. (GeV)	$\sigma/\mu(\%)$	$\sigma/\mu(\%)$
20	11.44±0.34	10.32±0.19
50	8.11±0.16	8.00±0.15
80	7.20±0.12	6.84±0.13
100	6.65±0.11	6.81±0.13
150	6.40±0.16	6.73±0.13
180	6.73±0.09	6.23±0.12
300	5.64±0.10	6.01±0.20
400	6.13±0.08	5.16±0.40
η=-0.35	Test Beam data	MC simulation
N. E. (GeV)	$\sigma/\mu(\%)$	$\sigma/\mu(\%)$
20	11.54±0.35	10.00±0.14
50	7.86±0.17	7.41±0.13
80	6.97±0.11	6.47±0.12
100	6.75±0.12	5.95±0.11
150	5.95±0.15	5.55±0.10
180	5.92±0.10	5.08±0.13
300	5.71±0.09	4.72±0.16
400	6.45±0.11	4.26±0.18
η=-0.45	Test Beam data	MC simulation
N. E. (GeV)	$\sigma/\mu(\%)$	$\sigma/\mu(\%)$
20	11.93±0.38	10.32±0.29
50	7.80±0.17	7.98±0.25
80	6.86±0.11	7.33±0.31
100	6.27±0.09	6.47±0.47
150	5.25±0.13	6.40±0.59
180	5.33±0.08	6.36±0.29
300	4.86±0.08	5.14±0.30
400	5.36±0.13	4.79±0.25
η=-0.55	Test Beam data	MC simulation
N. E. (GeV)	$\sigma/\mu(\%)$	$\sigma/\mu(\%)$
20	11.59±0.72	9.81±0.15
50	7.82±0.18	7.36±0.34
80	6.89±0.10	7.23±0.20
100	6.26±0.09	7.21±0.24
150	6.50±0.20	6.52±0.40
180	5.79±0.09	6.17±0.25
300	5.55±0.10	5.48±0.21
400	5.11±0.08	5.29±0.22

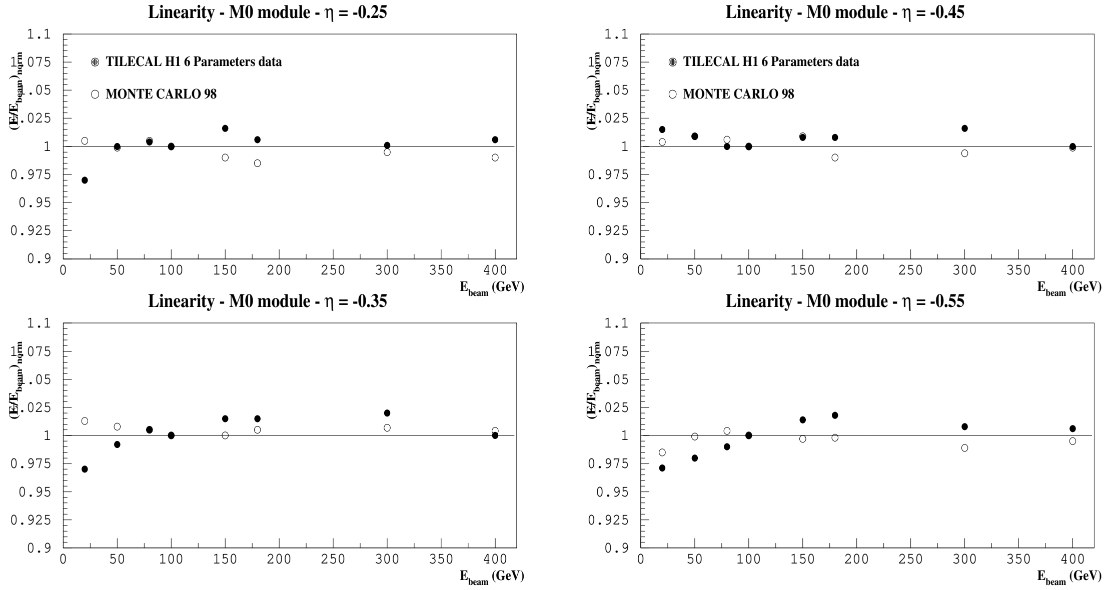

Figure 4.42: *Linearity after the parametrization with the beam energy for test beam data and Monte Carlo simulation. Left: For η=-0.25 (Top) and η=-0.35 (Bottom). Right: For η=-0.45 (Top) and η=-0.55 (Bottom).*

Table 4.23: *Statistical (a), constant (b), and noise (c) terms at four different η for test beam data and Monte Carlo simulation obtained after the parametrization.*

η	Test Beam data			MC simulation		
	a (%)	b (%)	c	a (%)	b (%)	c
-0.25	41.30	5.60	0.06	37.80	5.50	0.06
-0.35	41.10	5.30	0.06	42.20	3.90	0.06
-0.45	45.10	4.10	0.06	43.00	4.60	0.06
-0.55	43.40	4.70	0.06	37.70	5.10	0.06

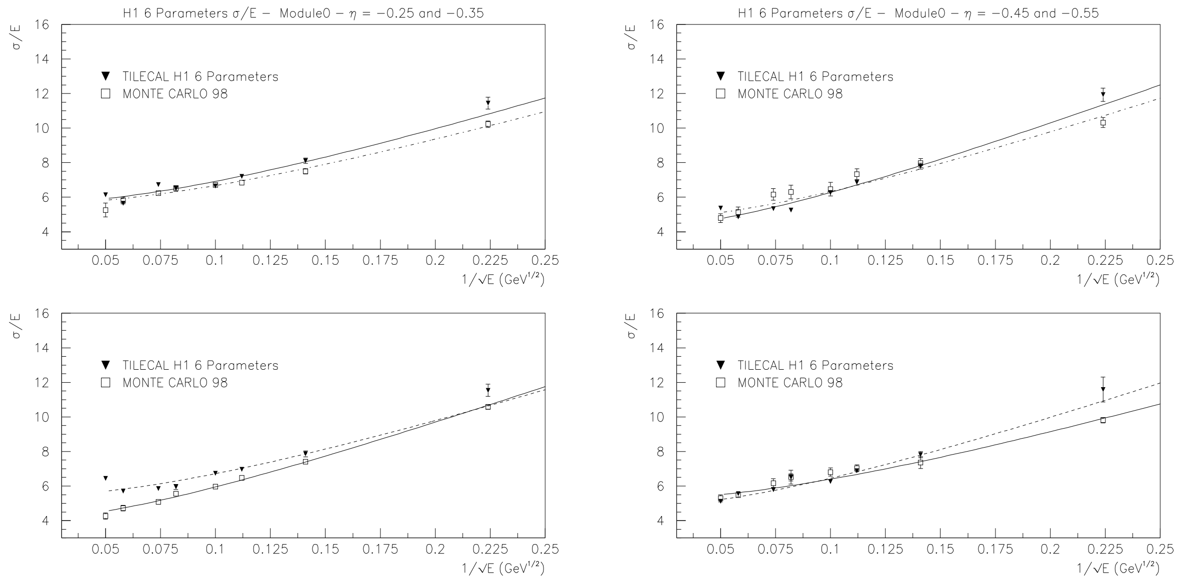

Figure 4.43: *Resolution after the parametrization with the beam energy for test beam data and Monte Carlo simulation. Left: For η=-0.25 (Top) and η=-0.35 (Bottom). Right: For η=-0.45 (Top) and η=-0.55 (Bottom).*

The drastic reduction from 112 to 6 parameters only represents an increase of 0.2 in the *rms*, both for Monte Carlo simulation and real data. For the resolution the statistical term from the fit is less in the Monte Carlo simulation than in the test beam data, this is because the resolution at low energy, where this term dominates, is better for the simulation than for the data.

4.5.2.2 Realistic energy reconstruction assuming no knowledge of the beam energy

The goal of this section is to reconstruct the pion energy in a real life experiment. The procedure was described in the section 4.2.3.3 [27].

We can reconstruct the energy using only 6 parameters and assuming no knowledge of the beam energy. This is shown in Figure 4.44

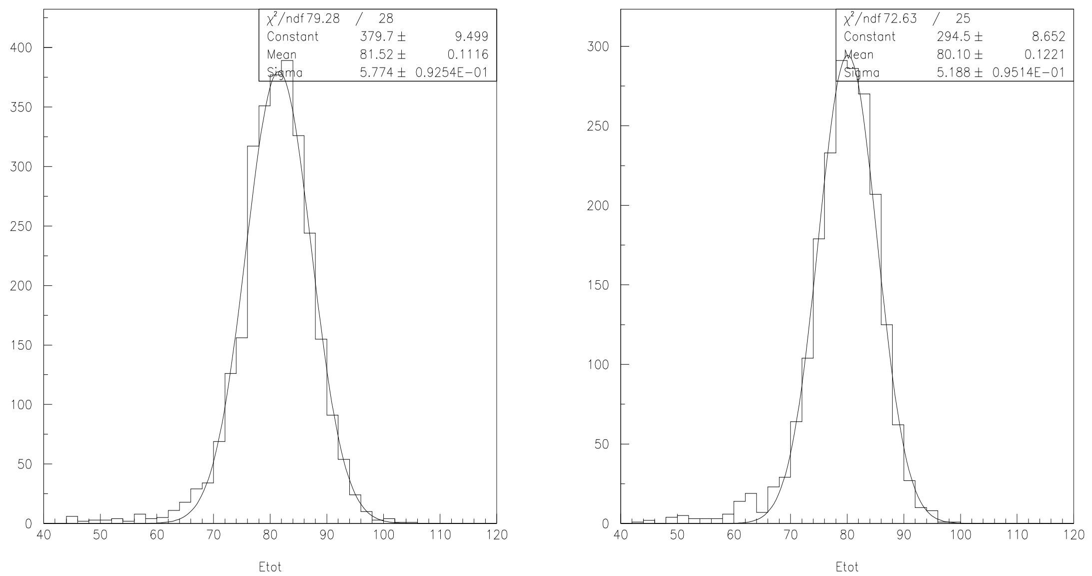

Figure 4.44: *Reconstructed energy using only 6 parameters and assuming no knowledge of the beam energy for pions at 80 GeV and η=-0.35. Left: test beam data. Right: Monte Carlo simulation.*

The mean, σ for η=-0.35 and resolution on the reconstructed energies are presented in tables 4.24 and 4.25. In figure 4.45 the linearity obtained by the *realistic* method is shown; the linearity remains as good as before. For test beam data the non-linearity ranges from 1.19% to 1.37% and from 0.48% to 0.85% for Monte Carlo simulation. The linearity given by the *realistic* method is compared with the linearity obtained using the known beam energy. Also the *rms* for the Monte Carlo simulation is less than for the test beam data.

Table 4.24: *Nominal energy, mean reconstructed energy and σ at various beam energies at η=-0.35 for test beam data and Monte Carlo simulation obtained assuming no knowledge of the beam energy.*

η=-0.35	Test Beam data		MC simulation	
N. E. (GeV)	μ (GeV)	σ (GeV)	μ (GeV)	σ (GeV)
20	19.51±0.06	2.22±0.06	20.58±0.05	2.16±0.04
50	50.22±0.09	3.93±0.07	50.87 ±0.07	3.82±0.07
80	81.79±0.11	5.69±0.09	79.44±0.09	5.16±0.09
100	101.5±0.1	6.86±0.10	98.80±0.11	5.92±0.11
150	154.7±0.3	9.27±0.22	149.9±0.2	8.07±0.16
180	186.8±0.2	11.07±0.16	177.2±0.2	9.19±0.22
300	311.7±0.4	18.01±0.27	297.2±0.5	13.13±0.49
400	406.7±0.5	26.45±0.45	395.7±0.6	15.72±0.60

The resolutions obtained with the realistic algorithm, as we can see in figure 4.46 present a slight degradation with respect to the values given in the previous parametrization that uses the nominal beam energy. This result is unavoidable due to event-to-event fluctuations of hadronic showers. The figure shows that the degradation of the resolution is more pronounced at low energy, as expected from the energy dependence of σ/E. At high energy, the resolution for the test beam data is greater than for the Monte Carlo simulation.

The final results for the test beam data and for the Monte Carlo simulation are shown in the table 4.26.

In this study we have proved that the linearity and resolution of the Barrel Module 0 improve using the H1 method. Also the good agreement between the Monte Carlo simulation and the Test beam data after applying H1 weighting technique for the four different values of η has been seen.

Respect to the linearity, using Lagrange multipliers we found a very good linear response over the range of studied energies, because 112 weights have been used for each module. With the parametrization of these weights using a total of 6 constants and assuming no knowledge of the particle energy the linearity is degraded but the average *rms* is around 1.5% and therefore inside the requirements. The linearity for the Monte Carlo simulation is better than for the test beam data but at high energies the hadronic shower simulation is insufficient and the shower description became quite far away from reality.

Table 4.25: *Nominal energy and resolution at various beam energies at four different η for test beam data and Monte Carlo simulation obtained assuming no knowledge of the beam energy.*

η=-0.25	Test Beam data	MC simulation
N. E. (GeV)	σ/μ(%)	σ/μ(%)
20	11.72±0.34	11.08±0.19
50	8.05±0.16	8.12±0.15
80	7.25±0.12	6.92±0.12
100	6.69±0.11	6.90±0.13
150	6.44±0.16	6.67±0.13
180	6.75±0.09	6.17±0.12
300	5.65±0.10	5.78±0.20
400	6.17±0.08	5.10±0.20
η=-0.35	Test Beam data	MC simulation
N. E. (GeV)	σ/μ(%)	σ/μ(%)
20	11.39±0.34	10.49±0.19
50	7.84±0.15	7.50±0.13
80	6.95±0.12	6.50±0.11
100	6.75±0.11	5.97±0.11
150	5.99±0.15	5.34±0.10
180	5.92±0.09	5.08±0.13
300	5.77±0.09	4.41±0.16
400	6.55±0.12	3.97±0.15
η=-0.45	Test Beam data	MC simulation
N. E. (GeV)	σ/μ(%)	σ/μ(%)
20	11.89±0.38	9.62±0.28
50	7.58±0.15	8.30±0.32
80	6.89±0.12	7.69±0.33
100	6.27±0.10	7.50±0.35
150	5.28±0.14	6.57±0.36
180	5.30±0.08	6.37±0.35
300	4.86±0.08	5.21±0.26
400	5.35±0.10	4.83±0.22
η=-0.55	Test Beam data	MC simulation
N. E. (GeV)	σ/μ(%)	σ/μ(%)
20	11.30±0.72	9.83±0.17
50	7.60±0.18	7.70±0.19
80	6.97±0.10	7.86±0.22
100	6.25±0.09	7.21±0.25
150	6.36±0.20	6.86±0.23
180	5.85±0.09	6.24±0.21
300	5.70±0.10	5.26±0.22
400	5.48±0.08	5.06±0.19

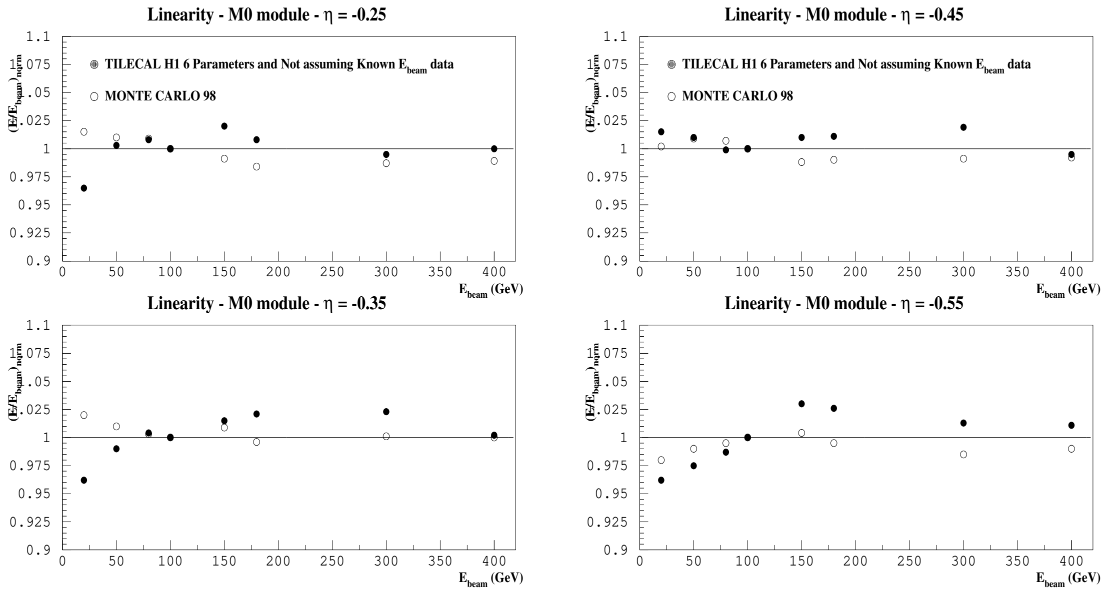

Figure 4.45: *Linearity plots without the beam energy knowledge for test beam data and Monte Carlo simulation. Left: For η=-0.25 (Top) and η=-0.35 (Bottom). Right: For η=-0.45 (Top) and η=-0.55 (Bottom).*

Table 4.26: *Statistical (a), constant (b), and noise (c) terms at four different η for test beam data and Monte Carlo simulation obtained assuming no knowledge of the beam energy.*

η	Test Beam data			MC simulation		
	a (%)	b (%)	c	a (%)	b (%)	c
-0.25	41.10	5.70	0.06	42.80	5.20	0.06
-0.35	40.80	5.30	0.06	45.70	3.70	0.06
-0.45	45.90	4.20	0.06	42.60	5.00	0.06
-0.55	43.20	4.80	0.06	39.00	5.10	0.06

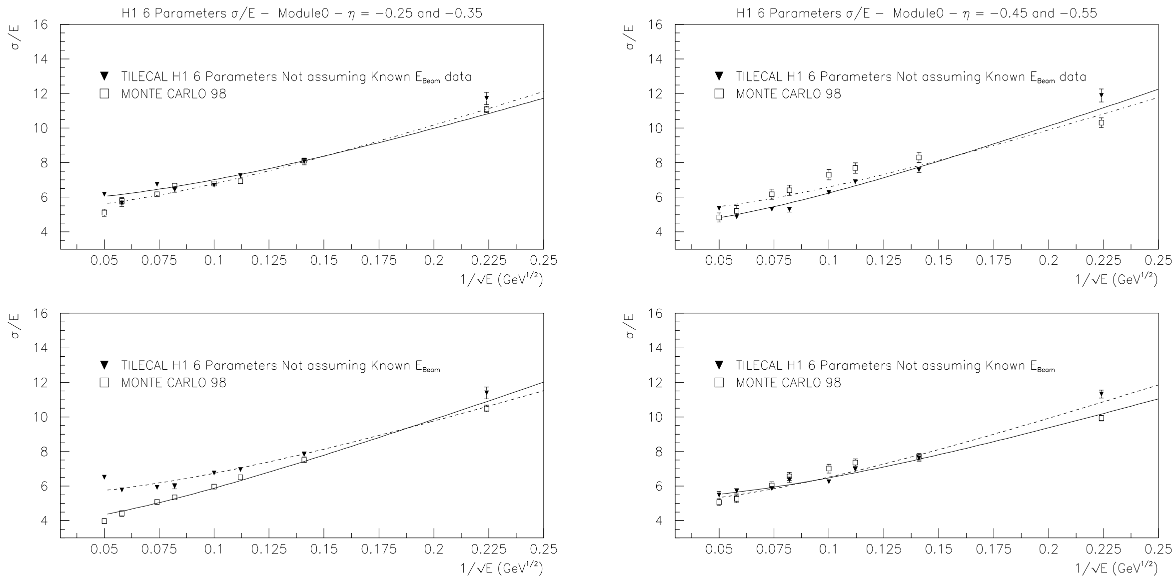

Figure 4.46: *Resolution plots without the beam energy knowledge for test beam data and Monte Carlo simulation. Left: For η=-0.25 (Top) and η=-0.35 (Bottom). Right: For η=-0.45 (Top) and η=-0.55 (Bottom).*

For the resolution, the use of all those weights improves significantly the resolution with respect to the raw data algorithm. As expected, the resolution degrades somewhat when no knowledge of the particle energy is assumed, been better than the obtained with the other methods. The statistical and the constant terms are very similar for the Monte Carlo simulation and test beam data having a mean value around 43% and 5%, respectively.

4.5.3 Leakages parametrization

The aim of this section is to parametrize the Module 0 leakages in order to improve the resolution. A prove that leakages exist is that in the Muon Wall located behind it there is signal.

A first idea was to apply cuts on the variable *MuBackHit* which represents the number of cells inside Back Muon Wall with signal greater than 0.7 mip. The figure 4.47 shows this variable for pion calibration beams with energies 20, 100 and 400 GeV at η=-0.45.

At high energies the *MubackHit* variable can reach values up to 10, 12 and, 14, while at low energies only 1 or 2. This is because at high energies the leakage in the Barrel Module 0 is greater than at low energies. We can make a cut on this variable to obtain better results in the resolution, reducing the leakages contribution.

For this pourpose we have reconstructed the raw energy detected in the Barrel Module 0 for η=-0.45 and pion beam energy 400 GeV without and with cut in *MubackHit* (*Mubackhit* < 3). This is shown in Figure 4.48. The resolution is better (evidently) when the cut is applied (from 5.7% to 5.0% for 400 GeV) but the number of entries has been strongly reduced (about 60% for 400 GeV) and also there is a clear reduction of the low energy tails. For this reason we decided to avoid the use of this cut.

Two alternatives have been tried to parametrize the leakages: with a gaussian or with an exponential. For the case where the main assumption is that the leakage is characterized by an exponential, the energy response of the ideal calorimeter (ideal resolution and correct energy scale) would have the shape:

$$R_0(e; E_0, \langle E_{leak} \rangle) = e^{-(E_0 - e)/\langle E_{leak} \rangle} \tag{4.18}$$

where E_0 is the nominal energy and $\langle E_{leak} \rangle$ is the mean value of the energy leaked out of the calorimeter. The formula is valid for $e \leq E_0$ and R_0 is equal to 0 otherwise.

Due to the e/h factor it becomes:

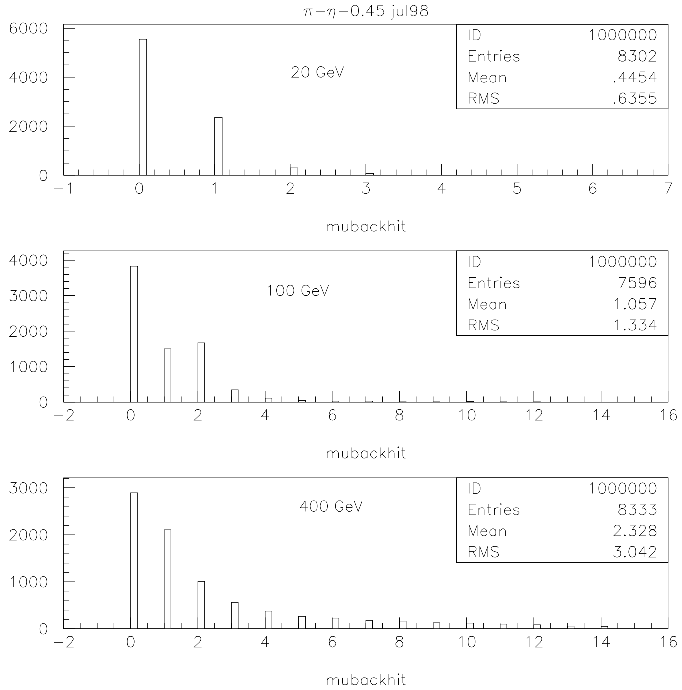

Figure 4.47: *Values of the MuBackHit variable for pion calibration beams at η=-0.45 and for three different energies.*

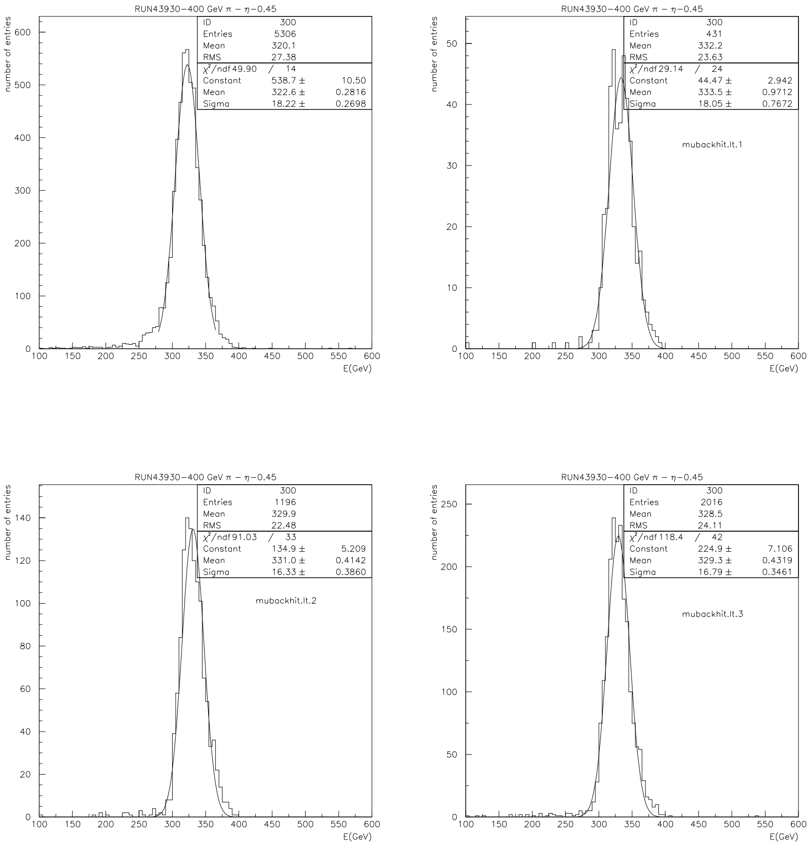

Figure 4.48: *Raw energy in the Barrel Module 0 for pions at 400 GeV and η=-0.45. Top left: without cut in MubackHit. Top right: with cut in MubackHit < 1. Bottom left: with cut in MubackHit < 2. Bottom right: with cut in MubackHit < 3.*

$$R_m(e; E_0, \langle E_{leak} \rangle) = e^{-(E_m - e)/\langle E_{leak} \rangle} \tag{4.19}$$

where E_m is a measured energy in the electromagnetic scale (it is lower that the nominal value E_0).

Because of the calorimeter resolution, each value e is smeared by the Gaussian distribution:

$$G(\epsilon; E_0, \sigma(e)) = e^{-(\epsilon - e)^2/(2\sigma^2(e))} \tag{4.20}$$

and consequently the measured response of the TileCal modules is (up to normalization factors):

$$\begin{aligned} R_{measured}(\epsilon) &= \int_0^{E_m} G(\epsilon; E_0, \sigma(e)) \times R_m(e; E_0, \langle E_{leak} \rangle) de \\ &= \int_0^{E_m} e^{-(\epsilon - e)^2/(2\sigma^2(e))} \times e^{-(E_m - e)/\langle E_{leak} \rangle} de \end{aligned} \tag{4.21}$$

and it contains three parameters:

1. The calorimeter response in the case of no leakage E_m.

2. The calorimeter resolution $\sigma(e)$. It might be constant $(\sigma(e) = \sigma(E_m))$ or energy-dependent according to the formula: $\sigma(e) = \sigma(E_m) \times \sqrt{e/E_m}$.

3. The mean energy leaked out of the calorimeter $\langle E_{leak} \rangle$.

In the case of no leakage ($\langle E_{leak} \rangle = 0$), the formula for $R_{measured}(\epsilon)$ contains an exponential function, with infinity large slope, which is equal to the $\delta(e - E_m)$ function and it becomes equal to the Gaussian distribution:

$$\begin{aligned} R_{measured}(\epsilon) &= \int_0^{E_m} G(\epsilon; E_0, \sigma(e)) \times \delta(e - E_m) de \\ &= e^{-(\epsilon - E_m)^2/(2\sigma^2)} \end{aligned} \tag{4.22}$$

Figure 4.49 shows the raw energy detected in the Barrel Module 0 for pion beam energy 400 GeV with cut in the *MubackHit* variable and parametrizing the leakages (low energy tails) with a gaussian and with an exponential. In the three cases the resolution is 5.2% but if we fit the whole distribution with two gaussians (signal and leakage) or

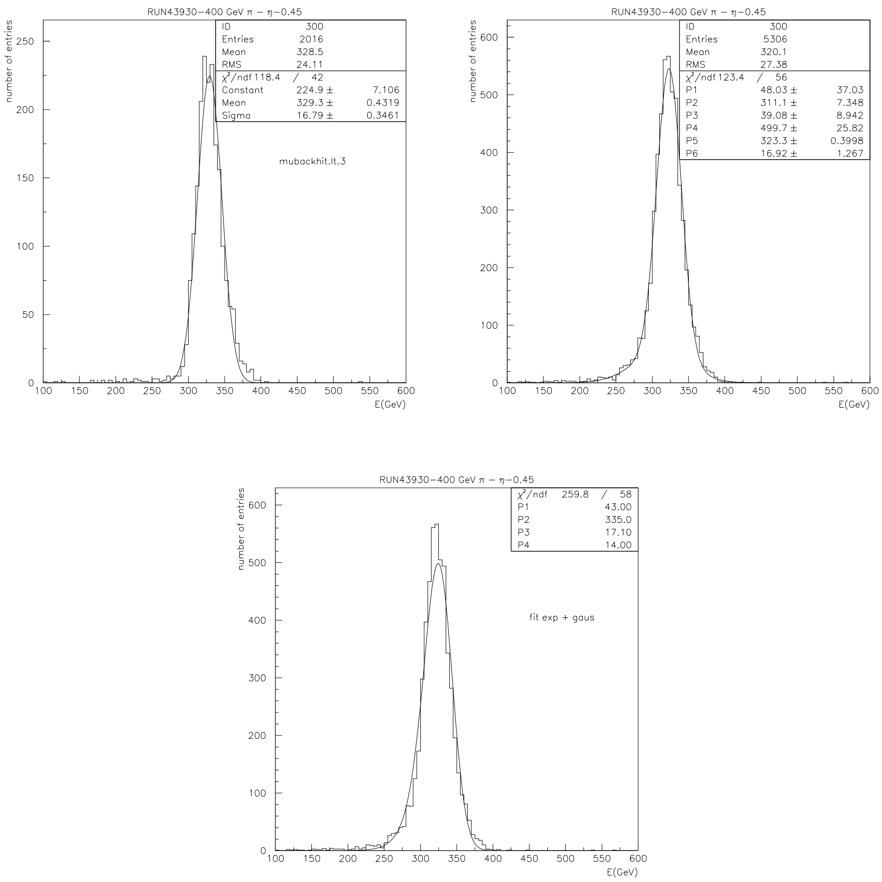

Figure 4.49: *Raw energy in the Barrel Module 0 for pions at 400 GeV and η=-0.45. a) With cut in MubackHit, b) parametrizing the leakages with a gaussian and c) characterizing the leakages with an exponential.*

with the convolution of the exponential and the gaussian, all the physical entries are used.

According with the expresion (4.17) we present in table 4.27 the results of μ, σ and σ/μ for $\eta = -0.45$ obtained from raw data and fitted with two gaussians; in table 4.28 the same results but using the convolution between the exponential and the gaussian are shown. Also the plots of linearity and energy resolution without to parametrize the leakage (top) and parametrizing the leakage with a gaussian (bottom) can be seen in figures 4.50 and 4.51, respectively. Figure 4.52 represents the energy resolution fitting with the convolution between the exponential and the gaussian.

Table 4.27: *Nominal energy, mean reconstructed energy , σ and resolution at various beam energies at $\eta = -0.45$ obtained from raw data and doing the fit with two gaussians.*

η=-0.45 N. E. (GeV)	μ (GeV)	σ (GeV)	σ/μ (%)
20	14.91 ± 0.02	2.06 ± 0.02	13.85 ± 0.13
50	38.62 ± 0.07	3.64 ± 0.05	9.42 ± 0.12
80	60.80 ± 0.46	4.63 ± 0.14	7.61 ± 0.23
100	77.98 ± 0.13	5.87 ± 0.37	7.52 ± 0.40
150	115.2 ± 0.7	6.73 ± 0.71	5.87 ± 0.60
180	143.4 ± 0.2	8.39 ± 0.22	5.85 ± 0.15
300	244.3 ± 0.3	14.83 ± 0.31	6.07 ± 0.13
400	323.3 ± 0.3	16.92 ± 0.90	5.23 ± 0.30

Table 4.28: *Nominal energy, mean reconstructed energy , σ and resolution at various beam energies at $\eta = -0.45$ obtained from raw data and doing the fit with the convolution between the exponential and the gaussian.*

η=-0.45 N. E. (GeV)	μ (GeV)	σ (GeV)	σ/μ (%)
20	14.91 ± 0.02	2.06 ± 0.03	13.85 ± 0.12
50	38.62 ± 0.06	3.64 ± 0.04	9.42 ± 0.15
80	63.20 ± 0.22	4.75 ± 0.17	7.81 ± 0.25
100	80.13 ± 0.15	6.01 ± 0.27	7.52 ± 0.33
150	119.17 ± 0.6	6.88 ± 0.75	5.91 ± 0.55
180	145.3 ± 0.3	8.87 ± 0.19	6.01 ± 0.17
300	248.3 ± 0.2	14.92 ± 0.34	6.02 ± 0.11
400	335.3 ± 0.2	17.10 ± 0.87	5.10 ± 0.33

The *rms* for the linearity is 2.5% when only one gaussian is used in the fit and 2.8% when two gaussians are fitted. The *rms* are quite similar because the two procedures

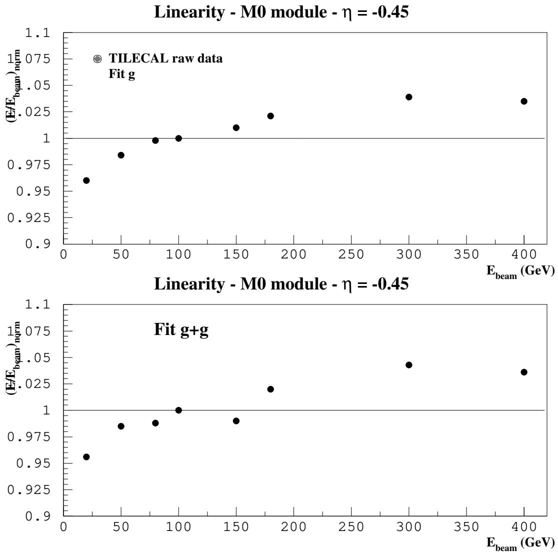

Figure 4.50: *Linearity of raw data doing the fit without to parametrize the leakage (top) and parametrizing the leakage with a gaussian (bottom) for $\eta = -0.45$.*

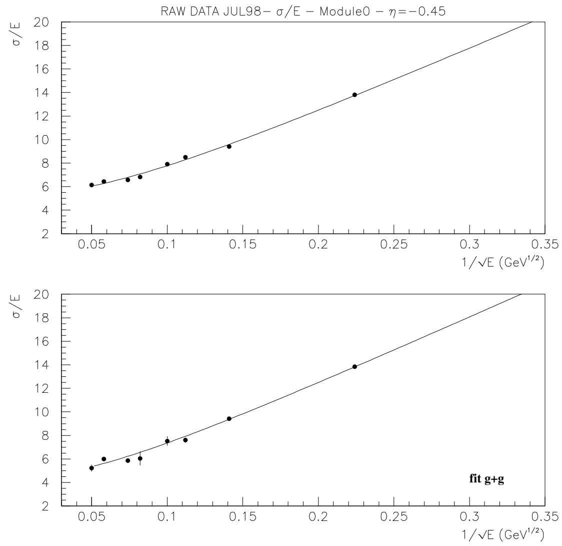

Figure 4.51: *Energy resolution of raw data doing the fit without to parametrize the leakage (top) and parametrizing the leakage with a gaussian (bottom) for $\eta = -0.45$.*

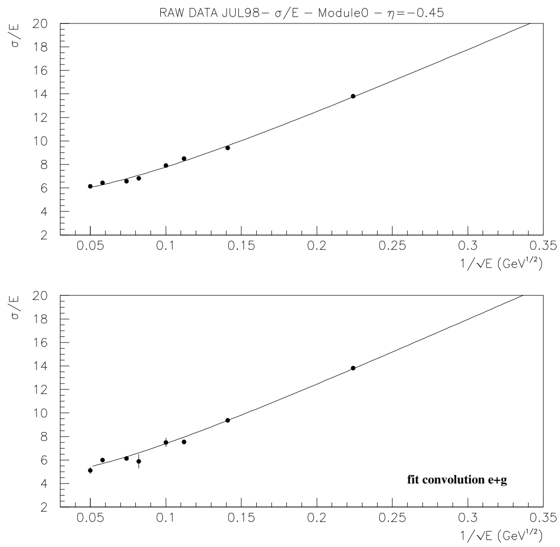

Figure 4.52: *Energy resolution of raw data doing the fit without parametrize the leakage (top) and parametrizing the leakage with an exponential (bottom) for $\eta = -0.45$.*

give practically the same value for the μ parameter.

For the resolution the fit results are presented in table 4.29, for the fit using one gaussian, two gaussians, the convolution between the exponential and the gaussian and the H1 method.

The statistical term is similar in the three cases (for the three fits) but the constant term is better when we parametrize the leakage with a gaussian or and exponential. This is because the resolution has been calculated with the gaussian distribution. And besides, the constant term for the H1 method and for the two leakage parametrization is similar due to the fact that the weighting itself already provides a reduction of the low energy tails (see figure 4.44).

Table 4.29: *Statistical (a) and constant (b) terms for $\eta = -0.45$ doing the fit with a gaussian , two gaussians, the convolution between the exponential and the gaussian and applying the H1 method. The noise (c) term have been fixed at 0.06 GeV.*

η	Fit (1 gaussian)		Fit (2 gaussians)		Fit (Conv. Exp. g.)		H1	
	a (%)	b (%)	a (%)	b (%)	a (%)	b (%)	a (%)	b (%)
-0.45	56.50	5.35	58.30	4.49	57.9	4.62	45.10	4.15

The figure 4.53 shows the comparison between the mean energy leaked out of the calorimeter $\langle E_{leak} \rangle$ when we parametrize the leakage with a gaussian (peak1-peak2) or with an exponential (slope of the exponent) and the energy dependence of the leakage.

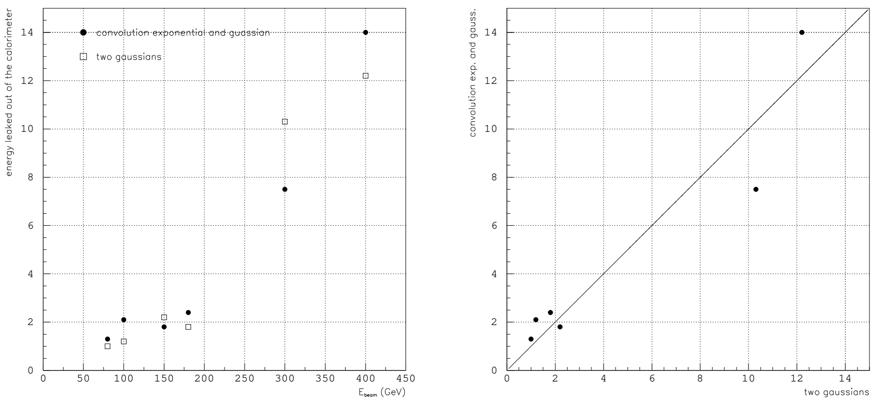

Figure 4.53: *Comparison between the mean energy leaked out of the calorimeter $\langle E_{leak} \rangle$ when we parametrize the leakage with a gaussian or with an exponential. a) Energy dependence. b) Correlation between both methods.*

In summary the two methods applied to parametrize the leakage give the same resolution and they provide the mean value of the energy leaked out of the calorimeter. The weighting technique already provides by itself a reduction of the low energy tails.

4.5.4 The e/h and the e/π ratios

The responses obtained for e and π give the possibility to determine the e/h ratio, an intrinsic characteristic of a non-compensated calorimeter. In our case the electron - pion ratios reveal complicated structures $e/\pi = f(E, \eta)$. Figure 4.54 shows the e/π ratios for Module-0 for $E =$ 20, 50 100, 180 and 300 GeV at $\eta = -0.35$, -0.45 and -0.55 and for Monte Carlo simulation at $\eta = -0.45$. The errors include statistical error and a systematic error of 1% (the error is due to the uncertainties on the value of the beam energy and on the leakage), added in quadrature. For extracting the e/h we have used the standard e/π method. The data have been fitted using equation (4.16) and a comparison with the Monte Carlo simulation at $\eta = -0.45$ has been done.

The e/h ratio of a sampling calorimeter with an iron-scintillator structure is expected to be > 1 for the conventional orientation of tiles perpendicular to incident hadrons. The results are presented in table 4.30. The e/h value is greater for η = -0.35 than for other $\eta' s$. That could be explained because the shower is better contained for η = -0.55

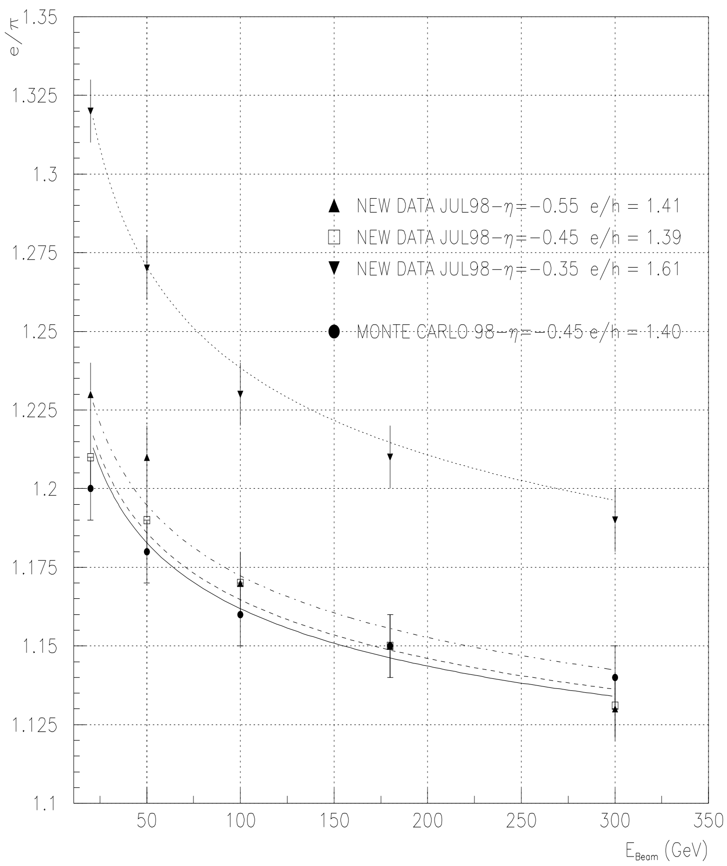

Figure 4.54: *The e/π ratio as a function of the beam energy for the Barrel Module 0 tested in the 1998 test beam at three different η's.The lines are the fits of the equation (4.16). The comparison for Monte Carlo data at η=-0.45 is also plotted.*

than for η = -0.35. Deviations from $e/h = 1$ contribute to the constant term in the energy resolution (see equation 4.7). This constant term is about 5.33 for η = -0.35 and 4.87 for η = -0.55.

The value $e/h = 1.39$ corresponding to η = -0.45 is in good agreement with the 1.36 obtained from previous precise studies and reported in the TDR [17].

Table 4.30: *The values of the e/h ratio for the Barrel module 0 at three differents η's using the equation (4.16). Also the Monte Carlo simulation, at η=-0.45 is given in the table.*

Module	η	e/h
M0	-0.35	1.61 $\pm$0.015
M0	-0.45	1.39 $\pm$0.012
M0	-0.55	1.41 $\pm$0.012
M. C.	-0.45	1.40 $\pm$0.013

4.6 Comparison between Extended Barrel and Barrel Module 0

Two Extended Barrel Modules 0 were exposed in 1997 to the calibration beams, the first was built in Barcelona (BCN), Spain, and the other at Argonne, USA. One Barrel Module 0 was exposed in 1998 to the calibrations beams.

The H1 weighting technique has been studied for both test beams. The table 4.31 shows the results obtained for the energy resolution after applying the H1 weighting technique to 1997 and 1998 test beam.

The average resolution for Extended Barrel is $\frac{\sigma}{E} = \frac{45.6\%}{\sqrt{E}} \oplus 3.0\% \oplus \frac{0.06}{E}$ and for the Barrel is $\frac{\sigma}{E} = \frac{42.7\%}{\sqrt{E}} \oplus 5.0\% \oplus \frac{0.06}{E}$. The statistical term is similar in the two cases and it is less than 50% (Hadronic calorimeter requirements [28]). The constant term is less in the Extedend Barrel than in the Barrel. As this term is related with the leakage, we can say that the Barrel Module 0 has more leakage than the Extended Barrel Modules 0 because the η values are higher than in the Barrel. For the Extended Barrel this term has a value around 3% (inside of the requirements) and for the barrel 5% (outside of the requirements).

The tables 4.32 and 4.33 show the *rms* for both Extended Barrel modules and for the Barrel Module 0 after applying the H1 weighting technique.

Table 4.31: *The statistical and constant term from the resolution curves for the two Extended Barrel modules (1997 test beam) and for the Barrel module 0 (1998 test beam) at differents η's .*

MODULE	η	a %	b %
BCN	-1.1	45.6 ± 0.7	2.71 ± 0.07
ANL	-1.1	47.8 ± 0.6	2.25 ± 0.06
BCN	-1.2	45.2 ± 0.7	3.10 ± 0.07
ANL	-1.2	43.7 ± 1.0	3.91 ± 0.07
M0	-0.25	41.1 ± 1.3	5.68 ± 0.08
M0	-0.35	40.7 ± 1.2	5.33 ± 0.08
M0	-0.45	45.9 ± 1.0	4.22 ± 0.08
M0	-0.55	43.2 ± 1.0	4.87 ± 0.10

Table 4.32: *The rms for both Extended Barrel modules and two values of η.*

η	-1.1	-1.2
BCN RMS (%)	1.2	3.0
ANL RMS (%)	1.8	2.9

The average *rms* for Extended Barrel modules is 2.2% and for the Barrel module is 1.5%. The linearity requirements for the hadronic calorimeter come from the study of quark compositness where the jet energy scale has to be linear within 2% up to a transverse energy of 4 TeV. The *rms* from the Barrel is less than this value.

The *e/h* ratio is very similar for both calorimeter prototypes (around 1.4) and there is a good agreement with previous precise studies and the Monte Carlo simulation. In the BCN extended barrel module, the *e/h* value increases when the shower is worse contained, and for the Barrel Module 0 we obtain the same behaviour [29].

Table 4.33: *The rms for the Barrel Module 0 at four different η's.*

η	-0.25	-0.35	-0.45	-0.55
RMS (%)	1.4	1.8	0.8	2.0

Bibliography

[1] R. Brun and F. Carminati, GEANT Detector Description and Simulation Tool, CERN Program Library, Long Writeup W5013, September 1993.

[2] C. Zeitnitz et al., The GEANT-CALOR Interface user's guide, CERN, AUG. 1995.

[3] S. Agnvall et al., Evaluation of FERMI Read-out of the ATLAS Tilecal Prototype, Nucl. Instr. and Meth. A403 (1998) 98-114.

[4] http://evalu20.ific.uv.es/sgonzale/cuts.html. Private comunication with B. Di Girolamo.

[5] N. Del Prete, F. Spanò, Cross-talk coefficients from muon data analysis, November 1997 AW; S. Burdin, Cross-talk coefficients determination from muon data analysis, March 1998 AW; S. Bravo, Cs data analysis, November 1997 AW; S. Nemecek, Cross-talk coeffcients from electrons data analysis, November 1997 and March 1998 AW.

[6] M. Cobal et al., Analysis of the first combined test of the LArgon and TILECAL barrel calorimeter prototypes, ATLAS Internal Note, TILECAL-No-67 (1995).

[7] H. Abramowicz et al., Nucl. Inst. and Meth. A180 (1981) 429.

[8] Private comunication with J. Kerstin.

[9] H1 Calorimeter Group, W. Braunschweig et al., DESY Internal report, DESY 89-022 (1989).

[10] F. Ariztizabal et al., Nucl. Inst. and Meth. A349 (1994) 384.

[11] A. E. Kiryunin, Study of the Hadron Energy Resolution of a Liquid Argon Calorimeter by Applying the H1 weighting technique, ATLAS Internal Note CAL-NO-016 (1993).

[12] H1 Calorimeter Group, B. Andrieu et al., Results from Pion Calibration Runs for the H1 Liquid Argon Calorimeter and Comparisons with Simulations, DESY internal report, DESY 93-047 (1993).

[13] M. P. Casado et al., ATLAS Internal Note TILECAL-NO-75 (1996).

[14] J. A. Budagov et al., Electron Response and e/h Ratio of ATLAS Iron-Scintillator Hadron Prototype Calorimeter with longitudinal Tile Configuration, Atlas Internal Note 02-02-1996.

[15] R. Wigmans, Nucl. Instr. and Meth. A265 (1988) 273.

[16] R. Wigmans, Nucl. Instr. and Meth. A259 (1987) 273.

[17] Tile Hadronic Calorimeter TDR, CERN/LHCC 96-42 (1996).

[18] DICE manual Version 0.10, CERN, Switzerland, Feb. 1995.

[19] M. Nessi et al., ATLAS Internal Note SOFT-NO-16 (1994).

[20] Comparison between the ATLAS/TileCal hadron barrel calorimeter prototype test beam data and Hadronic Simulation packge. I. Efthymiopoulos, 28-10-1996.

[21] M. Metcalf, Effective FORTRAN 77, CERN, Geneva, Switzerland

[22] J. Shiers et al., ZEBRA System, CERN Program Library, Long Writeup Q100/Q101, February 1995

[23] T. Sjostrand, High-Energy-Physics Event Generation with PYTHIA 5.7 and JETSET 7.4, CERN preprint CERN-TH.7111/93 and CERN-TH.7112/93.

[24] G. Marchesini et al., Comput. Phys. Commnu. 67 (1992) 465.

[25] F. E. Paige and S. D. Protopopescu, Manual ISAJET 7.13.

[26] C. W. Fabjan, CERN-PPE-94-61 (1994).

[27] F. Camarena et al., ATLAS Internal Note TILECAL-NO-99-001 (1999); F. Camarena, Estudios sobre el "Módulo 0" del TILECAL de ATLAS, tesis de licenciatura, Enero 1999.

[28] Calorimeter Performance, CERN/LHCC 96-40 (1997).

[29] Y. A. Kulchitsky et al., ATLAS Internal Note TILECAL-99-002 (1999).

[30] V. Castillo and S. González, ATLAS Internal Note TILECAL-99-020 (1999).